PREDICTING GAS SOLUBILITIES IN

SEMI-CRYSTALLINE BRANCHED POLYOLEFINS

Zur Erlangung des akademischen Grades eines

DOKTORS DER INGENIEURWISSENSCHAFTEN

von der KIT-Fakultät für Chemieingenieurwesen und Verfahrenstechnik des

Karlsruher Instituts für Technologie (KIT)

genehmigte

DISSERTATION

von

M.Sc. Simon Leube

aus Reutlingen

Tag der mündlichen Prüfung: *04. April 2025*

Erstgutachterin: *Prof. Dr. habil. rer. nat. Sabine Enders*

Zweitgutachter: *Prof. Dr. mont. Dr. rer. nat. Michael Fischlschweiger*

Danksagung

Die vorliegende Arbeit entstand zwischen September 2021 und Februar 2025 im Rahmen meiner Tätigkeit als wissenschaftlicher Mitarbeiter am Institut für Technische Thermodynamik und Kältetechnik des Karlsruher Instituts für Technologie.

Zuvorderst möchte ich meiner Doktormutter Sabine Enders danken für die vielen motivierenden Diskussionen und der gleichzeitig großen wissenschaftlichen Freiheit, die sie mir gewährt hat - gepaart mit der richtigen Portion Humor.

Michael Fischlschweiger danke ich für die Übernahme des Koreferats und die fachlichen Diskussionen.

Ich möchte meiner Arbeitsgruppe danken für die angenehme Atmosphäre, die konzentrierten Institutskolloquien und das regelmäßige Entkalken der Kaffeemaschine.

Ich danke meinen Eltern für die bedingungslose Untersützung und das fehlerfreie Auswendiglernen meines Promotionstitels.

Lena möchte ich danken für die moralische Untersützung und vertrauensvolle Art, auf die ich mich jederzeit freuen kann - und für das Ertragen der flexiblen Vorzüge einer Promotion.

Kurzfassung

Die genaue Abstimmung der Produkteigenschaften von Polyolefinen hinsichtlich ihrer Anwendungseigenschaften, welche durch die Produktion eingestellt werden, ist eine zentrale Herausforderung in der Verfahrenstechnik. Sowohl die Anwendungseigenschaften als auch die für die Produktion notwendigen physikalischen Größen hängen in komplexer Weise von den molekularen Parametern (Molmasse und Verzweigung) ab. Dies sei am Beispiel der Gaslöslichkeit in Polyolefinen erläutert. Einerseits hängt die Gaslöslichkeit stark von der Semikristallinität ab, die wiederum durch die Verzweigung beeinflusst wird. Anderseits bestimmt die Gaslöslichkeit die Verfahrensparameter bei der Produktion und bei der Einstellung der Anwendungseigenschaften.

Diese Arbeit widmet sich der Frage, wie die Gaslöslichkeit von reinen Gasen und Gasmischungen in Polyolefinen in Abhängigkeit der oben genannten molekularen Parameter mit einem physikalischen Modell berechnet werden kann. Die erste Herausforderung ist die Berechnung der Semikristallinität als Funktion der molekularen Parameter und der Temperatur. Die grundlegende Idee besteht in der Übertragung des sogenannten statistischen Car-Parking Problems (CPP), welches auf der Vorstellung von zufällig geparkten Autos auf einem langen Parkstreifen basiert, auf Polyolefine. Diese Idee berücksichtigt jedoch die Verzweigung nicht. Demzufolge wird in dieser Arbeit das CPP mit dem Flory-Ansatz für die Beschreibung der Kristallinität von statistischen Copolymeren (FCA), der die Verzweigung explizit berücksichtigt, kombiniert. Somit ist es möglich, die Semikristallinität in guter Übereinstimmung mit experimentellen Daten aus den molekularen Parametern und der Temperatur vorherzusagen.

Die Berücksichtigung der Semikristallinität in den thermodynamischen Gleichungen gelingt durch die Kombination mit der Kontinuumsmechanik. Die kristallinen Anteile verursachen einen Eigendruck, der mit kontinuumsmechanischen Ansätzen aus experimentell zugänglichen mechanischen Größen vorhergesagt werden kann.

Mittels des bestimmten Eigendruckes kann durch die Verwendung der Lattice-Cluster Theorie (LCT) die Gaslöslichkeit von reinen Gasen und Gasmischungen berechnet werden. Die LCT berücksichtigt die Molmasse und die Verzweigung direkt in der Helmholtzenergie. Die Reinstoffparameter können für Polyethylen anhand von PVT-Daten aus der Literatur bestimmt werden, wobei dieser Parametersatz unabhängig von den molekularen Parametern gilt. Die Beschreibung von Mischungen erfordert einen linear temperaturabhängigen binären Parameter, der an Löslichkeitsdaten im amorphen Zustand angepasst wird. Durch die Kombination mit dem Eigendruck, der wiederrum von den molekularen Parametern abhängt, kann die Gaslöslichkeit in semikristallinen Polyolefinen in sehr guter Übereinstimmung mit experimentellen Daten aus der Literatur vorhergesagt werden. Somit ist es erstmalig gelungen, den Einfluss der Verzweigung auf die Gaslöslichkeit theoretisch zu erfassen.

Abstract

Tailoring product properties of polyolefins regarding their application properties, which are adjusted during production, is one key challenge in chemical engineering. Both the application properties and the physical properties required for the production depend in a complex way on molecular parameters (molecular weight and branching). This is outlined using the example of the gas solubility in polyolefins. On the one hand, the gas solubility strongly depends on the semi-crystallinity, which in turn is influenced by the branching. On the other hand, the gas solubility predefines operational parameters during production and the adjustment of application properties.

This work addresses the question of how the gas solubility of pure gases and gas mixtures in polyolefins can be calculated as a function of the above mentioned molecular parameters using a physical model. The first challenge is the calculation of the semi-crystallinity as a function of the molecular parameters and the temperature. The basic idea is to transfer the so-called statistical car-parking-problem (CPP), which is based on the figurative problem of randomly parked cars on a long parking lot, to polyolefins. However, this concept does not consider branching. Consequently, in this work the CPP is coupled with the Flory approach for the description of the semi-crystallinity of statistical co-polymers (FCA), which explicitly considers branching. Through this, it was possible to predict the semi-crystallinity in good agreement with experimental data from the molecular parameters and the temperature.

The consideration of the semi-crystallinity in the thermodynamic equations is achieved by the combination with continuum mechanics. The crystalline domains create an eigen pressure, which is predicted from experimental accessible mechanical properties using a continuum mechanic approach.

With the help of the determined eigen pressure and the application of the Lattice-Cluster-Theory (LCT), gas solubilities of pure gases and gas mixtures can be calculated. The LCT considers the molecular weight and the branching directly in the Helmholtz energy. The pure substance parameters of polyethylene are determined using PVT-data from the literature, whereby this parameter set is valid independently of the molecular parameters. The description of the mixture requires a linear temperature-dependent binary parameter which is adjusted to solubility data in the amorphous state. By combining this with the eigen pressure, which in turn depends on the molecular parameters, the gas solubility in semi-crystalline polyolefins can be predicted in very good agreement with experimental data from the literature. Thus, for the first time, it is possible to theoretically characterize the influence of branching on the gas solubility.

Table of contents

Symbols

Symbol	Unit	Description
$a, b, c, d, e,$ f, g, m, n	-	Counting indices
a_0	$\mathrm{m^2\,mol^{-1}}$	Cross-sectional area of the polymer chain
br	$(1000\mathrm{C-atoms})^{-1}$	Branching degree
C	-	Car-Parking constant
C_{abc}	$\mathrm{J^a}$	Extended mean-field-contribution
D	-	Nucleation constant
F	J	Free energy
G	J	Free enthalpy
G	Pa	Shear modulus
h	$\mathrm{J\,mol^{-1}}$	Molar enthalpy
j	-	Number of crystalline sequences
K	Pa	Compression modulus
k_b	$\mathrm{J\,K^{-1}}$	Boltzmann constant
k_{ij}	-	Binary interaction parameter
M	-	Segment number
$\mathrm{M_N}$	$\mathrm{g\,mol^{-1}}$	Number average molecular weight
$\mathrm{M_W}$	$\mathrm{g\,mol^{-1}}$	Weight average molecular weight
N	-	Architecture coefficient
N	-	Permutation

N_{Av}	mol^{-1}	Avogadro constant
N_l	-	Number of lattice sites
n	mol	Amount of molecules
n_{br}	-	Number of units in the branch
p	Pa	Pressure
p^c, p^{eigen}	Pa	Constraint/eigen pressure
P	-	Probability
r	-	Variable chain unit
R	$\text{J}\,\text{mol}^{-1}\,\text{K}^{-1}$	Universal gas constant
S	J/K	Entropy
T	K	Temperature
V	m^3	Volume
V	-	Number of neighbours
W	-	Partition function
W	-	Wasted space
w	-	Weight fraction
v	$\text{m}^3\,\text{mol}^{-1}$	Molar volume
x_i	-	Mole fraction of component i
x	-	Interval length
z	-	Lattice coordination number

$\alpha,\ \eta,\ \kappa,\ \lambda,$ μ,π,τ,ω	-	Counting indices
α	wt%	Crystallinity
β	-	Lattice site vector
Δ	-	Difference
δ	-	Kronecker delta function
ϵ	J	Dispersion energy
ζ	-	Crystalline sequence length
ζ^*	-	Critical crystalline sequence length for linear chains
μ_i	$\mathrm{J\,mol^{-1}}$	Chemical potential of component i
ρ	-	Crystalline sequences in cross section
σ	-	Length of a cubic lattice cell
σ_e	$\mathrm{J\,m^{-2}}$	Surface energy
Φ	-	Segment fraction without consideration of void segments
ϕ	-	Segment fraction with consideration of void segments
χ	-	Flory-Huggins parameter

Subscript	Description
i	Component index
j	Component index
k	Type of architecture coefficient
m	Melting
occ	Occupied
v	Void
cr	Critical

Superscript	Description
AmPol	Reference to amorphous domains
ath	Athermal limit
G	Gas phase
L	Liquid (polymer) phase
lin	Linear chain
MF	Mean-field

Accent	Description
$\tilde{x}$	Reduced quantity
$\bar{x}$	Mean quantity

Abbreviation	Description
CPP	Car-Parking-Problem
EoS	Equation of state
DSC	Differential scanning calorimetry
FH	Flory-Huggins
FCA	Flory-Copolymer-Approach
HDPE	High-density-polyethylene
LCB	Long chain branching
LCT	Lattice-Cluster-Theory
LDPE	Low-density-polyethylene
LLDPE	Linear low-density-polyethylene
PE	Polyethylene
VLE	Vapour-liquid-equilibrium
SCB	Short chain branching
SL	Sanchez-Lacombe

List of Figures

List of Tables

1 Introduction

"Polyethylene can be thought of as being a schizophrenic polymer. One of its personalities is reflected by its simplicity. It is composed of only carbon and hydrogen. While the other personality is reflected by the diversity of ways these simple atoms can be combined to produce unique mixtures of macromolecules. It is this same complexity along with its semicrystalline nature that make it so difficult to characterize for the modern polymer chemist."

<div align="right">A. Willem deGroot [1]</div>

In the last decades, polymers have found their way into almost all aspects of our everyday life such as packaging, medicine, clothing, constructions and many other applications. One reason for the wide applicability of polymers is their flexibility in tailoring product properties for specific purposes. Even polyolefins, containing just carbon and hydrogen atoms, show various properties which can be adjusted by the architecture, e.g. the molecular structure in terms of chain length and side chain distribution. Affected by the molecular structure, polyolefins exhibit a complex crystallization behaviour, which is also a function of the pathway of crystallization, such as the heating rate and the thermal history of the sample.

In gas phase polymerization, for example, ethylene and longer α-olefin monomers are polymerized by an adequate catalyst and process conditions to achieve a specific architecture, which leads to a specific degree of crystallinity. However, some monomers remain unreacted in the environment and start to instantly penetrate the freshly produced polyolefin. These sorbed gas molecules change the product properties, leading to a melting point depression and softening of the polyolefin. This requires detailed knowledge of the competitive sorption behaviour of gases. When continuing to the processing of polyolefins, often high pressure and temperatures are applied, followed by an extrusion into ambient pressure. These heavily changing conditions affect the semi-crystallinity and the gas solubility. Degassing of gaseous components may lead to undesired product properties.

The semi-crystalline nature of polymers is a complex phenomenon affected by both equilibrium conditions and kinetics [2, 3]. Furthermore, the polyolefin's architecture including branches and chain length has a huge impact. Flory [4] was the first to develop a physical relationship (FCA) between the branching degree, the temperature and the crystalline degree of polymers. He considered a branched polyolefin as a co-polymer, only one type of monomer being crystallizable. While capturing the general dependencies of decreasing crystallinity with increasing branching degree, the main drawback is the description of the linear unbranched polymer, since Flory's theory gives 100 % for the limiting crystallinity. However, experiments have shown that unbranched polyolefins in fact do not crystallize completely [5, 6].

There are mainly two reasons for reduced crystallinity of linear polymers. A polymer melt consists of twisted, looped and knotted chains. These entanglements do not suddenly detangle shortly before crystallization and instead remain in the amorphous phase as uncrystallisable units, hence lowering the overall crystallinity [3]. Second, as crystallization progresses, certain sequences of the polymer chain become isolated and are then too short to build a stable crystallite, being forced to remain amorphous as well [3]. While chain entanglement is an issue widely discussed in literature [7–13], only a few have dealt with the issue of isolated, hence wasted space, during crystallization [14–17].

One way to determine the wasted space that emerges as crystallization progresses, is based on the figurative problem of cars being randomly placed along a curb without overlapping, also known as the Car-Parking-Problem (CPP) [18]. While this approach was applied successfully in the field of adsorption [19–21], it found barely attention in the field of crystallization. Gornick & Jackson [15] transferred the CPP to the crystallinity of polymer chains by calculating the wasted space that evolves between two sequences that have already crystallized but are too short to form another stable crystallite. Maltz & Mola [16, 22] introduced another point of view by considering the crystallization as a continuous process in which the sequences crystallize one after another resulting in different probabilities for different configurations. Independent from Maltz & Mola's extension [16, 22], Gornick & Freedman [23] derived the same relations 10 years later. Yet, both the statistical and the continuous approach were introduced at a merely academic level and, according to my knowledge, have not been further investigated.

When considering molten polyethylene, no crystallinity occurs. However, the polymer's architecture may affect the gas solubility directly. The influence of chain length has been investigated thoroughly [24–29]. Due to the increasing asymmetry between gas and polymer, the solubility decreases with increasing chain length [25, 26]. Yet, contradictory statements ex-

ist for the impact of the branching degree on the gas solubility in molten polyolefins [30–37], whereby more experiments are necessary in order to clarify this issue.

Various models have been used in the recent decades to describe gas solubilities in polyolefins. On the one hand, equations of state (EoS) from the SAFT-family (Statistical Associating Fluid Theory), such as the PC-SAFT (Perturbed Chain-SAFT) [38], are frequently used [25, 29, 39–41]. On the other hand, lattice theories, such as the Flory-Huggins (FH) theory [42, 43] and the Sanchez-Lacombe (SL) EoS [44] proved themselves as a useful tool for the calculation of gas solubilities in amorphous polyethylene [45–47]. Unfortunately, all these theories cannot be used for differently branched systems. Every polyethylene sample, each with its own unique architecture, would require a separate set of parameters for modeling. This drawback applies to my knowledge to all EoS, except for the Lattice-Cluster-Theory (LCT) [48, 49]. Here, the molecular structure is incorporated into the model a priori. The LCT was already applied successfully to solid-liquid-equilibria (SLE) and liquid-liquid-equilibria (LLE) of branched polymers [50–54] and vapour-liquid-equilibria (VLE) of small hydrocarbons [49]. The gas solubility in polymers and especially its dependence on branching had not been investigated so far.

When it comes to semi-crystalline gas solubilities, it could be shown that the sorption solely takes place in the amorphous domains of a semi-crystalline polyolefin [46, 47]. However, the solubility in the amorphous domains is strongly influenced by the surrounding crystalline domains by a constraining intrinsic stress. Different approaches exist to account for the altered solubility in the semi-crystalline state. Elastic approaches introduce a parameter denoting the fraction of tie chains that apply an elastic force and constrain the swelling of the polymer [55]. The non-equilibrium lattice fluid (NELF) approach regards the semi-crystalline state as a pseudo-glas-state, where the density of the amorphous state is in non-equilibrium and can be regarded as new parameter or calculated from corresponding swelling experiments [56]. Intrinsic pressure approaches introduce a constraint pressure, that is added to the equilibrium pressure and denotes the isotropic stress, acting from the crystalline on to the amorphous domains [47]. This constraint pressure was first used as an adjustable parameter. However, by coupling the constraint pressure approach with continuum mechanic, it could be predicted, using solely mechanical arguments from the polymer and the degree of crystallinity [46].

All these mentioned approaches regarding the altered solubility in the semi-crystalline state require the degree of crystallinity as input variable, which is often measured along the experimental gas solubilities. However, the crystallinity is a function of the temperature. When using the measured crystallinity, often measured at room temperature, and calculate phase equilib-

ria at the specified temperature of the sorption experiment, an error is introduced in the model that can lead to large deviation from the experimental data. To overcome this deficiency, the main aim of this work is the development of a consistent predictive framework, which is shown in figure 1.1.
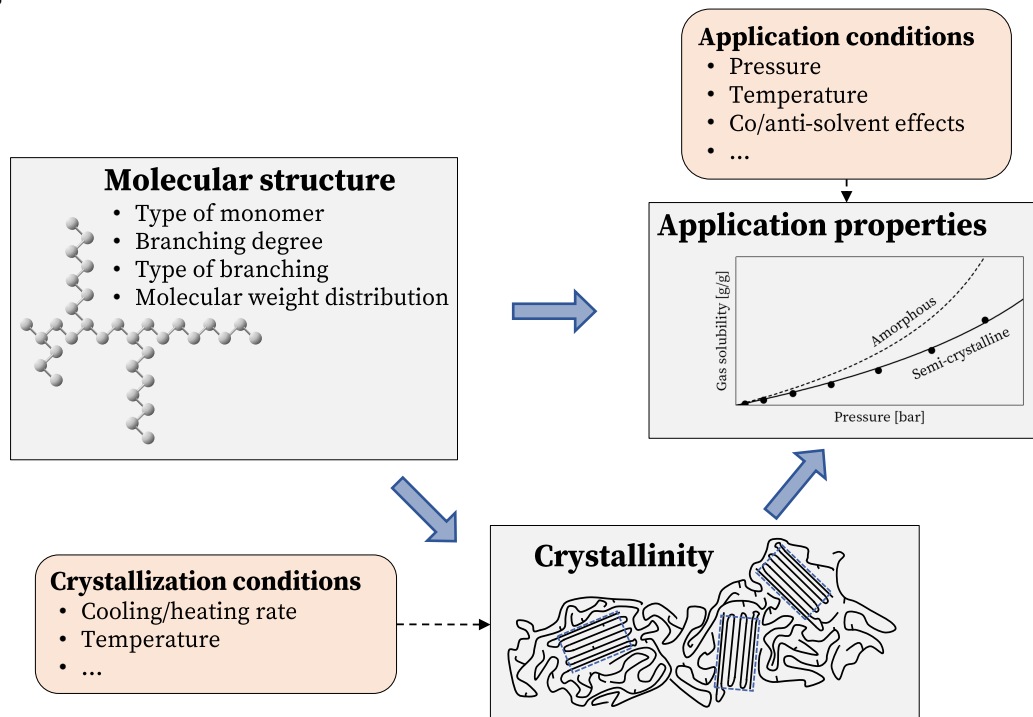
Figure 1.1: Schematic representation of dependencies between molecular structure, crystallinity and application properties.

Accordingly, three question will be addressed in the course of this work:

- How does the molecular structure (molecular weight and branching) affect the gas solubility in amorphous polyethylene?
- How does the molecular structure determine the crystallinity of polyethylene?
- How can a predictive framework be built that accounts for all these relationships between structure, crystallinity and experimental conditions?

The work is structured as follows: First, the challenges of classifying polyethylene and the modeling of polymer systems are outlined in chapter 2. Subsequently, approaches for considering the semi-crystalline state for gas solubility calculations are investigated in chapter 3. Withal, experimental methods are described to interpret experimental data, which is given afterwards. The theoretical approach, including the coupled CPP/FCA, the LCT and numerical implementations are given in chapter 4. Chapter 5 presents results regarding the calculated crystallinities. Finally, binary and ternary systems of gas solubilities in amorphous and semi-crystalline branched polyolefins are shown, discussed and compared with experimental data.

2 Background

In the following chapter, basic thermodynamic terminologies and physical relationships are explained, that are essential for further considerations and calculations throughout this work. Lattice theories in general and the Lattice-Cluster-Theory (LCT) in particular for modelling polymer systems are introduced. Further, polyethylene as divers macromolecule is characterized and the semi-crystalline state is introduced. Finally, basic physical relations of gas solubilities are described.

2.1 Phase equilibria for polymer systems

In order to describe macroscopic physical processes such as solubilities, the system has to be characterized thermodynamically. Of great importance here is the phase, a mechanical separated region, in which physical quantities exhibit no jump, i.e. homogeneous behaviour. Withal, one phase can be composed of several components. In case, a phase is in contact with an adjacent phase, i.e. connected by a phase boundary, a constant mass as well as energy transfer takes place. Driving force for these transfers and simultaneously definition for the thermodynamic equilibrium are the equilibrium conditions. These demand a mechanical equilibrium, i.e. uniform pressure p in all phases (eq. 2.1) as well as a thermal equilibrium, i.e. uniform temperature T in all phases (eq. 2.2). Moreover, a material equilibrium ensures uniform chemical potential μ_i in all phases for one component i each (eq. 2.3 - 2.4):

$$p^\alpha = p^\beta = ... = p^\pi \tag{2.1}$$

$$T^\alpha = T^\beta = ... = T^\pi \tag{2.2}$$

$$\mu_1^\alpha = \mu_1^\beta = ... = \mu_1^\pi \tag{2.3}$$

$$\vdots$$

$$\mu_i^\alpha = \mu_i^\beta = ... = \mu_i^\pi \tag{2.4}$$

The chemical potential is obtained by derivating the Helmholtz free energy F with respect to the amount of moles n_i of component i:

$$\mu_i = \left(\frac{\partial F(T, V, N)}{\partial n_i} \right)_{T,V,n_j \neq n_i} \tag{2.5}$$

When calculating vapour liquid equilibria such as gas solubilities in polymers, it is assumed that the polymer is only present in the liquid phase. Therefore, the material equilibrium condition (eq. 2.3) is only formulated for the gaseous component(s):

$$\mu_i^G(T, p, \Phi_i^G) = \mu_i^L(T, p, \Phi_i^L) \tag{2.6}$$

where μ_i^G and μ_i^L are the chemical potential of component i in the gas phase and liquid (polymer) phase respectively. T is the system temperature while Φ is the segment fraction. For a single gas solubility system, Φ_i^G turns 1.

2.1.1 Lattice theories

The ideal mixing law provides a simple relation for the description of mixtures. Eq. 2.7 equals the ideal entropy of mixing, with k_b being the Boltzmann constant and x_i the mole fraction of component i.

$$\frac{\Delta S^{ideal}}{k_b} = -\sum_i x_i \ln(x_i) \tag{2.7}$$

For the description of molecules having a similar size, the ideal mixing law provides an adequate correlation even in the presence of strong interactions. However, when considering polymer systems and in particular gas-polymer-systems, massive differences in the size of the molecules occur, leading to a significant deviation from eq. 2.7. For that reason, Flory [42] developed an approach for the calculation of polymer solutions. For that to happen, molecules are randomly placed in a perfect regular lattice consisting of identical sized lattice sites. Longer molecules are distributed onto multiple lattice sites in such a way that a lattice site accommodates similar sized parts of molecules (Fig. 2.1).

Hence, the mixing entropy of the athermal limits is written as [42]:

$$\frac{\Delta S^{ath}}{N_l k_b} = -\sum_i \frac{\Phi_i}{M_i} \ln(\Phi_i) \tag{2.8}$$
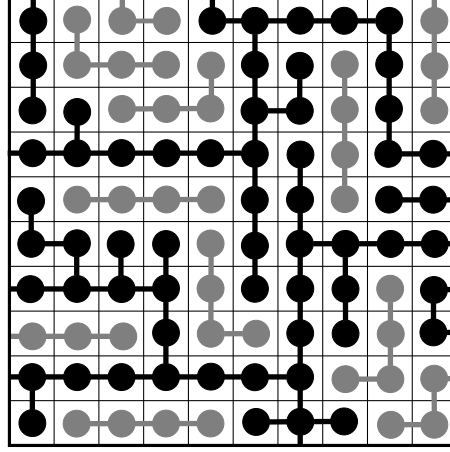
Figure 2.1: Exemplary arrangement of n-butane (grey) and polyethylene (black) in a lattice according to Flory's lattice theory. Each segment contains one CH_x-group.

with N_l being the overall number of lattice sites, Φ_i being the segment fraction and M_i being the number of segments of component i. The segment fraction Φ_i is calculated as follows:

$$\Phi_i = \frac{n_i M_i}{\sum n_j M_j} \tag{2.9}$$

whereby n_i is the amount of moles. Eq. 2.8 provides the basis for the Flory-Huggins-theory (FH) [42, 43]:

$$\frac{\Delta G^{FH}}{N_l k_b T} = \sum_i \frac{\Phi_i}{M_i} \ln(\Phi_i) + \sum_i \sum_j \chi_{ij} \Phi_i \Phi_j \tag{2.10}$$

With help of the FH-theory and the adjustable parameter χ_{ij}, incompressible polymer system can be calculated successfully. However, the FH-theory does not take into account any architecture of the molecules; χ_{ij} is used as a phenomenological empirical parameter, containing all the real effects, which cannot be described by the FH-theory.

2.1.2 Lattice-Cluster-Theory

The Lattice-Cluster-Theory (LCT) was developed by Freed and co-workers [57–61] (with the corrections from [62]) forming a consistent extension of the FH-theory. Starting from the mean-field-limit the partition function is corrected in a power series around the inverse lattice coordination number z^{-1} and the dispersion energy $\epsilon_{ij} k_b^{-1} T^{-1}$. Hence, the molecules architecture can be incorporated into the model a priori. The introduction of void lattice sites, regarded as one-segmented components without interactions, allows the description of compressible

systems [48]. The partition function of a linear chain in the athermal limit is given as follows [48]:

$$W_{lin}^{ath} = \prod_{\mu=1}^{k} \frac{1}{N_\mu! 2^{N_\mu}} \sum_{\substack{i_{1,1}^1 \neq i_{2,1}^1 \ldots \neq i_{M_1,1}^1 \\ \neq i_{1,2}^1 \neq i_{2,2}^1 \ldots \neq i_{M_1,2}^1 \\ \vdots \\ \neq i_{1,N_1}^1 \neq i_{2,N_1}^1 \ldots \neq i_{M_1,N_1}^1 \\ \vdots \\ \neq i_{1,N_k}^k \neq i_{2,N_k}^k \ldots \neq i_{M_1,N_k}^k}} \prod_{n_\mu=1}^{N_\mu} \left[\prod_{m_\mu=1}^{M_\mu-1} \sum_{\beta_{m,n}^\mu=1}^{z} \delta\left(i_{m,n}^\mu, i_{m+1,n}^\mu + \beta_{m,n}^\mu\right) \right] \quad (2.11)$$

whereby every distinguishable segment m_μ of a chain n of component μ occupies one lattice site $i_{m,n}^\mu$. The lattice site $i_{m,n}^\mu$ is connected by vectors $\beta_{m,n}^\mu$ to z adjacent neighbours. k gives the number of components, M the number of segments and N the number of chains. The Kronecker delta $\delta_{a,b}$ is given by:

$$\delta_{a,b} = \begin{cases} 1 & \text{if } a = b \\ 0 & \text{if } a \neq b \end{cases} \quad (2.12)$$

From eq. 2.11, the partition function of the mean-field-limit is calculated. Subsequently, the architecture of the considered molecules accompanied by excluded volume constraints as well as attractive interactions are incorporated into the LCT as deviations from the mean-field-limit [48]. In order to implement the molecular structure, the molecules involved are divided into united atom groups, being mostly CH_x-groups (Fig. 2.2). Now, the united atom model is represented by graphs involving the determination of the architecture coefficients (Table. 2.1). Finally, by calculating the cumulant diagrams, an expression for the free energy F is obtained, from which all thermodynamic quantities can be derived.
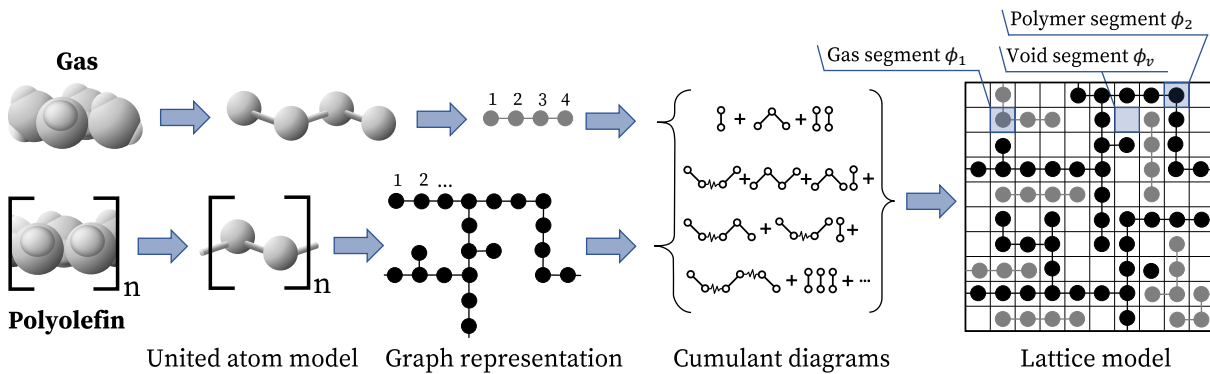
Figure 2.2: Schematic illustration of the LCT.
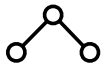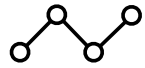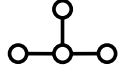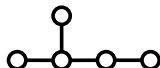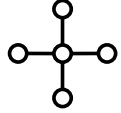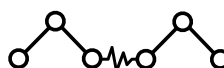
The original version of the LCT [48] requires nine architecture coefficients N_k alongside the segment number M, listed in Fig. 2.1. However, by means of graph invariants from Nemirovsky et al. [63] in eqn. 2.13 and 2.14, the number of required architecture coefficients can be reduced from nine to three, which are N_1, N_2 and N_3.

$$N_1 + 2N_2 + 2N_{1,1} - N_1^2 = 0 \tag{2.13}$$

$$2N_2 + 2N_3 + 3N_\perp + N_{1,2} - N_1 N_2 = 0 \tag{2.14}$$

Now, in terms of architecture, the free energy depends only on the number of one, two and three consecutive bonds as well as the number of segments. Since the LCT was only rearranged in an analytical way, the reduced version leads to the exact same result.

Table 2.1: Architecture coefficients used for the original version of LCT [48] and their description. Circles denote atom groups while lines are bonds between atom groups. Jagged lines stand for bonds on the same molecule being not consecutive.

Architecture coefficient	Graph representation	Description
M		Number of atom groups
N_1		Number of distinguishable ways to choose bonds between atom groups
N_2		Number of distinguishable ways to choose two consecutive bonds
N_3		Number of distinguishable ways to choose three consecutive bonds
$N_\perp$		Number of distinguishable ways to choose three bonds meeting at one atom group
$N_{\perp'}$		Number of distinguishable ways to choose four bonds, three of which meet at one atom group and one of which is appended
N_+		Number of distinguishable ways to choose four bonds meeting at one atom group
$N_{1,1}$		Number of distinguishable ways to choose two not consecutive bonds on the same molecule
$N_{1,2}$		Number of distinguishable ways to choose three bonds on the same molecule, two of which are consecutive
$N_{2,2}$		Number of distinguishable ways to choose four bonds on the same molecule, two of which are consecutive at a time

2.2 Classification of polyethylene

Polyethylene is a rather collective term for a whole series of different molecules, varying in architecture, e.g. molecular weight and branching. Every unique architecture leads to different physical and chemical properties. This section first describes how the kind and conditions of the synthesis predetermines the structure of polyethylene, namely the branching and the molecular weight. Afterwards, the semi-crystalline nature of polyethylene is investigated.

2.2.1 Synthesis

The polymers architecture is predetermined by the conditions of the synthesis, namely the polymerization type, the choice of catalysts and the composition of monomers, which can be seen in figure 2.3.
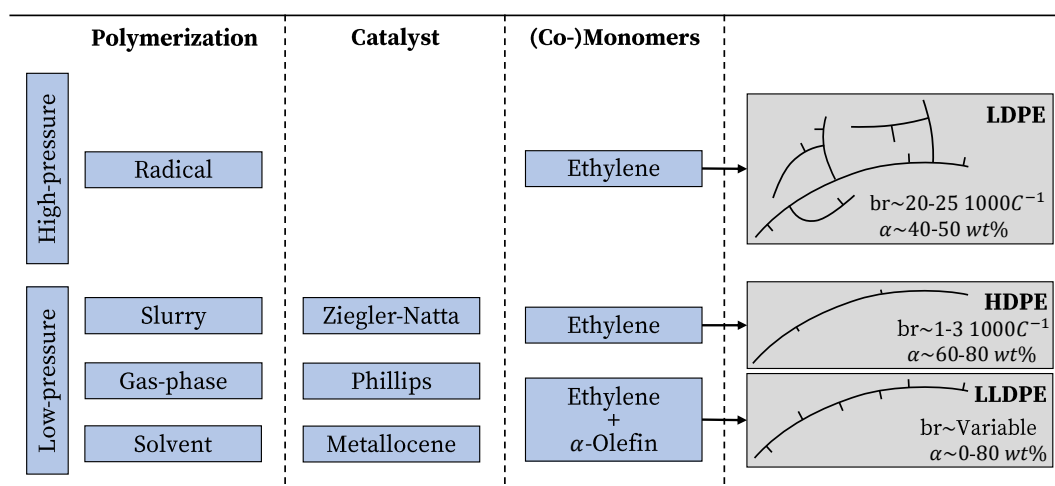
Figure 2.3: Relationship between synthesis conditions, architecture and properties of polyethylene. br denotes the branching degree while α is the crystallinity.

The right side of figure 2.3 shows a common classification of polyethylene types into LDPE (low density polyethylene), HPDE (high density polyethylene) and LLDPE (linear low density polyethylene). LDPE has both long and short chain branches resulting in a medium crystallinity. HDPE contains only few short branches resulting in a high crystallinity, whereas LLDPE has a varying amount of short chain branches and therefore varying crystallinity. While this helps as a rough categorization, for a detailed investigation on the polymers architecture, a more substantiated classification is necessary.

Polymerization

The polyethylene synthesis can be carried out either by a radical polymerization at high pressure or via catalysts at low pressure [64]. The high-pressure process takes place at 1800 bar to 3500 bar and temperatures between 180 °C and 350 °C. Ethylene is in the supercritical state and reacts via a radical chain mechanism to LDPE [64]. Approx. $0.5\,\text{br}\,1000\text{C}^{-1}$ to $1\,\text{br}\,1000\text{C}^{-1}$ long chain branches originate from intermolecular chain transfers, while ca. $20\,\text{br}\,1000\text{C}^{-1}$ to $25\,\text{br}\,1000\text{C}^{-1}$ short chain branches emerge via intramolecular chain transfers. Short chain branches include predominantly butyl branches, followed by ethyl branches [65]. The molecular weight can be controlled by the polymerization conditions: High pressure and low temperature leads to a higher molecular weight [66].

Low-pressure synthesis result in rather linear molecules with almost exclusively short chain branches (HDPE, LLDPE), which can be carried out in a slurry process, as gas phase polymerization and as solvent polymerization [64]. In the slurry process, ethylene is solved in a hydrocarbon solvent between 70 °C and 90 °C and 7 bar to 30 bar. The polyethylene particles produced are insoluble in the hydrocarbon solvent, and can be separated by filtration. In gas phase polymerization, a fluidized bed, including the monomers and catalyst particles, react to polyethylene between 85 °C and 100 °C and 20 bar to 30 bar. The heat of polymerization has to be dissipated via condensable components. In case of solvent polymerization, the monomers are solved in an appropriate solvent were the polyethylene produced is still in solution [64]. After adding the catalyst, the reaction starts rapidly, which is why the vessel has to be cooled externally to achieve a temperature between 140 °C and 150 °C and pressure between 7 bar to 70 bar. Solvent polymerization results in polyethylene of rather low molecular weight [64].

Catalyst

Contrary to the radical polymerization, low-pressure synthesis requires an adequate catalyst in which monomers coordinate at the surface of a transition metal [64]. First catalysts developed were Ziegler-Natta catalysts, based on titanium tetrachloride alongside a co-catalyst, which is mainly trialkylaluminum [65]. This results in highly linear chains (in case ethylene is the only monomer) and high molecular weight [67]. Phillips catalysts include chromium compounds impregnated on a silica-alumina support, leading to linear chains, having a broad molecular weight distribution, and a considerable amount of long chain branches [65]. The third class of catalysts are metallocene complexes of a transition metal, alongside a co-catalyst, being either an organoaluminium or methylalumoxane [65]. Metallocene catalysts allow to predetermine

11

the molecular weight and the molecular weight distribution of polyethylene, so a very narrow PDI (polydispersity index) can be obtained [65]. Also, the short-chain branching distribution is very low when using metallocene catalysts, in case co-monomers are used [65].

(Co-)Monomers

Key properties of polyethylene such as the crystallinity can be varied by adding co-monomers alongside ethylene during the polymerization process. This leads to the insertion of the co-monomers in the ethylene backbone which results in short chain branches [64]. Typical co-monomers are α-olefins such as 1-propene, 1-butene, 1-hexene and 1-octene corresponding to methyl, ethyl, butyl and hexyl branches. When using different monomers, it should be noted that the reactivity varies by orders of magnitude for different catalyst-monomer-pairs [64].

Additives

For fine-tuning the polymer for specific applications, additives such as degradation and stabilization aids, fillers, processing aids, anti-fogging agents, flame retardants, blowing agents and pigments are often used [68]. Production additives are usually added in a post-reaction step before the extruder. Additives do not directly alter the structure, but can have an influence on the phase equilibria such as the gas solubility. However, not only the consideration of these additives in phase equilibrium calculations would considerably increase the models complexity, but also the type and amount of additives that was admixed to the polymer is usually unknown.

2.2.2 Structure

The structure of polyolefins is defined by its branching degree and molecular weight. Depending on the synthesis both properties are no uniform values but distributions. The model of this work does not take into account the distributions of branching and molecular weight, hence all systems are considered as monodisperse.

Branching

Branched polyethylene is often synthesized as copolymer from ethylene and longer alkenes forming LLDPE. In this case the branching is usually expressed as the mole fraction of the co-monomer x_{Co} in the copolymer. From this the branching degree br per 1000 C-atoms can be determined by the following conversion:

$$\frac{br}{1000C} = 1000\frac{x_{Co}}{2 + n_{br}x_{Co}} \tag{2.15}$$

where n_{br} is the length of the branch (not the length of the co-monomer). In eq. 2.15, x_{Co} refers to ethylene as main monomer. Some refer the mole fraction of co-monomer to one carbon group, for example the group around Mandelkern [69]. If so, the 2 in the denominator becomes 1. The second term of the denominator comes from the fact that the branching degree refers to all C-atoms including those being inside the branch. If the weight fraction of the co-monomer w_{Co} is given, the conversion is as follows:

$$\frac{br}{1000C} = 1000\frac{w_{Co}}{n_{br} + 2} \tag{2.16}$$

Sometimes the branching degree is referred to 1000 backbone C-atoms br^{BB}, which can be converted by the following equation:

$$\frac{br}{1000C} = \frac{br^{BB}}{1 + n_{br}br^{BB}/1000} \tag{2.17}$$

Molecular weight

The molecular weight of a polymer represents its chain length, whereby the segment number can be determined by the following formula:

$$M = \frac{M_N}{M_{CH_2}} \tag{2.18}$$

whereby M_N is the number average molecular weight of the polymer and M_{CH_2} is the molecular weight of one segment, being a carbon atom with bonded H-atoms. Since the molecular weight is generally a distribution, polyethylene samples usually have a non-uniform polydispersity index (PDI), which is given as follows:

$$PDI = \frac{M_W}{M_N} \tag{2.19}$$

whereby M_W is the weight average molecular weight.

2.2.3 Crystallinity

The properties of polyolefins strongly depend on the crystallinity of the sample. Due to the macroscopic nature of polymers, polyolefins never crystallize completely, it may vary from almost zero to over 90 % [5]. So almost every polyolefin lies somewhere between the limiting amorphous and the limiting crystalline case. To investigate this semi-crystalline behaviour, figure 2.4 shows the specific volume of polyethylene over the temperature.
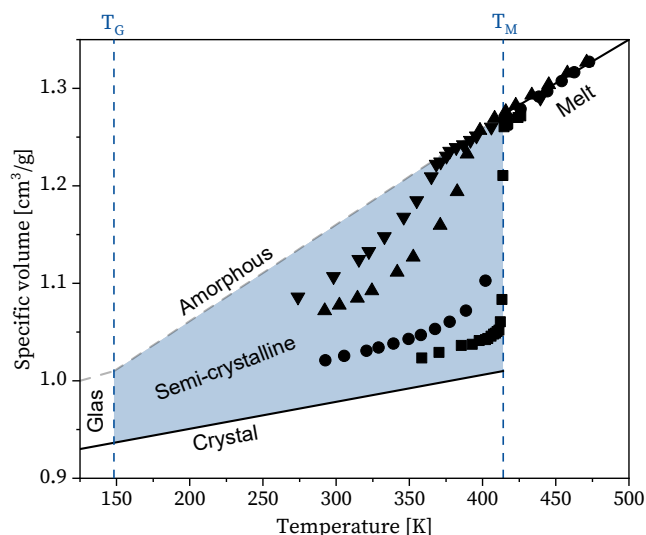
Figure 2.4: Volume-temperature relationship for polyethylene at 1 bar. T_G denotes the glas transition temperature while T_M is the equilibrium melting temperature for linear polyethylene. Experimental data of two linear samples (squares [70], circles [71]) and two branched samples (triangles up [71], triangles down [72]).

Let's start on the very right side of the graph, were the polymer is completely molten. By cooling down the system, the specific volume decreases approximately linearly until the melting temperature is reached. Here, smaller molecules would be in equilibrium with the solid, e.g. crystal phase, and the volume would decrease sharply at the melting temperature. However, polymers show a different behaviour. Depending on the architecture and the crystallization conditions, an either more or less sharp drop is discerned at the melting point, but the volume levels off and the pure crystal state is never reached. While in the molten state, different samples, varying in architecture, show very similar behaviour, they strongly differ in the amount of crystallinity below the melting point. In fact, branched samples follow the approximately linear curve of the melt below the equilibrium melting temperature of linear polyethylene, being a metastable liquid. Only below a significant lower temperature they show a soft decrease in specific volume and stay at a low degree of crystallinity. This is why Flory introduces the term melting transition instead of melting point [5].

When decreasing the temperature even further, another change in specific volume occurs: the glass transition. This is metastable thermodynamic state in which the polymer is in a kinetically locked state in contrast to the semi-crystalline state [73]. Yet, the glassy state is itself a complex matter and will not be the focus of this work.

Another message can be discerned from figure 2.4: Both branched samples in figure 2.4 are LDPE samples of comparable molecular weight, however, the crystallinity differs significantly. It appears that the classification into LDPE, HDPE and LLDPE is not sufficient enough, a more detailed look on the relationship between semi-crystallinity and architecture is necessary. For this, figure 2.5 shows a schematic representation of semi-crystalline polyethylene.
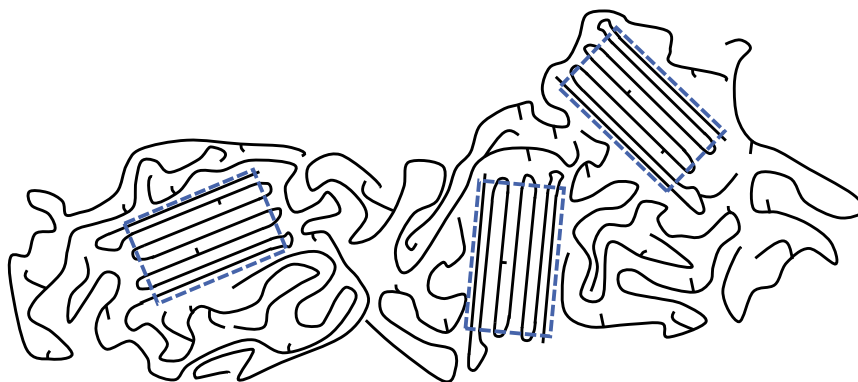
Figure 2.5: Schematic representation of a semi-crystalline scheme polyethylene having crystalline and amorphous domains. Blue boxes frame the crystalline domains.

The semi-crystalline state is divided into amorphous and crystalline domains, where the latter is usually shorter than the length of a polymer chain [5]. A polymer chain can exit one crystalline domain, meander through the intermediate amorphous region and enter either the same or another crystal. The question now arises as to what influences the degree of crystallinity. Generally, irregularities are excluded from a crystal domain, which include branches and chain ends. When talking about branches, it has to be distinguished between long-chain branching and short-chain branching. There is no clear separation between both terms, however, commonly branches having up to ten C-atoms are called short-chain branches, while long-chain branches can contain thousands of units [65]. The influence of long-chain branches on the crystallinity is of minor importance, since their number is relatively small [74]. LDPE, for example, usually has alongside approx. $20\,\mathrm{br}\,1000\mathrm{C}^{-1}$ to $25\,\mathrm{br}\,1000\mathrm{C}^{-1}$ short-chain branches $0.5\,\mathrm{br}\,1000\mathrm{C}^{-1}$ to $1\,\mathrm{br}\,1000\mathrm{C}^{-1}$ long-chain branches, HDPE and LLDPE even less [65]. Moreover, due to their length they can be incorporated in the crystal domains. Short-chain branches on the other side strongly decrease the crystallinity, as they would disrupt the aligned crystal state of the polymer chains [75–82], with the result that a sample having about $80\,\mathrm{br}\,1000\mathrm{C}^{-1}$ is almost

completely amorphous [82]. While branches are generally inhibited to be part of the crystal lattice, methyl branches due to their size can be accommodated in the crystal domain to a certain amount [81–86], whereby the amount of methyl branches in the lattice is estimated to approx. 20 % to 30 %.

The influence of the length of the short-chain branches on the crystallinity is of lesser importance compared to the degree of branching; however, longer branches appear to decrease the crystallinity to a higher extend [75, 77, 87]. The distribution of branches on the carbon backbone, which depends on the catalyst, does not influence the crystallinity to a distinct amount, an average branching degree appears to be an adequate factor [88].

2.3 Gas solubility

In this section, influencing parameters on the gas solubility in molten polyethylene will be addressed such as pressure, temperature, the polymers architecture as well as co-/ and anti-sorption effects. Subsequently, the solubility in semi-crystalline systems is outlined.

Molten polyethylene

The gas solubility in molten polyethylene generally increases with increasing system pressure. At very low solubilities, the relation between pressure and solubility is proportional and can be approximated with the Henry-law. For higher solubilities this relationship is not valid any more, resulting in a non-linear solubility. The isotherm eventually will pass into a liquid-liquid demixing by condensation of the gas. Light gases, on the other hand, may be in a supercritical state under the conditions of the experiment.

The influence of the temperature on the gas solubility is more complex. Most gas-polymer system show a decreasing solubility with increasing temperature. However, there are cases where the opposite is true, which is called inverse solubility [89]. This behaviour depends on the type of gas and on the conditions, e.g. temperature and pressure. For gases having a low critical temperature [27, 45, 90], the inverse solubility behaviour can be found at temperatures and pressure, where gas solubility plays a role. Nitrogen consistently shows an inverse solubility behaviour [33, 45, 91–94], while some experimental data of methane show an inverse solubility behaviour [32, 95] while others do not [33]. Experimental data of ethylene in polyethylene show a normal behaviour, e.g. decreasing solubility with increasing temperature. However, Maloney & Prausnitz [89], predicted with help of a free-volume theory a turnover point to inverse solubility behaviour at approx. 500 bar inside a temperature range of 150 °C and 300 °C. With help of

the Prigogine-Flory theory, Bogdanovic et al. [96] found out, that the turnover point to inverse solubility behaviour shifts towards lower pressure when increasing the temperature.

The influence of the molecular weight, i.e. the length of the polymer chains, on the gas solubility was addressed by several publications [24–29]. Generally, the gas solubility decreases with increasing molecular weight, which is due to the increasing asymmetry between the solvent and solute [25, 26]. The effect is especially pronounced at low molecular weights. Heuer et al. [24] studied the solubility of ethylene in polyethylenes and found significant differences between samples having M_N=0.476 kg mol^{-1}, 1.25 kg mol^{-1}, 1.94 kg mol^{-1} and 19.5 kg mol^{-1}. Gas solubility measurements of ethylene from Kobyakov et al. [97] with polyethylene samples having M_N=3.65 kg mol^{-1} and 4.95 kg mol^{-1} show a slightly higher solubility for the lower molecular weight. Meyer & Blanks [98] found no significant difference in the solubility of iso-butane in polyethylene having M_N=14 kg mol^{-1} and M_N=18 kg mol^{-1}. It is generally assumed, that the effect of the molecular weight is negligible from ca. 5 kg mol^{-1} [25, 99] to 10 kg mol^{-1} [27] onwards.

Literature regarding the branching influence on the gas solubility in melt are scarce and have to be conducted carefully in order to exclude other effects, such as molecular weight distribution, additives or buoyancy correction. Newman & Prausnitz [100] and Schreiber et al. [30] conducted gas-liquid chromatography experiments of hydrocarbons in different hydrocarbon-polyethylene-copolymers and calculated interaction parameters, which were mainly independent of the copolymer type and content. Banaszak et al. [101] carried out molecular simulations of the system ethylene in polyethylene observing the same effect. Moreover, Novak et al. [31] measured the solubility of ethylene and 1-hexene in molten polyethylene having different branching degrees, finding no significant influence of branching on the solubility. Measurements from Lundberg et al. [32, 33] of two different samples of unknown molar mass having different branching degree, showed very similar methane solubilities. Zimmermann et al. [36] measured the solubility of carbon dioxide in two different branched molten polyethylene samples finding no significant influence of chain branching. Furthermore, Cernia & Mancini [34] and Ehrlich [35] investigated high pressure phase equilibria of polyethylene and ethylene and stated that the effect of the polymers branching is negligible. On the contrary, Hasan et al. [37] measured the solubility of CO_2 in a branched and a linear polypropylene sample and claimed a significant dependence of the solubility on the chain branching.

When addressing ternary systems containing two gases solved in polyethylene, more complex relationships have to be considered. Measurements of these system consistently showed co-/ and anti-solvent effects [31, 41, 102–109], e.g. larger gases appear to enhance the solubility

of smaller gases, while at the same time, the smaller gases inhibit the sorption of bigger gases. These two counteracting effects may not completely cancel each other out and lead to a lower overall solubility compared to the sum of the pure cases [31, 109]. The experimental evidence has been confirmed by molecular simulations [101] and PC-SAFT modeling [39].

Semi-crystalline polyethylene

Semi-crystalline systems in general have already been classified in section 2.2.3. In the course of this, the influence of temperature and the polymers structure was addressed. Thus, when discussing the influence of these variables on the gas solubility in semi-crystalline systems, care must be taken as the relations interfere with each other. To give an example: The gas solubility in molten polyethylene usually decreases with increasing temperature, i.e. for semi-crystalline systems in the amorphous domains of the polymer. At the same time, the crystalline decreases with increasing temperature, which leads to an increasing gas solubility. So two counteracting effects take place when increasing the temperature in a semi-crystalline system.

Generally, the sorption takes place solely in the amorphous domains, since the crystalline domains do not provide enough space for the gas molecules to penetrate the defect free perfect crystal [46, 47]. This is why the solubility of gases in the semi-crystalline polymers w_{Gas}^{ScPol} is usually referred to the amorphous phase, which gives w_{Gas}^{AmPol} [110]:

$$w_{Gas}^{AmPol} = w_{Gas}^{ScPol} \cdot (1 - \alpha) \tag{2.20}$$

whereby α is the degree of crystallinity. Nevertheless, eq. (2.20) overestimates the solubility. This is due to the fact that the crystallinity has a strong influence on the gas solubility in the amorphous domains, by applying a stress on the amorphous domains [111, 112]. This leads to a decreasing solubility with increasing crystallinity. Methods, how to address this phenomenon are discussed in the following section.

3 State of the art

This chapter gives an overview of what has already been done in the literature. First, approaches for the description of gas solubilities in semi-crystalline polyolefins are introduced. Afterwards experimental methods, that are essential for the interpretation of experimental data are presented including the determination of the polyolefin's structure, its crystallinity and the gas solubility. Finally, experimental data is shown, starting with the crystallinity. Pure component data of gases are collected and discussed for the parametrization of LCT-parameters. Subsequently, gas solubility data are given and especially the data in molten polyethylene is discussed in detail, since appropriate measurements for the adjustment of the binary interaction parameter have to be chosen.

3.1 Approaches for modelling gas solubilities

A number of approaches exist in literature considering the complex modelling of gas solubilities in semi-crystalline polymers. Generally, the sorption takes place solely in the amorphous domains, since the crystalline domains do not provide enough space for the gas molecules to penetrate the defect free perfect crystal [46, 47]. However, even when restricting gas molecules from the crystalline phase, models strongly overestimate the solubility in the amorphous domains. This discrepancy is addressed by various approaches which can be categorized into elastic, non-equilibrium and intrinsic pressure approaches.

3.1.1 Elastic approach

Michael & Hausslein [55] introduced an approach for the decrease of solubility in the semi-crystalline state by adding an elastic term to the solvent activity:

$$\ln(a_1) = \ln(v_1) + v_2 + \mathcal{X} v_2^2 + \frac{\langle a \rangle_0^2 f \rho v_1 v_2^{1/2}}{M_c} \tag{3.1}$$

where the first three terms denote the activity of a solvent in an amorphous polymer according to the FH-theory [42, 43], the last terms comes from the Flory-Rehner equation [113]. v_1 and v_2 are the volumes of the solvent respectively the polymer while $\mathcal{X}$ is the FH-parameter. $\langle a \rangle_0^2$ denotes the mean end-to-end distance of the unrestricted polymer chain, ρ the unswollen polymer density and M_c the length of the elastic segments. The mass fraction of elastically effective chains is given by f, which can be adjusted to experimental data [55]. These elastically affected tie segments apply an elastic force and therefore constrain the swelling of the amorphous domains of the semi-crystalline polymer. The original approach was coupled with group contribution approaches [114], the PC-SAFT equation of state [101] and the Saku-Wu-Prausnitz-EoS [108] and was able to describe the lowered solubility in semi-crystalline polyethylene. The results showed that the parameter f was strongly influenced by the polymer type [114], but only slightly by the type of solved gas [101, 108] and to a certain extend on the temperature [108]. The latter publication [108] was proceeded by an approach where the melting temperature was fitted while assuming a fixed value for f [115]. With this, experimental could be described satisfactorily. This again shows that the reduced solubility is mainly due to the polymer properties, which likewise manifests itself in the melting temperature.

3.1.2 Non-equilibrium approach

Doghieri & Sarti [56] introduced the non-equilibrium lattice fluids (NELF) approach, originally developed for glassy polymers, taking the expression for the Gibbs free energy from Sanchez & Lacombe [44] as basis. However, the density of the polymer is an internal state variable, which no longer depends on the EoS. The altered density therefore takes account for the constraints induced by the crystalline domains. Yet, the determination of this amorphous density remains a challenging task, which is sometimes used as adjustable parameter. Bonavoglia et al. [116] applied the NELF approach to semi-crystalline systems, whereby the amorphous density was calculated from swelling measurements of the corresponding gas-polymer system. This approach revealed high agreement with experimental sorption data. However, preliminary experiments are necessary which are often not available.

3.1.3 Intrinsic pressure approach

Based on the works of Memari et al. [117, 118], Minelli & De Angelis [47] introduced an additional pressure representing the isotropic stress, which acts from the crystalline on the amorphous domain. This constraint pressure p^c is added to the equilibrium pressure p, which prevails in

the gas phase, which alters eq. 2.6 as follows:

$$\mu_i^G(T, p, \Phi_i^G) = \mu_i^L(T, p + p^c, \Phi_i^L)$$ (3.2)

Minelli & De Angelis [47] implemented the constraint pressure into the SL-EoS [44] and used it as an adjustable parameter. The binary interaction parameter k_{ij}, accounting for the gas-polymer interactions was adjusted to the solubility of the corresponding gas in molten polyethylene. With this, they [47] were able to model gas solubilities successfully. The findings showed that the constraint pressure is a function of the crystallinity: The higher the crystallinity, the higher the isotropic stress onto the amorphous phase. With vanishing crystallinity, e.g. by increasing the temperature, p^c turns zero. At the same time the sort of solved gas appears to have a moderate influence of the constraint pressure as well.

Fischlschweiger et al. [46] enhanced the proposed constraint model from Minelli & De Angelis [47] by coupling the SL-EoS with continuum mechanics. With this, a constraint pressure, a so-called eigen pressure can be predicted from mechanical arguments, namely the compression modulus K and the shear modulus G:

$$p^{eigen} = \left[K \left(\frac{\phi_v^{L,0} - \phi_v^L}{\phi_v^{L,0}} \right) + 2.5G \right] \alpha$$ (3.3)

Eq. (3.3) is a modification of the original equation [46], which uses the SL-EoS. For using the LCT, the corresponding quantities $\phi_v^{L,0}$ and ϕ_v^L are inserted, representing the void segment fractions of the pure liquid phase and the liquid mixture respectively while α depicts the crystallinity. The first term in eq. (3.3) represents the elastic mismatch coming from the isotropic imbalance between the amorphous and the crystalline phase due to gas sorption. Since it involves the void segment fraction of the liquid mixture, it depends on the amount and sort of sorbed gas, which in turn is a function of the temperature. The second term in eq. (3.3) represents the initial formation of micro void expansion due to island like clusters formed when first gas molecules enter the polymer matrix [46]. To account for the temperature dependence of the eigen pressure, Zimmermann et al. [119] extended the prediction by use of temperature dependent mechanical properties.

3.2 Experimental techniques

This section covers experimental methods used for determining the polymers architecture, the crystallinity and the gas solubility. The listing does not raise any claim to completeness, but is intended to deliver an overview which is useful for discussions in the further work.

3.2.1 Structural Characterization

Although being at a first glance a very simple molecule, polyethylene shows various unique architectures, which strongly affect its properties. This is why the characterization of the polymers structure is of central importance. However, most detectors are not especially sensitive to carbon and hydrogen atoms, which makes the characterization challenging [1]. Key parameters for the structural characterization of polyolefines are the molecular weight distribution, short-chain branching (SCB) distribution and long-chain branching (LCB) [120].

In contrast to smaller molecules, polymers are generally not uniform in their length. This is why the chain length or molecular mass is not a single value, but a distribution. The high temperature gel permeation chromatography (GPC) or size exclusion chromatography is a useful tool for the determination of the molecular weight distribution [1]. GPC is a liquid chromatography, where the column is packed with microporous gel particles, having small pores through which the molecules have to pass. The separation takes place according to the hydrodynamic volume of the molecules in solution, which leads to a different elution time depending on the size of the molecules [121]. Preliminary to the characterization, a calibration with known standards have to be carried out, in order to relate the elution time with the molecular mass [121]. Due to the polydisperse nature of polymers, a molecular weight distribution is obtained, from which moments such as the number average molecular weight M_N or the weight average molecular weight M_W can be deduced [1].

The most widely used technique for the determination of SCB is nuclear magnetic resonance (NMR) spectroscopy. In ^{13}C NMR, electromagnetic radiation interacts with the nuclear spin of C-atoms, which give a specific resonance depending on the type of bonding [1]. A spectrum is obtained, with peaks proportional to the number of contributing nuclei, which are assigned to the groups -CH-, -CH$_2$- and -CH$_3$, for example [122]. With NMR, not just the SCB content but also the length of side chains can be determined. Another possibility to access information about SCB are crystallization-based techniques such as temperature rising elution fractionation (TREF), crystallization analysis fractionation (CRYSTAF) and crystallization elution frac-

tionation (CEF). With these methods, the distribution, but not the length of side chains can be deduced [1]. Long-chain branching (LCB) influences rheological properties such as the viscosity and melt strength and can be detected for example by GPC combined with light scattering [1]. However, since the relative number of LCB compared to SCB is negligible and the influence of LCB on crystallinity and solubility is of minor importance [74], the focus is on SCB.

3.2.2 Crystallinity

The determination of the crystalline fraction of a semi-crystalline polymer can be accessed by various methods, including differential scanning calorimetry, density differences, x-ray scattering as well as raman, infrared and nuclear magnetic resonance spectroscopy [121], which will be discussed briefly.

Differential scanning calorimetry

On of the most used technique for the determination of the crystalline content is differential scanning calorimetry (DSC), providing an effective technique, that requires only a small amount of sample [123]. Here, the mass-based content of crystallinity is calculated via the ratio of the samples heat of fusion and the heat of fusion of the purely crystalline polymer. By analysing the area under the melting peak, the heat of fusion is obtained. One challenge is the availability of the purely crystalline heat of fusion, often done by extrapolation [124]. Care must be taken when drawing the baseline for determining the area so as to take into account the change in heat capacity during melting [125]. For an accurate calculation of the crystallinity, the temperature dependence of the purely crystalline heat of fusion has to be considered, especially for polymers where melting occurs over a wide temperature range [125].

Density difference

The determination of the crystallinity by density difference is based on the assumption of a two phase mixture of amorphous and crystalline phases, each with its own density. With help of the density of the completely amorphous and the completely crystal phase, the crystalline content can be calculated by a mass balance [125]. However, the distinction of these phases is challenging and especially the completely amorphous density varies with temperature and the thermo-mechanical history of the sample [121]. Moreover, some loosely ordered non-crystalline areas will have an impact on the degree on crystallinity which cannot be considered by this two-phase-model [121].

X-ray scattering

X-ray scattering is normally used to characterize the structure of a semi-crystalline sample. By analyzing the intensity of the thin diffraction peaks, corresponding to crystals as well as the very diffuse peak corresponding to the amorphous phase, the amount of crystallinity can be determined [121]. However, the calculation of the crystallinity from x-ray scattering relies on a number of assumptions, introducing inaccuracies, such as incoherent scattering and the crystalline disorder [126]. Moreover, the interpretation of the X-ray diffractogram is challenging [126].

Spectroscopy

Spectroscopic methods rely on the absorption of electromagnetic radiation over various wavelengths, revealing the structure and morphology of the sample. Infrared spectroscopy and Raman spectroscopy involves the excitation of bonds of specific atomic groupings, which differ, if they are part of a crystal or part of the amorphous phase [125]. Nuclear magnetic resonance spectroscopy, which is also used for the determination of chain branching, uses the fact, that electromagnetic radiation interacts with the nuclear spin of atoms or isotopes. Different resonances can be attributed to disordered amorphous carbon atoms or carbon atoms, which are embedded in an ordered crystalline region [125]. As with X-ray-scattering, the exact attribution of bands to crystalline and amorphous regions is challenging and leads to inaccuracies [127].

3.2.3 Gas solubility

In the last decades there have been evolved numerous methods for determining solvent solubilities in polymers. The majority of those techniques can be grouped into four categories, based on its measurement type: Gravimetric methods, piezoelectric methods, manometric methods and chromatography.

Gravimetric

The gravimetric methods cover measurement techniques, were the amount of gas is determined by direct weighting of the sample. One way to achieve this, is by a quartz spring balance, were the extension of a spring, proportional to the weight of load is measured by a cathetometer. A preliminary calibration relates the elongation of the spring to the solubility using Hooke's Law. Since McBain [128] is one of the first, using this technique it is commonly referred as McBain balance. The method is suitable for highly soluble gases. However, the sensitivity is

low, which is why it is not applicable sorption of light gases [129]. Moreover, the temperature dependence of the spring constant has to be addressed.

An electronic microbalance provides a method having a very high sensitivity, making it suitable for the sorption of light gases [129]. Since less amount of specimen has to be used, the experiment time is considerably lower. Electronic microbalances, which are frequently used, make use of a beam on which the polymer sample is placed, whereby its imbalance is monitored either by a variable gain amplifier or by a current in a coil that changes while the beam is within a permanent magnet field. Figure 3.1 shows a schematic electronic microbalance from Cahn. The measurement is usually operated under constant temperature and pressure and the gas is purified from any condensable component via columns of charcoal and silica gel [130]. Some electronic microbalances use a weight decay technique, were in a first step, polymer sample and gas is put in the chamber until equilibrium is reached. Subsequently the chamber is depressurized, the sample is placed in the microbalance and the weight loss is monitored [131].
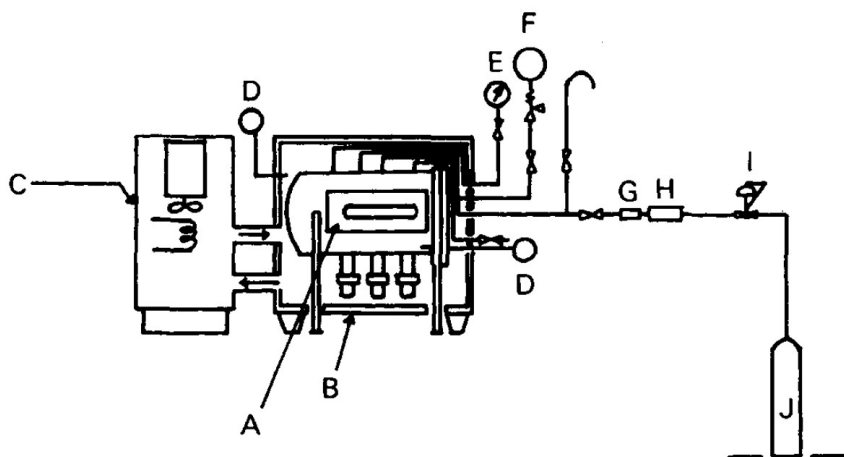
Figure 3.1: Electronic microbalance from Cahn, adopted from [130]: (A) pressure chamber containing electronic microbalance, (B) thermostatically controlled air bath, (C) temperature controller, (D) thermometer, (E) manometer, (F) safety valve, (G) flow meter, (H) columns of active charcoal and silica gel, (I) pressure regulator and (J) sample gas cylinder.

A magnetic suspension balance has similar advantages compared to electronic microbalances such as high sensitivity and short experiment time but is more suitable to high pressure and temperature areas due to a contactless weight measurement. For this, the sample holder is attached to a free-floating suspension magnet, transmitting magnetic attraction force to the electronic balance, which is isolated from the sorption chamber [131].

Gravimetric methods offer a high sensitivity for a broad range of gases and polymers. However, there is one problematic aspect of gravimetric methods, which needs to be considered:

During the experiment, solved gas particles will result in a sample swelling, leading to a higher volume. At the same time, a high pressure leads to a shrinkage effect of the sample. Therefore a buoyancy correction has to be implemented, as the specific volume of the sample increases and the specific volume of the gas atmosphere decreases when elevating the pressure. A swelling correction is often done by photometric methods or by the use of an equation of state, whereby the latter can lead to huge inaccuracies.

Piezoelectric

The quartz crystal microbalance uses the piezoelectric effect to measure gas solubilities. The oscillation frequency of the vibration of a piezoelectric crystal, which is coated by a thin film polymer is measured by electronic methods [129]. Preliminary calibration of uncoated and coated piezoelectric crystal are required. Due to the small amount of sample, which is necessary for the polymer film, this method requires short experiment time. Moreover very small weight changes can be measured resulting in a high sensitivity. However, the preparation of the thin polymer films on the crystal is challenging.

Manometric

Manometric methods require the measurement of the pressure or the volume of the gas sorbed in the polymer film [129], while the temperature is predefined. A volume calibration of the chamber has to be carried out in advance of the experiment. Once the polymer is in equilibrium with the gas, all the ambient gas has to be removed from the chamber, without withdrawing sorbed gas from the polymer and the pressure or volume change is monitored [131].

Another frequently used manometric technique is the pressure decay method (figure 3.2). In this method, the polymer sample is place into the chamber with predefined temperature and volume. Afterwards, a preheated gas in introduced into the chamber while monitoring the pressure change [132]. One challenge is the compensation of the polymer swelling due to gas sorption. Furthermore, the pressure decay technique requires a long measurement time, since a large amount of sample has to be used [131].

Chromatography

Apart from the static methods mentioned above, chromatography offers a dynamic measurement technique. Here, the sample is not in a static equilibrium with the gas, but the sorption of a gas flow is measured. This is done by measuring the retention time of the mobile phase (gas) over the static phase (polymer) and comparing it to the retention time of a carrier gas [129].
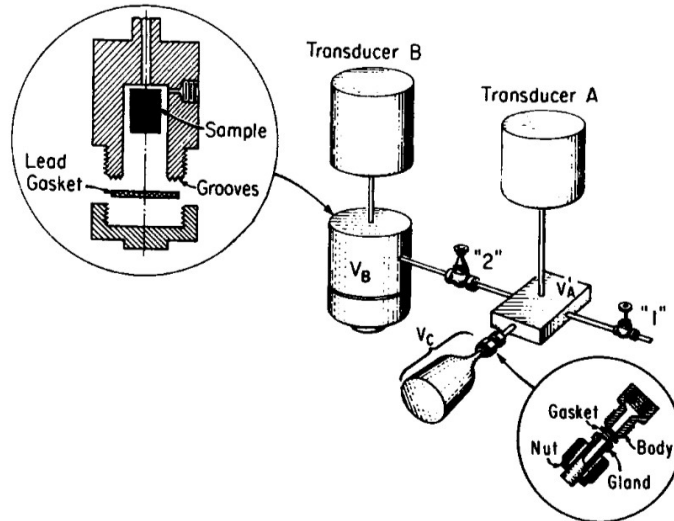
Figure 3.2: Pressure decay method with 2 sorption cells, adopted from [132]: V_A and V_B are two sorption cells while V_C is the reference reservoir. The pressure of each cell is measured by the transducers.

While the experiment time is shorter compared to static methods, the sorption measurements can be limited by diffusion [131]. Furthermore, the solubility of the carrier gas (mostly nitrogen or helium) influences the solubility of the desired gas, which leads to inaccuracies.

Other methods

All the above mentioned methods involve an in situ measurement, e. g. the amount of dissolved gas is directly or indirectly determined in the sorption chamber. Some experimenters rely on a ex situ technique were the sample with sorbed gas is measured externally either gravimetrically or manometrically. This simplifies the measurement setup but introduces inaccuracies due to a potential partial desorption while the sample is measured ex situ at ambient pressure [133].

Another possible way to access experimental solubility data is via diffusion measurements. Here, the diffusion and permeation can be measured by a static flow of the desired gas through a thin polymer membrane [131], which is then converted to the solubility.

3.3 Experimental data

3.3.1 Crystallinity

Figure 3.3 shows an overview of the existing experimental data [31, 75, 77, 87, 134–153] regarding the crystallinity of branched polyethylene measured by differential scanning calorimetry. Experimental data involving other experimental methods were excluded, due to questionable assumptions when determining the crystallinity and to keep the observations comparable.

The experimental data are underlying a clearly recognisable trend where the maximal crystallinity of unbranched polyethylene lies around 60 % to 70 % while completely amorphous polyethylene lies in the region of around $100 \, br \, 1000C^{-1}$ to $150 \, br \, 1000C^{-1}$. The measurements may be divided into two groups: Slowly cooled samples having cooling rates between $20 \, K \, min^{-1}$ and cooling in oil baths as well as quenched samples having maximal possible cooling rates. Moreover, the target temperature at which the samples are cooled is an issue as well as the heating rate of the DSC measurement. Furthermore, amount and type of branching as well as molar mass, molar mass distribution and polymerization method have to be considered. Since information on the above-mentioned influencing variables is often lacking and, in addition, all the variables are interrelated, it is difficult to extract clear dependencies from Figure 3.3.

No significant trend can be observed regarding the type of cooling, although the target temperature of the quenched samples is mostly lower, which makes a comparison challenging. It appears that the crystallinity decreases as the branch length increases, when comparing different samples [75, 77, 87, 141, 142, 151] with ethyl-, butyl- and hexyl branched polyethylene at the same crystallization conditions. At the same time, Voigt-Martin et al. [140] measured no significant difference between ethyl- and hexyl-branched samples.

Methyl-branches can be accommodated in the crystalline lattice up to a certain extend [81, 82, 85, 86, 154] which may explain why these systems [134–136] (black symbols in Figure 3.3) exhibit a slightly higher crystallinity than the general trend.

The same superposition of influences appears when studying the effect of the target temperature on crystallinity. There seems to be a trend of higher crystallinities at lower temperatures, when considering experimental data having apart from that similar conditions. Androsch et al. [148] measured the crystallinity of two hexyl-branched samples at −40 °C and 20 °C exhibiting a significant higher crystallinity for the lower temperature. Also methyl-branched samples from Han-Adebekun et al. [136] at 40 °C have a significantly lower crystallinity than methyl-branched measurements from Ver Strate [135] at room temperature.
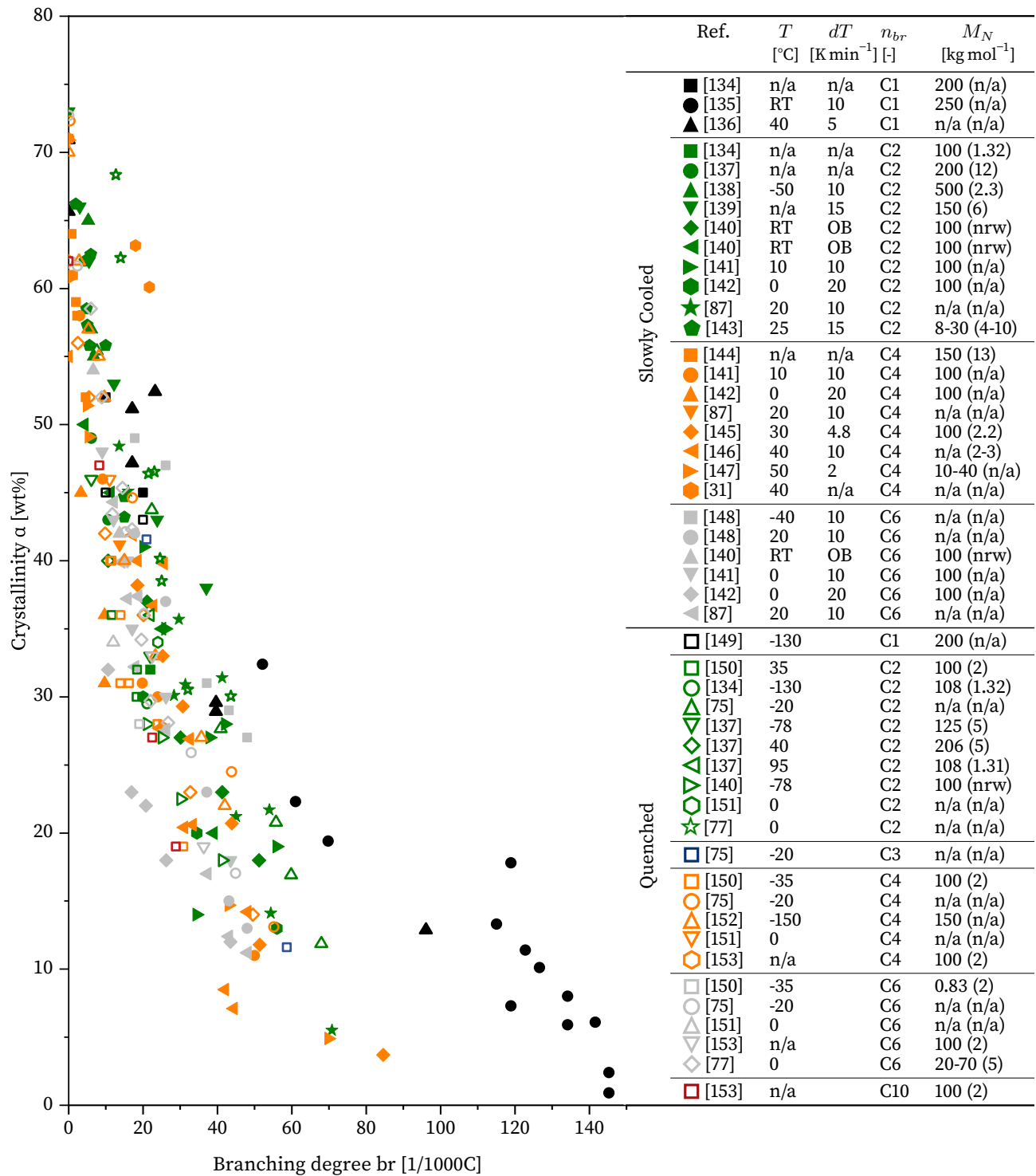
Figure 3.3: Experimental data concerning the crystallinity of polyethylene as a function of the branching degree br for slowly cooled and quenched samples. All experiments were conducted via differential scanning calorimetry with a heating rate of $2\,\mathrm{K\,min^{-1}}$ to $20\,\mathrm{K\,min^{-1}}$. The colour of the symbols denotes the type of branching. For slowly cooled samples the first temperature indicates the target temperature (RT denotes room temperature) while the second one (dT) is the cooling rate (OB denotes oil bath). For quenched samples, just the target temperature is given. n_{br} represents the length of the branch, where C1 is methyl, C2 is ethyl, etc. M_N indicates the molar mass with a molecular weight distribution given in brackets where available. nrw denotes a narrow distribution while n/a means not available.

On the other hand, quenched samples in figure 3.3 show no large scatter across the crystallinity, although the range of target temperature (−130 °C to 95 °C) is much higher than for the slowly cooled systems (−50 °C to 30 °C).

3.3.2 Pure component data of gases

For characterizing the gases with adjustable parameters, appropriate experimental data has to be used. Wherever possible, experimental data from the Perry's Chemical Engineers' handbook [155] was used, due to the consistent quality and the wide temperature range of data, which applied to n-butane, nitrogen, methane, carbon dioxide, ethylene and propylene. For n-pentane and n-hexane, data from Young [156] respectively and Reynolds [157] were used, since just these sets of data were available, covered a wide temperature range and were consistent. For heptane, data from Reynolds [157] and McMicking [158] was found. Since the data from the latter scatters, especially the saturated volumes, and covers a smaller temperature range, data from Reynolds [157] was used.
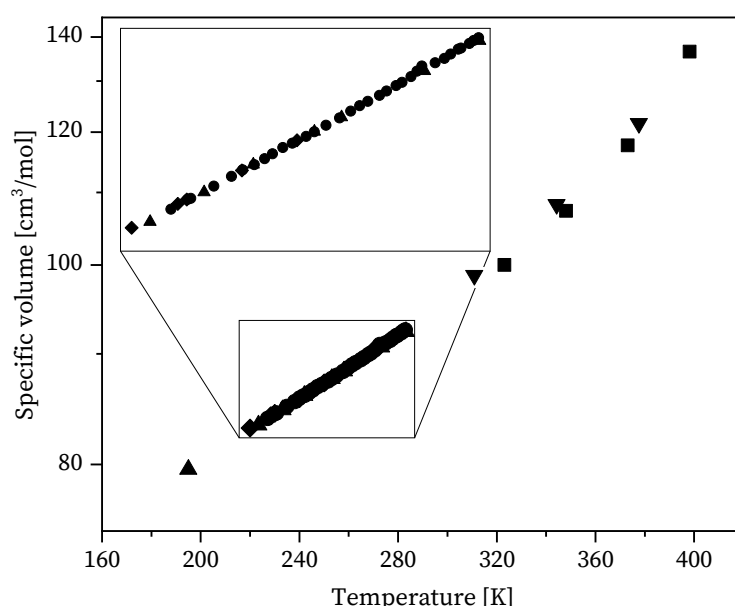
Figure 3.4: Experimental data considering saturated liquid volumes of 1-butene from [159] (squares), [160] (circles), [161] (triangles up), [162] (triangles down), [163] (diamonds). A magnification shows the medium-temperature range in more detail.

Multiple experimental data sets exist for 1-butene [159–164]. For the vapour pressure, combined data sets from Luo & Miller [163] and Ihmels et al. [164] are used in order to cover a wide temperature range. Measurements of saturated liquid volumes from 1-butene, which are shown in figure 3.4 are numerous, but cover just small temperature ranges and are partly inconsistent. Data from Beattie & Marple [159] is significantly lower compared to the other data

sets. Combined saturated liquid volume data from Wackher et al. [161] and Olds et al. [162] are used, which are in agreement with other experimental data [160, 163] and cover a sufficient temperature range.

For 1-hexene, plenty measurements of both vapour pressure and saturated liquid density can be found in literature [155, 165–171] (see Betken et al. [172] for an extensive research), whereby the vapour pressure was mainly measured in the temperature range below 378 K. Below this temperature, there is a high consistency between sets of experimental data [166–169] except those of Perry [155] (figure 3.5). Only Ma et al. [165] conducted measurements beyond 378 K, but the vapour pressure is significantly higher when comparing the trend of other experimental data [166–169]. For comparison, an empirical regression from Perry [155] (with data compiled from [171] and [173]) is included in figure 3.5, which is in perfect agreement with other sets of experimental data [166–169], but is clearly below experimental data from Ma et al. [165]. For this reason, combined vapour pressure data from Camin & Rossini [167] and Moodley [168] are used, which are in agreement with other experimental data [166, 169] and cover a sufficient temperature range. Saturated volume data were taken from Kireev [170] due to the wide temperature range.
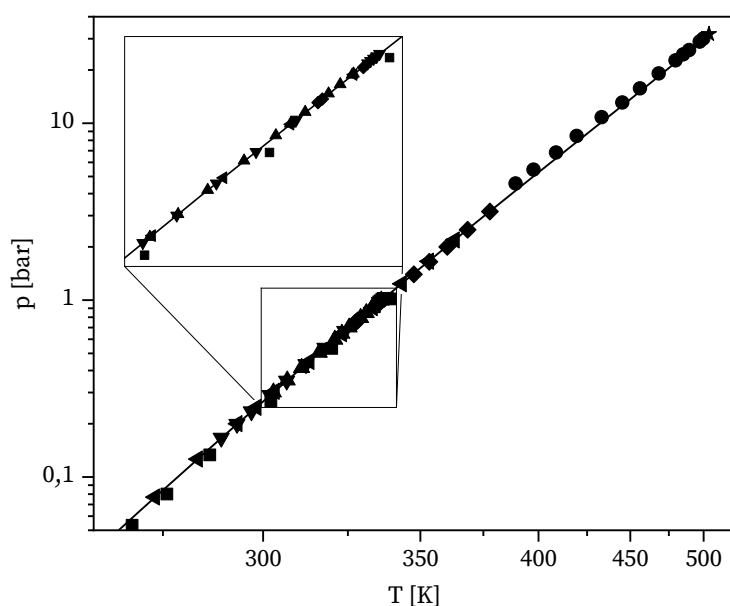
Figure 3.5: Experimental data considering vapour pressure of 1-hexene from [155] (squares), [165] (circles), [166] (triangles up), [167] (triangles down), [168] (diamonds), [169] (triangles left). The star denotes the critical point from [165], while the line is an empirical regression from [155]. A magnification shows the medium-temperature range in more detail.

3.3.3 Gas solubility

In this subsection, an overview of gas solubility measurements in PE is given, including single- and multi-gas systems. Subsequently, single gas solubility in amorphous PE is discussed in more detail, since an adequate data set has to be chosen for the adjustment of the k_{ij}. Finally, solubility data in semi-crystalline PE is discussed, which are used in the further work for the comparison with the model results. Table 3.1 shows data, that is available in literature.

Table 3.1: Experimental data of binary and ternary gas solubility in amorphous and semi-crystalline PE.

Gas	State	M_N	br	Method	Ref.
		$[\mathrm{kg\,mol^{-1}}]$	$[\mathrm{br\,1000C^{-1}}]$		
	am	28	n/a	c	[34]
	am	31.7	n/a	b	[92]
	am	16.6	25.5	d	[27, 89]
	am	1.94	31.8	a	[24]
	am	100-140	n/a	a	[40]
	am	2.2	n/a	c	[174]
	am	3.65	n/a	n/a	[97]
	am	n/a	n/a	d	[175][f]
	am	12.6/16.7	n/a	a	[176]
	am	1.1	n/a	c	[177]
	am	250	n/a	c	[178]
Ethylene	sc	11.5-40.4	n/a	a	[106]
	sc	n/a	n/a	c	[179]
	sc	n/a	n/a	a	[180]
	sc	n/a	n/a	a	[102]
	sc	24.6/27.2	n/a	a	[109]
	sc	20-60	30-50	c	[108, 115]
	sc	34.3	n/a	a	[40]
	sc	n/a	0-20	a	[31]
	sc	12.6/16.7	n/a	a	[176]
	sc	38/45	21/26	e	[153][f]
	sc	n/a	n/a	c	[181]
	sc	6.4-35.3	n/a	a	[182]
	sc	n/a	n/a	c	[107]

Gas	State	M_N	br	Method	Ref.
		[kg mol^{-1}]	[br 1000C^{-1}]		
1-propene	am	1.94	31.8	a	[24]
	sc	15.8-27.5	n/a	c	[183]
	sc	n/a	n/a	c	[184]
1-butene	am	1.94	31.8	a	[24]
	am	1.94	31.8	a	[104]
	sc	20-60	n/a	c	[108, 115]
	sc	n/a	n/a	a	[185]
	sc	18	n/a	a	[186]
1-hexene	am	n/a	n/a	a	[101][f]
	am	n/a	n/a	a	[31]
	am	10-50	n/a	d	[187][f]
	sc	n/a	n/a	a	[31]
	sc	100	9-104	a	[188]
	sc	24.6/27.2	n/a	a	[109]
	sc	10-35	n/a	a	[189]
	sc	20-60	n/a	c	[108, 115]
	sc	n/a	n/a	a	[185]
	sc	11.5-40.4	n/a	a	[106]
	sc	11.7-57.1	n/a	a/c	[114]
	sc	6.4-35.3	n/a	a	[182]
	sc	10-30	n/a	a	[190]
Carbon dioxide	am	15.2	n/a	a	[191]
	am	8.16	n/a	c	[45]
	am	n/a	n/a	c	[94]
	am	n/a	n/a	c	[192][f]
	am	n/a	n/a	a	[193]
	am	11.3/4.5	22/5	a	[36]
	sc	n/a	n/a	a	[194]
	sc	n/a	n/a	d	[195]
	sc	n/a	n/a	c	[196]
	sc	n/a	n/a	a	[197]

Gas	State	M_N [kg mol^{-1}]	br [br 1000C^{-1}]	Method	Ref.
Carbon dioxide	sc	38/45	21/26	e	[153][f]
	sc	n/a	n/a	a	[198]
	sc	26-400	1.5-300	e	[111, 112][f]
	sc	15/33	2/16	e	[199][f]
	sc	11.3/4.5	22/5	a	[36]
Nitrogen	am	n/a	n/a	c	[32]
	am	0.80	n/a	a	[91]
	am	8.16	n/a	c	[45]
	am	350	n/a	a	[200]
	am	n/a	n/a	a	[93]
	am	31.7	n/a	b	[92]
	am	n/a	n/a	c	[94]
	sc	n/a	n/a	a	[194]
	sc	n/a	n/a	a	[102]
	sc	15/33	2/16	e	[199][f]
	sc	26-400	1.5-300	e	[111, 112][f]
	sc	n/a	n/a	c	[196]
	sc	38/45	21/26	e	[153][f]
Methane	am	n/a	n/a	c	[32]
	am	n/a	n/a	b	[95]
	am	n/a	n/a	c	[33]
	sc	n/a	n/a	d	[195]
	sc	n/a	n/a	a	[197]
	sc	n/a	n/a	a	[102]
	sc	38/45	21/26	e	[153][f]
	sc	26-400	1.5-300	e	[111, 112][f]
n-butane	am	n/a	n/a	c	[201]
	sc	18.0	n/a	a	[186]
	sc	24.9	n/a	a	[202]

Gas	State	M_N [kg mol^{-1}]	br [br 1000C^{-1}]	Method	Ref.
n-pentane	am	76	n/a	c	[203]
	sc	24.9	n/a	a	[202]
n-hexane	am	16.6	n/a	d	[27][f]
	am	35.0	n/a	d	[100][f]
	am	n/a	n/a	d	[204]
	sc	n/a	n/a	c	[181]
	sc	20-60	30-50	c	[108, 115]
	sc	24.9	n/a	a	[202]
	sc	26.4	n/a	d	[205]
	sc	n/a	n/a	a	[206]
	sc	n/a	n/a	a	[207]
	sc	n/a	n/a	c	[107]
n-heptane	am	10-50	n/a	d	[175][f]
	sc	24.9	n/a	a	[202]
	sc	13.7	n/a	a	[208]
Ethylene + 1-butene	am	1.94	31.8	a	[24, 104]
Ethylene + 1-propene	sc	n/a	n/a	a	[209]
Ethylene + 1-hexene	sc	25.6	n/a	a	[106]
	sc	24.6	n/a	a	[109]
	sc	n/a	0-20	a	[31]

a: gravimetric type, b: piezoelectric type, c: manometric type, d: chromatographic type,
e: indirect via diffusion and permeation measurement, f: Henry-coefficients at ambient pressure.

3.3.3.1 Melt

Figure 3.6 shows experimental data considering the solubility of ethylene in molten polyethylene at temperatures ranging from 393.15 K to 573.15 K. Although, a general trend can be observed many of the experimental data sets are scattered and inconsistent.
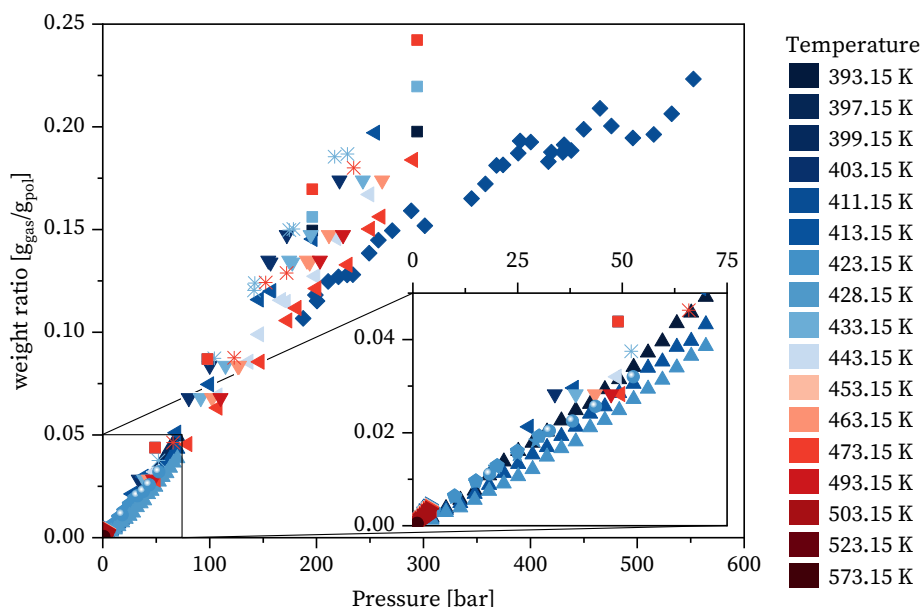
Figure 3.6: Solubility of ethylene in molten polyethylene at different temperatures. Experimental data from [97] (squares), [27] (circles), [92] (triangles up), [174] (triangles down), [89] (diamonds), [24] (triangles left), [176] (triangles right and hexagons), [40] (stars), [31] (pentagons), [178] (spheres) and [177] (stars). A magnification shows the low-pressure range in more detail.

All data sets show an increasing solubility with decreasing temperature except those of Kobyakov et al. [97]. The original publication is not accessible and the data is obtained from Wohlfahrts handbook [133], so the experimental method cannot be examined. Due to the contradicting temperature influence, data from Kobyakov [97] is excluded from adjustment. Spahl & Luft [177] conducted measurements using a manometric technique after sample-taking with low molecular polyethylene having a molar mass of $1.1 \, kg \, mol^{-1}$. Due to the low molecular weight and hence short chains (around 80) of this sample, these data points show significant higher solubility compared to all other measurements. Low-pressure experiments from Jiang et al. [176] using an electronic microbalance and Maloney & Prausnitz [27] using inverse chromatography were excluded as well, in order to cover a wide range of solubility. Since in the further course of the work, predictions are made for significant lower temperatures, temperature dependent interaction parameters are used were possible. For this reason, experimental data from Novak et al. [31] and Chmelar et al. [40], who used a magnetic suspension balance, as well as data from Davis et al. [178], who used a dual chamber pressure decay technique, and

Maloney & Prausnitz [89], measured by inverse chromatography, are excluded from the adjustment, since they just measured a single isotherm. However, these data sets can be used for the validation of other experimental data. While the experimental measured solubility from Cheng & Bonner [92] via a piezoelectric quartz crystal microbalance is significant lower compared to other sets in the same pressure range, solubility data from Rousseaux et al. [174], measured monometrically, is higher compared to other data sets. The measured solubility isotherms from Heuer et al. [24], determined by averaged gravimetrical and manometrical means after sample-taking, are mainly consistent with single isotherms from Novak et al [31], Chmelar et al. [40] and Davis et al. [178]. Moreover, Heuer et el. [24] characterized the used polyethylene in terms of molecular weight and branching, required as input variable for the LCT. For these reasons, experimental data from Heuer et al. [24] are used for the adjustment of the binary interaction parameter.

For the solubility of propylene in molten polyethylene, just data from Heuer et al. [24] were found in literature. The data, including three isotherms were measured over a wide pressure range, seems consistent. Additionally, the polyethylene sample was well characterized in terms of branching and molar mass.

Heuer et al. [24] also conducted measurements of 1-butene in well characterized molten polyethylene at three different temperatures by averaging gravimetric and manometric means after sample-taking (figure 3.7).
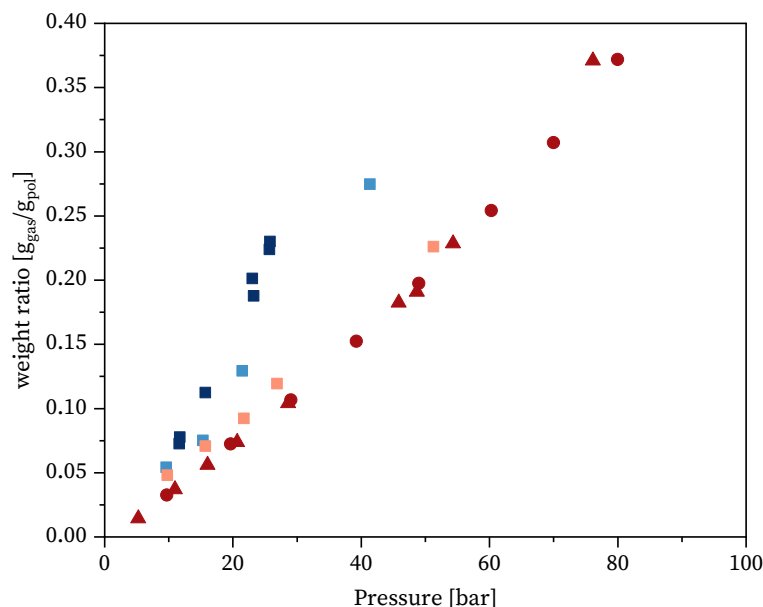
Figure 3.7: Solubility of 1-butene in molten polyethylene at 428.15 K (dark blue), 438.15 K, 468.15 K and 493.15 K. Experimental data from [24] (squares), [104] (circles), [133] (triangles up).

The same working group around Wohlfahrt published in a proceeding publication a data set at 493.15 K [104]. Additionally, Wohlfahrt published another set of data at 493.15 K in his book [133], referring to his own publication [104]. Although the data at 493.15 K is consistent, it appears to be another set of experiments. The three lower isotherms seem consistent, with the exception of two data points at high pressure (around 40 bar and 50 bar respectively), which appear to have a lower solubility compared to the other isotherms. The three lower isotherms are used for adjusting the binary interaction parameter while the single isotherms at 493.15 K from the other publications [104, 133] are just used for validation as it is not sure whether it is the same polymer sample and the same measurement run.

Solubility experiments of 1-hexene in molten polyethylene are scarce. Only Novak et al. [31] measured a single isotherm at 423.15 K by a magnetic suspension balance. Although measurements for the calculation of the Henry-coefficients were conducted at different temperatures [101, 187], those measurements were carried out at very low-pressures below 1 bar. This is why the data set from Novak et al. [31] is used for adjusting the binary interaction parameter.

Experimental data considering the solubility of carbon dioxide in molten polyethylene is shown in figure 3.8. Data from Chaudhary & Johns [193], measured by a magnetic suspension balance, is scattered and contradicts all other experimental data sets. Furthermore, extrapolation of the isotherms to zero pressure does not go through the origin.

Figure 3.8: Solubility of carbon dioxide in molten polyethylene at different temperatures. Experimental data from [193] (squares), [191] (circles), [36] (triangles up), [45] (diamonds) and [94] (triangles left).

The solubility was also investigated by Areerat et al. [191] by a magnetic suspension balance and Sato et al. [45] by the pressure decay technique, both measuring three isotherms over a wide pressure range. Durrill & Griskey [94] measured a single isotherm in the low-pressure area via the pressure decay technique. The data sets from Areerat et al. [191] and Sato et al. [45] are mainly consistent. However, the data from Sato et al. [45] is slightly scattered, while data from Areerat et al. [191] seems consistent and is in well agreement with low-pressure data from Durrill & Griskey [94]. Due to that reason, measurements from Areerat et al. [191] are used for the adjustment of the binary interaction parameter.

Measurements of nitrogen in molten polyethylene are shown in figure 3.9. A consistent inverse solubility over the whole pressure range of experiments can be observed, where the solubility is increasing with increasing temperature. The only exception is the data from Azimi [200], which not only show an opposing temperature dependence, but also a significantly higher solubility than all other measurements. The swelling correction was done by an equation of state, which may introduce inaccuracies [200]. Moreover, no experiment time is given in the publication [200]. However, neither explains the large deviation and the inconsistent temperature influence. Plenty of experiments were conducted in low-pressure area up to 150 bar, whereby data from Lee & Flumerfelt [91], measured by chromatography, is considerable higher compared to all other data, which is probably due to the low molecular weight of $0.8\,\mathrm{kg\,mol^{-1}}$.
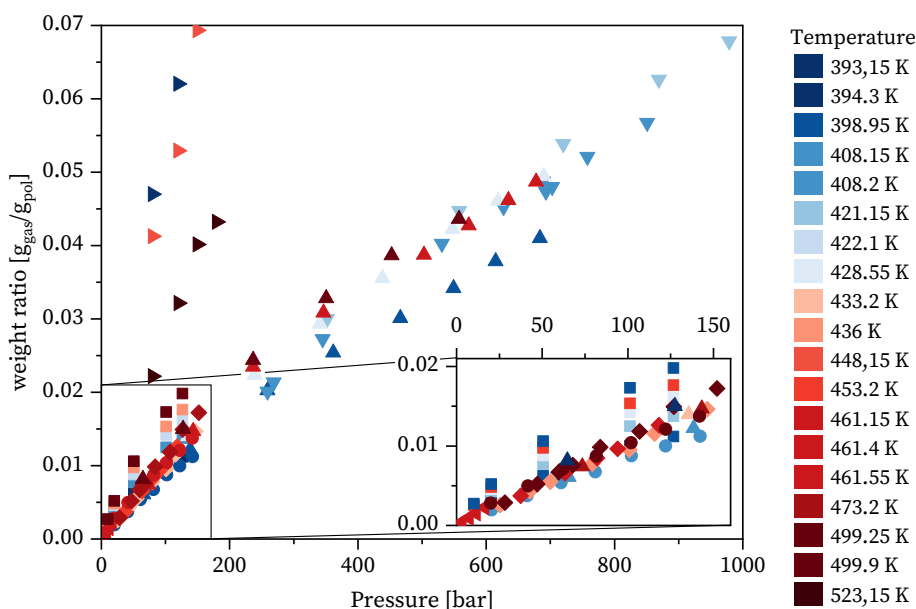
Figure 3.9: Solubility of nitrogen in molten polyethylene at different temperatures. Experimental data from [91] (squares), [92] (circles), [33] (triangles up), [93] (triangles down), [45] (diamonds), [94] (triangles left) and [200] (triangles right). A magnification shows the low-pressure range in more detail.

Experimental data from Cheng & Bonner [92], measured via a piezoelectric quartz crystal microbalance, as well as from Sato et al. [45] and Durrill & Griskey [94], measured by the pressure decay technique, only cover the low-pressure range. The measurements from Lundberg [33], determined by pressure decay technique cover a wide pressure range and are consistent with data from Cheng & Bonner [92] and Sato et al. [45] in the low-pressure range as well as Atkinson [93] in the middle pressure range. At pressures higher than 500 bar, solubilities from Lundberg [33] are slightly higher compared to Atkinsons [93]. This could be due the reason that Atkinsons [93] measured the gas solubility externally after sample-taking. In high-pressure experiments, the subsequent pressure drop could lead to partial desorption before the exact amount of dissolved gas is determined. At the same time, data from Lundberg [33] show a slightly scattered behaviour at higher pressure (>500 bar). This could be due to the novelty and experimental difficulties of the method at that time. Furthermore, swelling behaviour of the sample was ignored [32], which could introduce inaccuracies especially at high pressure. Nonetheless, Lundbergs measurements [33] show high consistency over a wide pressure range, which is why this data set until 500 bar is used for the parametrization.

The solubility of methane in molten polyethylene, which is shown in figure 3.10, was investigated by Lundberg et al. [32], Lundberg [33] and Bonner [95]. The different isotherms, covering a temperature range from about 400 K to 500 K, lie very close to each other, which makes it difficult to observe a temperature dependence.
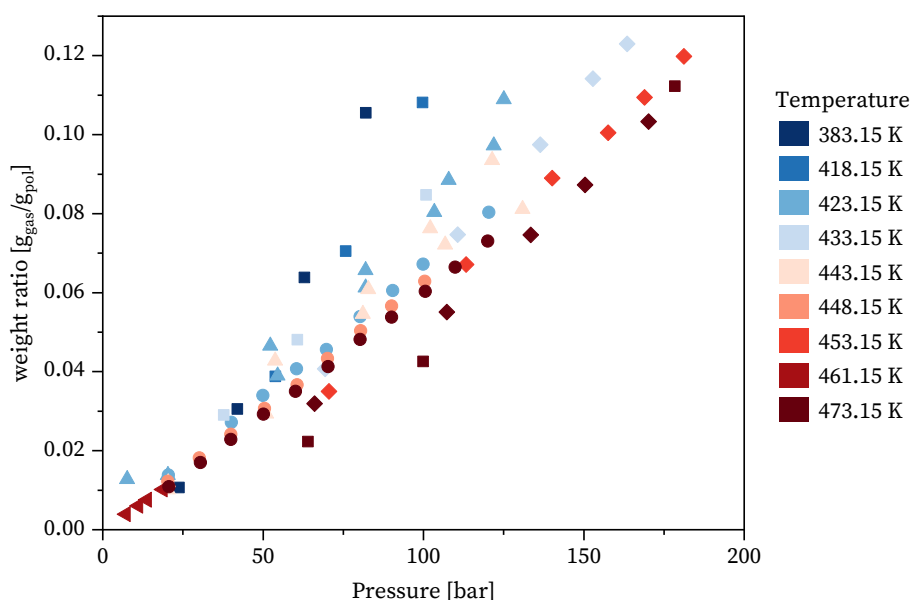

Figure 3.10: Solubility of methane in molten polyethylene at different temperatures. Experimental data from [32] (squares), [95] (circles) and [33] (triangles up).

Lundberg et al. [32] conducted measurements via pressure decay technique mainly at high pressures exhibiting an inverse solubility effect, e.g. an increasing solubility with rising temperature [32]. Lundberg [33] published experimental data of another polyethylene sample in the lower and medium pressure range being partly consistent with the data published in the earlier work [32]. Here, the inverse solubility effect is discernible for the higher temperatures, while the lowest isotherm (413.19 K) still results in the highest solubility. Experimental data from Bonner [95], measured via a piezoelectric quartz spring microbalance in the low-pressure area, revealed an inverse solubility effect as well. Considering all the experimental data sets, there could be a point of change to inverse solubility behaviour in the range of experimental data. Only one isotherm from Lundberg [33] shows normal solubility behaviour, which could also be due to experimental uncertainty, since the isotherm lie very close to each other. Due to the consistent data from Lundberg et al. [32], this data set is used for the adjustment of k_{ij}.

For the system n-butane in molten polyethylene, only measurements Wang et al. [201] via pressure decay technique were found in literature. Four isotherms over a wide pressure were published, providing a well data basis for the adjustment of the binary interaction parameter. The solubility of n-pentane in molten polyethylene was only investigated by Surana et al. [203] by the pressure decay technique, measuring two isotherms over a wide range of pressure.

Figure 3.11 shows experimental data considering the solubility of n-hexane in polyethylene. Brockmeier et al. [204] conducted experiments up to a pressure of 5 bar using a chromatographic technique. Measurements from Newman [100] and Maloney [27] at 1 atm, measured by chromatography as well and among themselves consistent, show significantly higher solubility. Additionally, the curvature of the isotherms from Brockmeier et al. [204] seem unlikely for a gas having such a high critical point. The isotherms of n-pentane, 1-hexene and n-heptane for example start to bend upwards significantly at around 5 bar. Reasons for this could be the novelty and experimental difficulties of the method at that time, which was already pointed out by Bonner et al. [210]. This is accompanied by the fact the gas chromatography measurement is a dynamic method, were the system is not in a static equilibrium. Moreover, a carrier gas has to be used, which is nitrogen in this case. Although the solubility of nitrogen is considerably lower compared to n-hexane, nitrogen acts as a so-called anti-solvent lowering the solubility of n-hexane, especially towards higher pressure, which may lead to the missing upwards bend. For this reason, with the exception of the lowest temperature, the data set of Maloney [27] is used for the adjustment of the binary interaction parameter. The data point at 397.15 K is excluded, since at this temperature, partial crystallization cannot be ruled out. For the solubility

of n-heptane in molten polyethylene, only data from Liu et al. [187] at 1 bar, measured by chromatography, was found in literature which is used for the adjustment of k_{ij}.
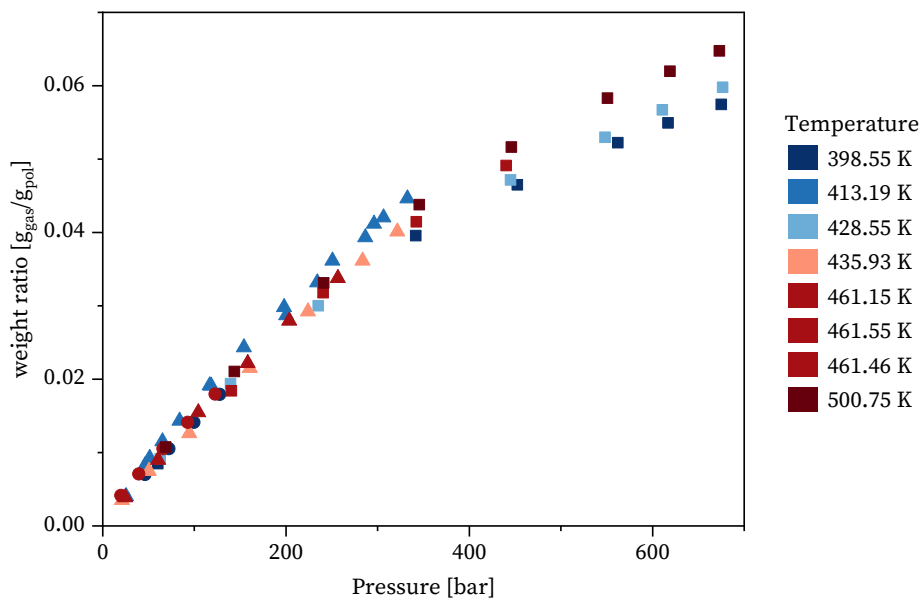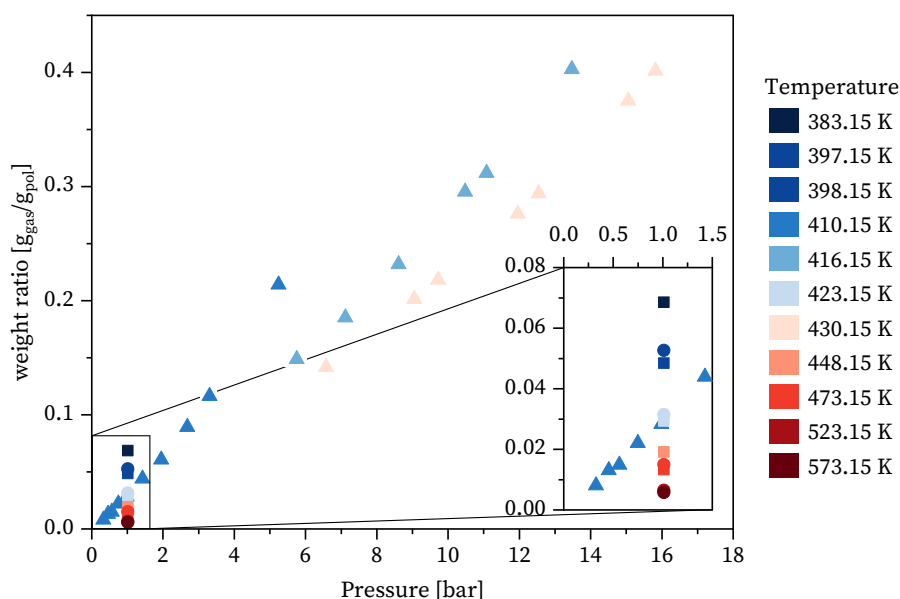

Figure 3.11: Solubility of n-hexane in molten polyethylene at different temperatures. Experimental data from [100] (squares), [27] (circles) and [204] (triangles up). A magnification shows the low-pressure range in more detail.

Ternary systems, including the solubility of two gases in molten polyethylene, were investigated by Wohlfahrt et al. [104] for ethylene and 1-butene, where a sample was withdrawn from the reactor and the solubility was determined by gravimetrical and manometrical means. The solubility of ethylene and 1-hexene was measured by Novak et al. [31] via magnetic suspension balance.

3.3.3.2 Semi-crystalline

Experimental data considering the solubility of gases in semi-crystalline polyethylene are numerous (table 3.1). Since information about the polymers architecture are necessary for both the combined CPP/FCA approach and the LCT, experimental data with insufficient characterization in terms of branching are mainly excluded. The group around Greenhalgh [108] published well characterized data including the solubility of ethylene, 1-butene, 1-hexene and n-hexane [108, 115], measured by the pressure-decay method. The solubility of ethylene was also investigated by Jiang et al. [176] via an electronic microbalance while Jin et al. [188] measured the solubility of 1-hexene with help of a quartz spring balance. Measurements of Yao et al. [183] via pressure-decay method and Castro et al. [202] via electronic microbalance are not characterized in terms of the branching degree but provide information about the crystallinity

and its measurement conditions, which can serve as indirect information about the polymers architecture.

The solubility of small gases in differently branched polyethylene samples at ambient pressure was investigated by Michaels & Bixler [111, 112] and Laguna et al. [153] for carbon dioxide, nitrogen and methane as well as for carbon dioxide and nitrogen by Pino et al. [199]. Here, the solubility was indirectly determined by the measurement of the diffusion and permeation via time-lag-method and subsequently converted to the solubility.

The ternary system of ethylene and 1-hexene in semi-crystalline polyethylene was investigated both by Moore et al. [106] and by Sun et al. [109] via an electronic microbalance. Yoon et al. [209] conducted measurements of ethylene and 1-propene in polyethylene via a quartz spring balance.

4 Theoretical approach

In this chapter, the theoretical framework of this work is outlined. First, the Lattice-Cluster-Theory as well as the Car-Parking-Problem and Flory's co-polymer approach for branching are presented. Finally, numerical implementations of this work will be given.

4.1 Lattice-Cluster-Theory

For the sake of lucidity, the free energy of mixing ΔF is expressed following Langenbach et al. [49] in form of a series expansion according to the lattice coordination number z, the segment fraction of void lattice sites ϕ_v and the segment fraction of occupied lattice sites ϕ_{occ}:

$$
-\frac{\Delta F(M_i, N_{k,i}, z, \Phi_i, \phi_v, T, \epsilon_{ij})}{N_l k_b T} = \frac{\Delta S^{MF}(M_i, z, \Phi_i, \phi_v)}{N_l k_b}
$$
$$
+ \sum_{a=0}^{2} \sum_{b=0}^{2} \sum_{c=1}^{6} (k_b T)^{-a} z^{a-2} \phi_v^b \phi_{occ}^c C_{abc}(M_i, \tilde{N}_{k,i}, \Phi_i, \epsilon_{ij})
\tag{4.1}
$$

whereby the mean field contribution ΔS^{MF} is equivalent to Flory's [11] entropy of mixing in the athermal limit in eq. (2.8) and equals:

$$
\frac{\Delta S^{MF}(M_i, z, \Phi_i, \phi_v)}{N_l k_b} = -\phi_v \ln(\phi_v) - \sum_{i \neq v}^{n} \frac{\phi_i}{M_i} \ln(\phi_i)
\tag{4.2}
$$

At that, C_{abc} are the extended mean field contributions, Φ_i is the segment fraction of component i without consideration of void lattice sites, ϕ_i the segment fraction of component i considering the void lattice sites and T is the temperature. Φ_i is calculated as follows:

$$
\Phi_i = \frac{\phi_i}{1 - \phi_v}
\tag{4.3}
$$

while the reduced architecture coefficients $\tilde{N}_{k,i}$ read:

$$
\tilde{N}_{k,i} = \frac{N_{k,i}}{M_i}
\tag{4.4}
$$

The contributions to the athermal limit packing entropy of the C_{0bc} arise due to excluded volume constraints and are calculated for a n-component mixture as follows [48, 49]:

$$C_{001} = \sum_{\kappa \neq v}^{n} (-2\tilde{N}_{1,\kappa}\tilde{N}_{3,\kappa} - \tilde{N}_{2,\kappa}^2 - z\tilde{N}_{1,\kappa}^2 - \frac{2}{3}\tilde{N}_{1,\kappa}^3 + 4\tilde{N}_{1,\kappa}^2\tilde{N}_{2,\kappa} - 2\tilde{N}_{1,\kappa}^4)\Phi_\kappa \tag{4.5}$$

$$C_{002} = \sum_{\kappa \neq v}^{n} \sum_{\lambda \neq v}^{n} (2\tilde{N}_{1,\kappa}\tilde{N}_{3,\lambda} + 2\tilde{N}_{2,\kappa}\tilde{N}_{2,\lambda} + z\tilde{N}_{1,\kappa}\tilde{N}_{1,\lambda})\Phi_\kappa\Phi_\lambda \tag{4.6}$$

$$C_{003} = \sum_{\kappa \neq v}^{n} \sum_{\lambda \neq v}^{n} \sum_{\mu \neq v}^{n} (\frac{2}{3}\tilde{N}_{1,\kappa}\tilde{N}_{1,\lambda}\tilde{N}_{1,\mu} - 4\tilde{N}_{2,\kappa}\tilde{N}_{1,\lambda}\tilde{N}_{1,\mu})\Phi_\kappa\Phi_\lambda\Phi_\mu \tag{4.7}$$

$$C_{004} = \sum_{\kappa \neq v}^{n} \sum_{\lambda \neq v}^{n} \sum_{\mu \neq v}^{n} \sum_{\eta \neq v}^{n} (2\tilde{N}_{1,\kappa}\tilde{N}_{1,\lambda}\tilde{N}_{1,\mu}\tilde{N}_{1,\eta})\Phi_\kappa\Phi_\lambda\Phi_\mu\Phi_\eta \tag{4.8}$$

The energy contributions of first-order C_{1bc} and second-order C_{2bc} contain the dispersion energies ϵ_{ii} and $\Delta\epsilon_{ij}$ taking account of the attracting interactions. For a n-component mixture, C_{1bc} reads [48, 49]:

$$C_{102} = \sum_{\kappa \neq v}^{n} \sum_{\lambda \neq v}^{n} c_1^{\kappa\lambda}(2, -1, 0, 0, 2, 2, -1)\Delta\epsilon_{\kappa\lambda}\Phi_\kappa\Phi_\lambda \tag{4.9}$$

$$C_{103} = \sum_{\kappa \neq v}^{n} \sum_{\lambda \neq v}^{n} \sum_{\mu \neq v}^{n} c_1^{\kappa\lambda}(-2, 2, -1, -1, -1, -1, 0)\Phi_\kappa\Delta\epsilon_{\lambda\mu}\Phi_\lambda\Phi_\mu \tag{4.10}$$

$$C_{104} = \sum_{\kappa \neq v}^{n} \sum_{\lambda \neq v}^{n} \sum_{\mu \neq v}^{n} \sum_{\eta \neq v}^{n} c_1^{\kappa\lambda}(2, -1, 0, 2, 0, 0, 0)\Delta\epsilon_{\mu\eta}\Phi_\kappa\Phi_\lambda\Phi_\mu\Phi_\eta \tag{4.11}$$

$$C_{105} = \sum_{\kappa \neq v}^{n} \sum_{\lambda \neq v}^{n} \sum_{\mu \neq v}^{n} \sum_{\eta \neq v}^{n} \sum_{\omega \neq v}^{n} c_1^{\kappa\lambda}(0, 0, 0, -1, 0, 0, 0)\Delta\epsilon_{\eta\omega}\Phi_\kappa\Phi_\lambda\Phi_\mu\Phi_\eta\Phi_\omega \tag{4.12}$$

$$C_{111} = \sum_{\kappa \neq v}^{n} c_1^{\kappa\lambda}(0, 0, 0, 0, 2, 2, -2)\epsilon_{\kappa\kappa}\Phi_\kappa \tag{4.13}$$

$$C_{112} = \sum_{\kappa \neq v}^{n} \sum_{\lambda \neq v}^{n} c_1^{\kappa\lambda}(-2, 2, -1, 0, -2, -2, 0)\epsilon_{\kappa\kappa}\Phi_\kappa\Phi_\lambda \tag{4.14}$$

$$C_{113} = \sum_{\kappa \neq v}^{n} \sum_{\lambda \neq v}^{n} \sum_{\mu \neq v}^{n} c_1^{\kappa\lambda}(4, -2, 0, 2, 0, 0, 0)\epsilon_{\kappa\kappa}\Phi_\kappa\Phi_\lambda\Phi_\mu \tag{4.15}$$

$$C_{114} = \sum_{\kappa \neq v}^{n} \sum_{\lambda \neq v}^{n} \sum_{\mu \neq v}^{n} \sum_{\eta \neq v}^{n} c_1^{\kappa\lambda}(0, 0, 0, -2, 0, 0, 0)\epsilon_{\eta\eta}\Phi_\kappa\Phi_\lambda\Phi_\mu\Phi_\eta \tag{4.16}$$

$$\begin{aligned} c_1^{\kappa\lambda}(a, b, c, d, e, f, g) &= a\tilde{N}_{1,\kappa}\tilde{N}_{2,\lambda} + b\tilde{N}_{1,\kappa}\tilde{N}_{1,\lambda} + c\tilde{N}_{1,\lambda}\tilde{N}_{2,\kappa} \\ &\quad + d\tilde{N}_{1,\kappa}\tilde{N}_{1,\lambda}\tilde{N}_{1,\mu} + e\frac{z}{2}\tilde{N}_{1,\kappa} + f\frac{1}{2}\tilde{N}_{3,\kappa} + g\frac{z^2}{4} \end{aligned} \tag{4.17}$$

The second-order energy contributions C_{2bc} depend on the product of two dispersion energies and are calculated for a n-component mixture as follows [48, 49]:

$$C_{202} = \sum_{\kappa \neq \upsilon}^{n} \sum_{\lambda \neq \upsilon}^{n} c_2^{\kappa\lambda}(1, -2, 1, 1) \Delta\epsilon_{\kappa\lambda}^2 \Phi_\kappa \Phi_\lambda \tag{4.18}$$

$$C_{203} = \sum_{\kappa \neq \upsilon}^{n} \sum_{\lambda \neq \upsilon}^{n} \sum_{\mu \neq \upsilon}^{n} \Bigg[c_2^{\kappa\lambda}(-4, 4, -2, -2) \Delta\epsilon_{\kappa\lambda}\Delta\epsilon_{\lambda\mu} + c_2^{\kappa\lambda}(0, 1, 0, 0)\Delta\epsilon_{\lambda\mu}^2$$
$$+ c_2^{\kappa 0}(-2, 0, 0, 0)\Delta\epsilon_{\kappa\mu}\Delta\epsilon_{\lambda\mu} + c_2^{\kappa 0}(0, 2, -1, 0)\Delta\epsilon_{\kappa\lambda}\Delta\epsilon_{\kappa\mu} \Bigg]\Phi_\kappa \Phi_\lambda \Phi_\mu \tag{4.19}$$

$$C_{204} = \sum_{\kappa \neq \upsilon}^{n} \sum_{\lambda \neq \upsilon}^{n} \sum_{\mu \neq \upsilon}^{n} \sum_{\eta \neq \upsilon}^{n} \Bigg[c_2^{\kappa\lambda}(2, -4, 2, 1)\Delta\epsilon_{\kappa\lambda}\Delta\epsilon_{\mu\eta} + c_2^{\kappa\lambda}(4, -4, 1, 0)\Delta\epsilon_{\lambda\mu}\Delta\epsilon_{\mu\eta}$$
$$+ c_2^{\kappa\lambda}(2, 0, 0, 0\Delta\epsilon_{\kappa\mu}\Delta\epsilon_{\kappa\eta}) + c_2^{\kappa\lambda}(4, 0, 0, 0)\Delta\epsilon_{\kappa\mu}\Delta\epsilon_{\lambda\eta} \Bigg]\Phi_\kappa \Phi_\lambda \Phi_\mu \Phi_\eta \tag{4.20}$$

$$C_{205} = \sum_{\kappa \neq \upsilon}^{n} \sum_{\lambda \neq \upsilon}^{n} \sum_{\mu \neq \upsilon}^{n} \sum_{\eta \neq \upsilon}^{n} \sum_{\omega \neq \upsilon}^{n} \Bigg[c_2^{\kappa\lambda}(-8, 3, -1, 0)\Delta\epsilon_{\lambda\mu}\Delta\epsilon_{\eta\omega}$$
$$+ c_2^{\kappa\lambda}(-2, 0, 0, 0)\Delta\epsilon_{\mu\eta}\Delta\epsilon_{\eta\omega} \Bigg]\Phi_\kappa \Phi_\lambda \Phi_\mu \Phi_\eta \Phi_\omega \tag{4.21}$$

$$C_{206} = \sum_{\kappa \neq \upsilon}^{n} \sum_{\lambda \neq \upsilon}^{n} \sum_{\mu \neq \upsilon}^{n} \sum_{\eta \neq \upsilon}^{n} \sum_{\omega \neq \upsilon}^{n} \sum_{\tau \neq \upsilon}^{n} c_2^{\kappa\lambda}(3, 0, 0, 0)\Delta\epsilon_{\mu\eta}\Delta\epsilon_{\omega\tau} \Phi_\kappa \Phi_\lambda \Phi_\mu \Phi_\eta \Phi_\omega \Phi_\tau \tag{4.22}$$

$$C_{211} = \sum_{\kappa \neq \upsilon}^{n} c_2^{\kappa 0}(0, -2, 1, 2)\epsilon_{\kappa\kappa}^2 \Phi_\kappa \tag{4.23}$$

$$C_{212} = \sum_{\kappa \neq \upsilon}^{n} \sum_{\lambda \neq \upsilon}^{n} \Bigg[c_2^{\kappa\lambda}(-4, 4, -2, -2)\epsilon_{\lambda\lambda}\Delta\epsilon_{\kappa\lambda} + c_2^{\kappa 0}(0, 2, 0, 0)\epsilon_{\lambda\lambda}^2$$
$$+ c_2^{\kappa\lambda}(-2, 4, -2, -2)\epsilon_{\kappa\kappa}\epsilon_{\lambda\lambda} + \epsilon_{\kappa\kappa}\Delta\epsilon_{\kappa\lambda}c_2^{\kappa\lambda}(0, 4, -2, -2) \Bigg]\Phi_\kappa \Phi_\lambda \tag{4.24}$$

$$C_{213} = \sum_{\kappa \neq \upsilon}^{n} \sum_{\lambda \neq \upsilon}^{n} \sum_{\mu \neq \upsilon}^{n} \Bigg[c_2^{\kappa\lambda}(4, -8, 4, 2)\epsilon_{\mu\mu}\Delta\epsilon_{\kappa\lambda}$$
$$+ c_2^{\kappa\lambda}(4, -4, 1, 0)\epsilon_{\lambda\lambda}\epsilon_{\mu\mu} + c_2^{\kappa\lambda}(4, -4, 1, 0)\epsilon_{\mu\mu}\Delta\epsilon_{\lambda\mu}$$
$$+ c_2^{\kappa\lambda}(4, -4, 1, 0)\epsilon_{\lambda\lambda}\Delta\epsilon_{\lambda\mu} + c_2^{\kappa\lambda}(8, -4, 2, 2)\epsilon_{\kappa\kappa}\Delta\epsilon_{\lambda\mu} \Bigg]\Phi_\kappa \Phi_\lambda \Phi_\mu \tag{4.25}$$

$$C_{214} = \sum_{\kappa \neq \upsilon}^{n} \sum_{\lambda \neq \upsilon}^{n} \sum_{\mu \neq \upsilon}^{n} \sum_{\eta \neq \upsilon}^{n} \Bigg[c_2^{\kappa\lambda}(-16, 6, -2, 0)\epsilon_{\eta\eta}\Delta\epsilon_{\lambda\mu} + c_2^{\kappa\lambda}(-8, 6, -2, 0)\epsilon_{\lambda\lambda}\Delta\epsilon_{\mu\eta}$$
$$+ c_2^{\kappa\lambda}(-4, 0, 0, 0)\epsilon_{\eta\eta}\Delta\epsilon_{\mu\eta} + c_2^{\kappa\lambda}(-2, 0, 0, 0)\epsilon_{\mu\mu}\epsilon_{\eta\eta} \Bigg]\Phi_\kappa \Phi_\lambda \Phi_\mu \Phi_\eta \tag{4.26}$$

$$C_{215} = \sum_{\kappa \neq \upsilon}^{n} \sum_{\lambda \neq \upsilon}^{n} \sum_{\mu \neq \upsilon}^{n} \sum_{\eta \neq \upsilon}^{n} \sum_{\omega \neq \upsilon}^{n} (\epsilon_{\mu\mu}\Delta\epsilon_{\eta\omega}c_2^{\kappa\lambda}(12, 0, 0, 0)\Phi_\kappa \Phi_\lambda \Phi_\mu \Phi_\eta \Phi_\omega \tag{4.27}$$

$$C_{221} = \sum_{\kappa \neq v}^{n} c_2^{\kappa 0}(0, 2, -1, -2)\epsilon_{\kappa\kappa}^2 \Phi_\kappa \tag{4.28}$$

$$C_{222} = \sum_{\kappa \neq v}^{n} \sum_{\lambda \neq v}^{n} \left[c_2^{\kappa\lambda}(4, -8, 4, 4)\epsilon_{\kappa\kappa}\epsilon_{\lambda\lambda} + c_2^{\kappa\lambda}(2, -4, 1, 0)\epsilon_{\lambda\lambda}^2 \right] \Phi_\kappa \Phi_\lambda \tag{4.29}$$

$$C_{223} = \sum_{\kappa \neq v}^{n} \sum_{\lambda \neq v}^{n} \sum_{\mu \neq v}^{n} \left[c_2^{\kappa\lambda}(-16, -12, -4, 0)\epsilon_{\lambda\lambda}\epsilon_{\mu\mu} + c_2^{\kappa\lambda}(-2, 0, 0, 0)\epsilon_{\mu\mu}^2 \right] \Phi_\kappa \Phi_\lambda \Phi_\mu \tag{4.30}$$

$$C_{224} = \sum_{\kappa \neq v}^{n} \sum_{\lambda \neq v}^{n} \sum_{\mu \neq v}^{n} \sum_{\eta \neq v}^{n} c_2^{\kappa\lambda}(12, 0, 0, 0)\epsilon_{\mu\mu}\epsilon_{\eta\eta} \Phi_\kappa \Phi_\lambda \Phi_\mu \Phi_\eta \tag{4.31}$$

$$c_2^{\kappa\lambda}(a, b, c, d) = a\frac{1}{4}\tilde{N}_{1,\kappa}\tilde{N}_{1,\lambda} + b\frac{1}{4}\tilde{N}_{1,\kappa} + c\frac{1}{4}\tilde{N}_{2,\kappa} + d\frac{1}{16}z \tag{4.32}$$

The dispersion energy is assumed to have a temperature dependence as follows:

$$\epsilon_{ii}(T) = \epsilon_{ii}^{(1)} + \frac{\epsilon_{ii}^{(1)}\epsilon_{ii}^{(2)}}{T} \tag{4.33}$$

while the dispersion energy between unlike molecules $\Delta\epsilon_{ij}$ is assumed to obey the geometrical mixing rule:

$$\Delta\epsilon_{ij}(T) = \epsilon_{ii} + \epsilon_{jj} - 2\sqrt{\epsilon_{ii}\epsilon_{jj}}(1 - k_{ij}(T)) \tag{4.34}$$

$$k_{ij}(T) = a_{ij} + b_{ij} \cdot T \tag{4.35}$$

whereby k_{ij} is the binary interaction parameter whose coefficients a_{ij} and b_{ij} are adjusted to experimental data.

The molar volume v of a mixture with same sized lattice sites equals:

$$v = \frac{\bar{M}\bar{v}_v}{\phi_{occ}} \tag{4.36}$$

$$\bar{v}_v = \sum_i \Phi_i v_{v,i} \tag{4.37}$$

$$v_{v,i} = \sigma_i^3 N_{Av} \tag{4.38}$$

$$\bar{M} = \phi_{occ}\left(\sum_i \frac{\phi_i}{M_i}\right)^{-1} \tag{4.39}$$

with $\bar{M}$ being the mean segment number, $\bar{v}_v$ the mean lattice site volume of a mixture and $v_{v,i}$ lattice site volume of the pure component i. N_{Av} stands for the Avogadro-constant.

The system pressure p becomes:

$$p = \frac{RT}{v_v}\left\{ -\ln(\phi_v) - \phi_{occ} + \frac{\phi_{occ}}{\bar{M}} + \sum_{c=1}^{4} z^{-2}(1-c)\phi_{occ}^c C_{00c} \right.$$

$$+ \sum_{b=0}^{1}\sum_{c=1}^{4}(zk_bT)^{-1}\left[(1-b-c)\phi_v^b\phi_{occ}^c + b\phi_v^{b-1}\phi_{occ}^c\right]C_{1bc} \qquad (4.40)$$

$$\left. + \sum_{b=0}^{2}\sum_{c=1}^{6}(k_bT)^{-2}\left[(1-b-c)\phi_v^b\phi_{occ}^c + b\phi_v^{b-1}\phi_{occ}^c\right]C_{2bc} \right\}$$

and chemical potential of the component i is calculated as:

$$-\frac{\mu_i}{k_bT} = -\frac{1}{k_bT}\left(\frac{\partial\Delta F}{\partial n_iM_i}\right)_{T,V,n_jM_j\neq n_iM_i} = \frac{1}{k_b}\left(\frac{\partial\Delta S^{MF}}{\partial n_iM_i}\right)_{T,V,n_jM_j\neq n_iM_i}$$

$$+ \sum_{a=0}^{2}\sum_{b=0}^{2}\sum_{c=1}^{6}(k_bT)^{-a}z^{a-2}\left\{\left[(n_{v,i}+1)\phi_v^b\phi_{occ}^c(1-b-c) + bn_{v,i}\phi_v^{b-1}\phi_{occ}^c + c\phi_v^b\phi_{occ}^{c-1}\right]C_{abc}\right.$$

$$\left. + \phi_v^b\phi_{occ}^{c-1}n_{occ}M_{occ}\left(\frac{\partial C_{abc}}{\partial n_iM_i}\right)_{T,V,n_jM_j\neq n_iM_i}\right\}$$

$$(4.41)$$

with the derivatives of the mean field entropy and the amount of mole of component i being:

$$\frac{1}{k_b}\left(\frac{\partial\Delta S^{MF}}{\partial n_iM_i}\right)_{T,V,n_jM_j\neq n_iM_i} = -n_{v,i}\ln(\phi_v+1) - \frac{1}{M_i}\ln(\phi_i+1) + (n_{v,i}+1)\left(\frac{\phi_{occ}}{\bar{M}} + \phi_v\right)$$

$$(4.42)$$

$$n_{v,i} = \left(\frac{\partial n_v}{\partial n_iM_i}\right)_{T,V,n_jM_j\neq n_iM_i} = \frac{1}{\phi_{occ}}\left(\phi_v - \frac{v_{v,i}}{\bar{v}_v}\right) \qquad (4.43)$$

When considering a pure component, $n_{v,i}$ turns -1. The derivatives of the extended mean-field-contributions are calculated according to the following pattern:

$$\left(\frac{\partial C_{abc}}{\partial n_iM_i}\right)_{T,V,n_jM_j\neq n_iM_i} = C_{abc}\sum_{\alpha\in\kappa,\lambda,\mu,...}\left(\frac{\delta_{\alpha,i}}{\Phi_\alpha} - 1\right) \qquad (4.44)$$

where the number of counting indices $\alpha \in \kappa,\lambda,\mu,...$ depends on the number of sums in C_{abc}. The Kronecker delta is defined according to eq. (2.12).

Determination of architecture coefficients

As previously mentioned, for calculations with the LCT using the simplifications of Nemirovsky et al. [63] in eqn. 2.13 and 2.14, just the three architecture coefficients N_1, N_2 and N_3 are required instead of nine architecture coefficients from table 2.1. N_1, the number of bonds is simply calculated via the number of segments:

$$N_1 = M - 1 \tag{4.45}$$

For linear molecules, the determination of N_2 and N_3 is straightforward:

$$N_1^{lin} = M - 2 \tag{4.46}$$

$$N_2^{lin} = M - 3 \tag{4.47}$$

Since the direct determination of N_2 and N_3, i.e. the number of two and three consecutive bonds becomes quite complex for heavily branched molecules, these can be obtained by an approach from Langenbach & Enders [211]. For this purpose, the number of neighbours of second-order $V_{2,m}$ and third-order $V_{3,m}$ of each united atom group m is determined and summed up over all segments M:

$$N_2 = \frac{1}{2} \sum_m^M V_{2,m} \tag{4.48}$$

$$N_3 = \frac{1}{2} \sum_m^M V_{3,m} \tag{4.49}$$

This method is applicable for smaller molecules, where the effort of counting every united atom group and its neighbours is reasonable. When it comes to bigger molecules such as polymers, this is not the case. At the same time, the exact molecular structure of polymers is often not ascertainable. Usually, measurements of the molar mass are available, which can be used to determine the number of united atom groups. The architecture of the polymers can be determined by spectroscopic measurements, providing the branching degree, i.e. the number of threefold and fourfold branching points per 1000 C-atoms br_3 and br_4 respectively. According to Langenbach [212], the architecture coefficients can be extracted from this information as

follows:

$$N_2 = M - 2 + br_3 + 3br_4 \tag{4.50}$$

$$N_3 = M - 3 + 2br_3 + 6br_4 \tag{4.51}$$

Eq. (4.51) is only valid, if branching points are not directly adjacent to each other and if side chains contain at least two segments. In case, such detailed information about the branching is at hand, eq. (4.49) has to be used. Due to the fact, that polyethylene exhibits almost exclusively threefold branching points, br_4 is assumed to be negligible.

4.2 Car-parking-framework

For the general treatment of the crystallinity, polymer configurations are accommodated in a lattice [213]. In this context, a crystalline region is characterized by ζ, the number of repeating structural units, which in case of polyolefins may be CH_2-units. The crystallinity α of the polyolefin is then defined as:

$$\alpha = \frac{j\zeta}{M} \tag{4.52}$$

where j is the number of crystalline sequences and M is the segment number of the entire chain, whereby one segment is formed by a structural CH_2-unit. The segment number is given directly by the molecular weight and the molar mass of a unit. However, ζ and j are unknown. For this reason, the former considers the free energy change in forming a crystallite, while for j, the Car-Parking-Problem is applied to polymer crystallization.

4.2.1 Crystalline sequence length

Based on the works of Flory [214], Mandelkern [215] found an implicit expression for the free energy change ΔF in forming a crystallite, depending on the crystalline sequence length ζ, the number of crystalline sequences in cross section ρ, the number of polymer molecules N, the chain length M, the system temperature T, the melting enthalpy of one segment Δh_m, the melting temperature T_m^0, the surface energy σ_e and the cross-sectional area of the polymer chain a_0 [215]:

$$\Delta F = 2\sqrt{\pi\rho}\zeta\sigma_u - RT\rho\ln(D) - \zeta\rho\frac{\Delta h_m}{2}\frac{T_m^0 - T}{T_m^0} - RT\left[N\ln\left(1 - \frac{\zeta\rho}{NM}\right) + \rho\ln\left(\frac{M - \zeta + 1}{M}\right)\right] \tag{4.53}$$

In the original publication [215], the second term of eq. (4.53) in squared brackets has a different sign. This was corrected after comparison with preceding publications [214, 216]. Δh_m is divided by 2 as it refers to one ethylene-unit, which contains two segments. $\ln(D)$ is defined as follows:

$$\ln(D) = \frac{-2\sigma_e a_0}{RT} \tag{4.54}$$

whereby D is regarded by Flory [214] as nucleation constant. σ_u is the lateral interfacial free energy of a molecule. With help of the first term of a Taylor series expansion, the first term of eq. (4.53) in squared brackets $N \ln\left(1 - \frac{\zeta\rho}{NM}\right)$ can be written as $-\zeta\rho/M$. Strictly speaking, this is only valid at small crystallinities. However, the error should be minor compared to general inaccuracies when dealing with crystallinities. ΔF does not exhibit a maximum or minimum, but shows a saddle point where the free energy derivatives $\left(\frac{\partial \Delta F}{\partial \zeta}\right)_\rho$ and $\left(\frac{\partial \Delta F}{\partial \rho}\right)_\zeta$ equal zero [215]. At this extremum, the critical properties ρ^* and ζ^* are obtained. Combining both equation leads to the critical crystalline sequence length ζ^*:

$$\frac{\zeta^*}{2}\left(\frac{\Delta h_m}{2}\frac{T_m^0 - T}{T_m^0} - \frac{RT}{M} + \frac{RT}{M - \zeta^* + 1}\right) + RT\ln\left[\frac{D(M - \zeta^* + 1)}{M}\right] = 0 \tag{4.55}$$

whereby σ_u vanishes. While Δh_m and T_m^0 are substance properties, which are directly experimental accessible, σ_e is a property coming from crystallization growth kinetics, whose estimation may be accompanied by large uncertainties. For lower molecular weights there is probably an effect of chain length on σ_e [217] which will be disregarded here for the sake of simplification. Parameters for eq. (4.55) are given in table 4.1.

Table 4.1: Parameters used for the model predictions in eqn. 4.55 and 4.77.

Quantity	Value	Method	Ref.
Δh_m [kJ $(\text{mol}_{\text{C2H4}})^{-1}$]	8.284	a)	[218]
T_m^0 [K]	414.6	b)	[70]
a_0 [$\text{m}^2\,\text{mol}^{-1}$]	$1.1 \cdot 10^5$	-	[213]
σ_e [mJ m^{-2}]	168	c)	[81]

a): Differential Scanning Calorimetry with solution-grown crystals, b): extrapolation of linear chain homologs, c): nucleation kinetics of polyethylene droplets

4.2.2 Car-Parking-Problem

The idea for the Car-Parking-Problem (CPP) was constructed by Renyi [18] in 1958. In this 1-dimensional random space filling problem, the following question was posted: Having a given interval $(0, x)$, how many unit segments, j, can be placed so that no points are overlapping. The question is similar to the illustration of identical cars, randomly parked along a curb, which is why the problem is known as the Car-Parking-Problem. Renyi [18] postulated the following continuous recursion for the number of units j, that can be placed on $(0, x)$:

$$j(x) = \begin{cases} 0 & \text{if } x < 1 \\ 1 + \dfrac{2}{x-1} \displaystyle\int_0^{x-1} j(y)dy & \text{if } x \geqslant 1 \end{cases} \tag{4.56}$$

Forming the limit of the unit density $j(x)/x$ for an infinite interval, one obtains the famous Car-Parking-constant C:

$$C = \lim_{x \to \infty} \frac{j(x)}{x} = \int_0^\infty \exp\left(-2\int_0^t \frac{1-e^{-u}}{u}du\right)dt \approx 0.7476 \tag{4.57}$$

4.2.2.1 Statistical treatment
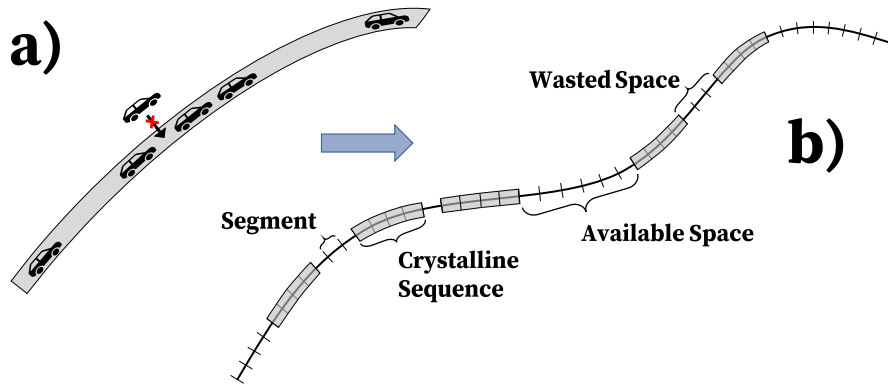
Figure 4.1: a) Model concept of the CPP. b) Application to crystallization of a polymer chain.

Gornick & Jackson [15] applied the CPP to the crystallization of polymers by considering a polyolefin chain consisting of M segments in which j sequences of length ζ are crystallized (figure 4.1b)). In this case, $N(M, j, \zeta)$ describes the number of possibilities, arranging those j sequences in the polymer chain. In other words, $N(M, j, \zeta)$ is the number of permutations of

j with $M - j\zeta$ amorphous segments [15].

$$N(M, j, \zeta) = \frac{(M - j\zeta + j)!}{(M - j\zeta)!j!} \tag{4.58}$$

The probability P, that the first interval δ_1 equals a value r, is [15]:

$$P(\delta_1 = r) = \frac{N(M - r - \zeta, j - 1, \zeta)}{N(M, j, \zeta)} = \frac{(M - j\zeta + j - r - 1)!}{(M - j\zeta + j)!} \frac{(M - j\zeta)!}{(M - j\zeta - r)!} j \tag{4.59}$$

Gornick & Jackson [15] simplified eq. (4.59) for $M \to \infty$, $j \to \infty$ and large ζ, in order to solve the equation analytically. In this work, however, to study the influence of the segment number and the crystalline sequence length, eq. (4.59) is solved without simplification. Since the calculation of faculties for high segment numbers is extremely CPU-intensive, in this work, eq. (4.59) is approximated with help of the Stirling's formula with 3 terms.

$$n! \simeq \sqrt{2\pi n} \left(\frac{n}{e}\right)^n \tag{4.60}$$

$$P(r) = j \frac{\sqrt{2n\pi(M - j\zeta)} \left(\frac{M - j\zeta}{e}\right)^{M - j\zeta}}{\sqrt{2n\pi(M - j\zeta - r)} \left(\frac{M - j\zeta - r}{e}\right)^{M - j\zeta - r}}$$

$$\times \frac{\sqrt{2n\pi(M - j\zeta + j - r - 1)} \left(\frac{M - j\zeta + j - r - 1}{e}\right)^{M - j\zeta + j - r - 1}}{\sqrt{2n\pi(M - j\zeta + j)} \left(\frac{M - j\zeta + j}{e}\right)^{M - j\zeta + j}} \tag{4.61}$$

$$= e \sqrt{\frac{(M - j\zeta)(M - j\zeta + j - r - 1)}{(M - j\zeta - r)(M - j\zeta + j)}} \left[\frac{\zeta}{\alpha} - \zeta + 1 - \frac{r + 1}{j}\right]^{-1} \left[1 - \frac{r + 1}{M - j\zeta + j}\right]^j$$

$$\times \left[1 + \frac{1}{\frac{\zeta}{\alpha} - \zeta - \frac{r}{j}} - \frac{1}{M - j\zeta - r}\right]^{M - j\zeta - r} \left[1 + \frac{1}{\zeta}\left(\frac{\alpha}{1 - \alpha}\right)\right]^{-(M - j\zeta)} \tag{4.62}$$

$$= e \sqrt{\frac{(M - j\zeta)(M - j\zeta + j - r - 1)}{(M - j\zeta - r)(M - j\zeta + j)}} \left[\frac{\zeta}{\alpha} - \zeta + 1 - \frac{r + 1}{j}\right]^{-1} \left[1 - \frac{r + 1}{M - j\zeta + j}\right]^j$$

$$\times \left[1 + \frac{1}{\frac{\zeta}{\alpha} - \zeta - \frac{r}{j}} - \frac{1}{M - j\zeta - r}\right]^{-r} \left[\frac{1 + \frac{1}{\zeta/\alpha - \zeta - r/j} - \frac{1}{M - j\zeta - r}}{1 + \frac{1}{\zeta}\left(\frac{\alpha}{1 - \alpha}\right)}\right]^{M - j\zeta} \tag{4.63}$$

For long polymer chains, depending on the configuration of M, j, ζ and r, either eq. (4.62) or eq. (4.63) is numerically favourable.

For intervals being too small in order to accommodate a crystalline sequence, one has $r < \zeta$. One obtains the segment fraction of wasted space W with the following expression, in case

enough amorphous segments remain for the accommodation of a further sequence [15]:

$$\forall (M - j\zeta) \geqslant \zeta : \; W = \frac{j+1}{M} \sum_{r=1}^{\zeta - 1} r P(r) \tag{4.64}$$

The factor $j + 1$ results from the reference to the entire chain. Technically speaking, there are configurations of $P(r)$, where less intervals than $j + 1$ exist, due to crystalline sequences placed directly adjacent to each other. However, for long chains this effect is negligible, which can be explained phenomenologically: An elongating chain is considered as a constant chain having shorter segments, i.e. the same chain is much more finely segmented. The shorter the segments, the less likely crystalline sequences are to be adjacent to each other. Hence, one can assume the number of intervals being $j + 1$.

The index of summation r of eq. (4.64), i.e. the length of the first interval, may go from 1 to $\zeta - 1$. This works, if an interval can reach the value $\zeta - 1$. In case of long crystalline sequences or high crystallinities there may be no space to accommodate another sequence. In these cases, r goes from 1 to $M - j\zeta - 1$, i.e. the remaining segments not occupied by crystalline sequences. For this consideration, in this work, another term is included:

$$\forall (M - j\zeta) < \zeta : \; W = \frac{j+1}{M} \sum_{r=1}^{M - j\zeta - 1} r P(r) \tag{4.65}$$

Another particular case arises, the moment r reaches $M - j\zeta$. This case corresponds to the configuration, where all the remaining amorphous segments lie together forming one big interval, which cannot be calculated with eqn. 4.62 and 4.63 due to arising zero in the denominator. Hence, in this work, the last addend in eq. (4.65) is calculated as follows:

$$W = \frac{1}{M} r P(\delta_1 = M - j\zeta) \tag{4.66}$$

Since one big interval is considered, the factor $j + 1$ vanishes. The number of possibilities if the first interval δ_1 has the length $M - j\zeta$ is just equal to 1, because all the remaining amorphous segments are accommodated in this interval. One can see this as well by inserting $r = M - j\zeta$

and $j = 1$ into eq. (4.59). With help of the Stirling formula (eq. (4.60)) it follows:

$$P(r = M - j\zeta) = \frac{1}{N(M, j, \zeta)} = \frac{(M - j\zeta)!\, j!}{(M - j\zeta + j)!} \tag{4.67}$$

$$= \frac{\sqrt{2\pi (M - j\zeta)} \left(\frac{M - j\zeta}{e}\right)^{M - j\zeta} \sqrt{2\pi j} \left(\frac{j}{e}\right)^{j}}{\sqrt{2\pi (M - j\zeta + j)} \left(\frac{M - j\zeta + j}{e}\right)^{M - j\zeta + j}} \tag{4.68}$$

$$= \sqrt{\frac{2\pi j (M - j\zeta)}{(M - j\zeta + j)}} \left(\frac{M - j\zeta}{M - j\zeta + j}\right)^{M - j\zeta} \left(\frac{j}{M - j\zeta + j}\right)^{j} \tag{4.69}$$

$$= \sqrt{\frac{2\pi j (M - j\zeta)}{(M - j\zeta + j)}} \left[1 + \frac{1}{\zeta}\left(\frac{\alpha}{1 - \alpha}\right)\right]^{-(M - j\zeta)} \left[\frac{\zeta}{\alpha} - \zeta + 1\right]^{-j} \tag{4.70}$$

Besides the limitation of crystallinity due the combinatorial reasons another limitation applies for long crystalline sequences: For $\zeta/M > 0.5$, after placing a first sequence which now covers more than half of the polymer chain, no further sequence can be accommodated in the polymer. This natural limitation is:

$$\alpha_{j=1} = \frac{\zeta}{M} \tag{4.71}$$

and equals therefore eq. (4.52) in case of $j = 1$. The wasted space of this limit is calculated as follows:

$$W_{j=1} = 1 - \alpha_{j=1} = 1 - \frac{\zeta}{M} \tag{4.72}$$

4.2.2.2 Continuous treatment

While the approach of Gornick & Jackson [15] is a purely statistically consideration of the problem, Maltz & Mola [16, 22] introduced a continuous view on the problem. In this approach the chronology of the crystalline sequences comes into play, which is elucidated in Fig. 4.2.

For the left-hand side in figure 4.2, eq. (4.58) can be applied, resulting in a probability $1/6$ for one of the possible arrangements 1-6. For the calculation of the right-hand side, one has to calculate the possibility of the black sequence to find its place in an empty compartment, which is $1/5$ in all configurations. The probability of introducing the grey sequence into 1a is $1/3$, respectively $1/2$ for 1b resulting in an overall probability of configuration 1 of $P = 1/5 \cdot 1/3 + 1/5 \cdot 1/2 = 1/6$. The same accounts for configurations 2-4. However, configuration 5 and 6 equal a probability of $2/15$ respectively $1/5$. While the statistical treatment assigns the same
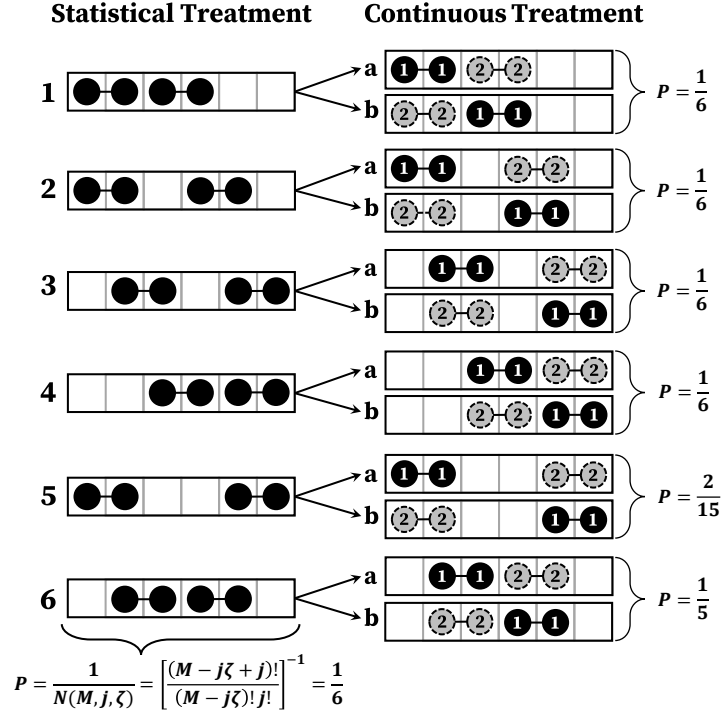
Figure 4.2: Probability of filling two two-segment sequences into a compartment of six segments. On the left-hand side the purely statistical approach. On right-hand side the continuous treatment: First, a black sequence is inserted, followed by a grey sequence. Adopted from [22].

probability to every configuration, the different configurations have different probabilities in continuous treatment.

For the calculation of the wasted space two natural constraints have to be considered. If the crystalline sequence length ζ is larger than the length of the polymer chain M, all space is wasted. Secondly, if ζ equals the chain length, however improbable, the hole chain crystallizes at ones, resulting in a wasted space of zero [16]:

$$\forall(M < \zeta): \ W(M, \zeta) = 1 \tag{4.73}$$

$$\forall(M = \zeta): \ W(M, \zeta) = 0 \tag{4.74}$$

The recursive formalism in case ζ is smaller than M is as follows [16]:

$$\forall(M > \zeta): \ W(M, \zeta) = \frac{M - \zeta}{M(M - \zeta + 1)} \left[(M - 1)W(M - 1, \zeta) + 2W(M - \zeta, \zeta) \right] \tag{4.75}$$

Freedman & Gornick [219] addressed the same issue 10 years later and reached the same result (eqn. 4.73-4.75) independently of Maltz & Mola [16, 22].

4.2.3 Flory-approach for branching

A fundamental predictive model for estimating the crystallinity α as function of the branching degree br was introduced by Flory [4]. As can be seen in figure 4.3, the polymer chain is divided into units A (main monomer) and units Co (co-monomer), with just A-units being crystallizable.
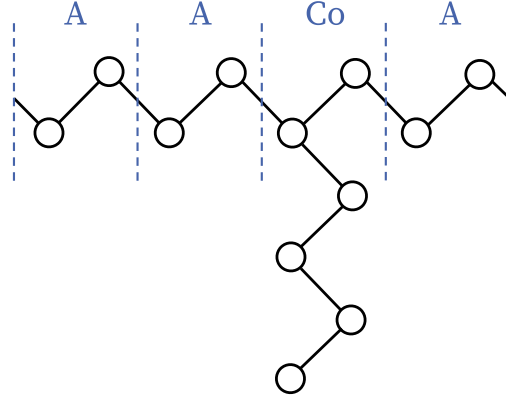

Figure 4.3: Model concept of Flory's copolymer approach (FCA) having crystallizable units A as well as non-crystallizable units Co using the example of an ethylene-hexene-copolymer (the side chain would be butyl in this case).

The crystallinity of branched polyolefins is given by [4]:

$$\alpha = \frac{\frac{\phi_A}{p}(1-p)^2 p^{\zeta_{cr}} \left[\frac{p}{(1-p)^2} - \frac{e^{-\theta}}{(1-e^{-\theta})^2} + \zeta_{cr} \left(\frac{1}{1-p} - \frac{1}{(1-e^{-\theta})} \right) \right]}{1 - \frac{\phi_A}{p} p^{\zeta_{cr}} \left(\frac{1-p}{1-e^{-\theta}} \right)^2 \left[\zeta_{cr}(1-e^{-\theta}) + e^{-\theta} \right]} \tag{4.76}$$

$$\theta = \frac{\Delta h_m}{R} \left(\frac{1}{T} - \frac{1}{T_m^0} \right) \tag{4.77}$$

where ϕ_A is the volume fraction of A-units, which is used instead of the mole fraction x_A, since monomers A and Co do not have the same volume:

$$\phi_A = \frac{x_A}{\left(\frac{n_{br}+2}{2} \right)(1-x_A) + x_A} \tag{4.78}$$

with n_{br} being the number of units in the branch. p in eq. (4.76) is the probability of a monomer being an A unit and equals the mole fraction x_A for random co-polymers:

$$p = x_A = 1 - \frac{2br}{1000 - n_{br}br} \tag{4.79}$$

with br being the number of branches per 1000 C-atoms. A critical crystalline length ζ_{cr} is calculated using eq. (4.80) which is a function of the temperature. Solely sequences composed

of A-units which are at least be equivalent to ζ_{cr} are able to crystallize.

$$\zeta_{cr} = \frac{-1}{\theta + \ln(p)} \left[\ln\left(\frac{D\phi_A}{p}\right) + 2\ln\left(\frac{1-p}{1-e^{-\theta}}\right) \right] \tag{4.80}$$

where the nucleation constant D is given by eq. (4.54). Δh_m is the melting enthalpy of one A-unit, T_m^0 the melting temperature of the unbranched linear polymer. The same parameters are used as for the calculation of the linear crystalline sequence length given in table 4.1. The second term in the denominator of eq. (4.76) differs from Flory's original approach [4]. This correction was shown up by Kilian [220], Baur [221] and Wunderlich [222] and considers the fact that just amorphous sequences are available for further crystallization.

4.3 Numerical implementations

Parametrization

The pure component parameters of the LCT for polyethylene are fitted to experimental data of the liquid volume, while parameters of gases are adjusted to experimental vapour pressure and saturated liquid volume data. A parameter set θ is obtained by minimizing a least square function:

$$\min_{\Theta} F(\Theta) = \frac{1}{N_v} \sum_{i=1}^{N_v} \left(\frac{v_i^{exp} - v_i^{calc}(\Theta)}{v_i^{exp}} \right)^2 + \frac{1}{N_p} \sum_{j=1}^{N_p} \left(\frac{p_j^{exp} - p_j^{calc}(\Theta)}{p_j^{exp}} \right)^2 \tag{4.81}$$

No weighting was introduced, the sum terms were normalized to the number of data points available. For finding the optimum of eq. (4.81), a simplex method was used due to its robustness, whereby the problem of local minima was solved by performing multiple minimizations from different initial values.

Thermodynamic framework

Gas solubility calculations were carried according to figure 4.4. First, the limiting crystallinity for a linear polyethylene chain is calculated with help of the temperature, the molar mass and crystalline sequence length via the CPP (eqns. (4.64)-(4.66), (4.71) and eqns. (4.73)-(4.75)). This is multiplied by the crystallinity of the branched chain via the FCA (eq. (4.76)) as a function of temperature and the polymers architecture.
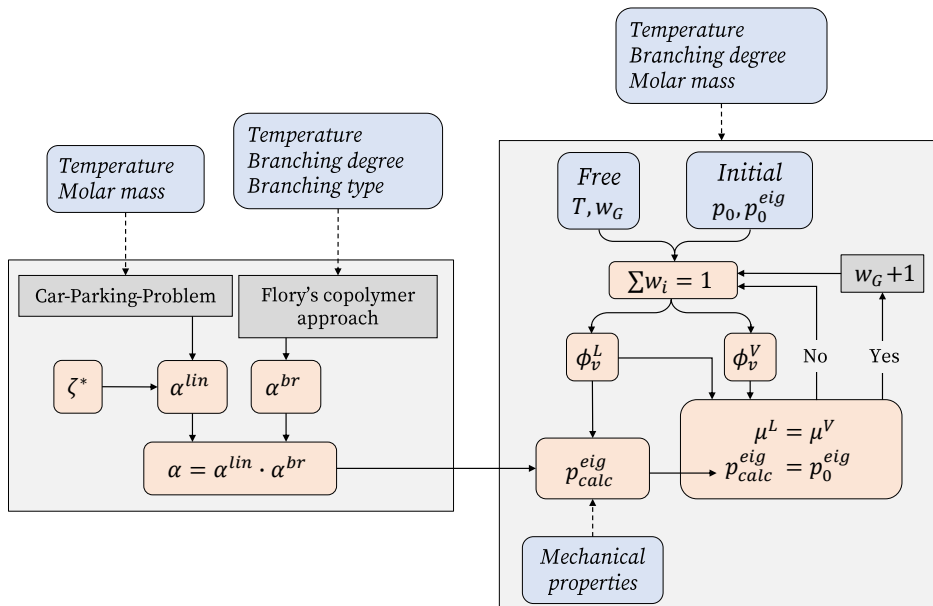

Figure 4.4: Numeric procedure for prediction of gas solubilities in semi-crystalline systems. The left side is the CPP/FCA for the determination of the crystallinity, while the ride side stands for the phase equilibria calculations with the LCT. Blue are input variables, orange calculations.

Subsequently, the thermodynamic phase equilibrium for binary systems is determined by the LCT. The system pressure is iterated at a given temperature and weight fraction of the solved gas in the liquid phase. A suitable value for the system pressure and for the eigen pressure has to be guessed, whereby $2.5G$ suits as an initial value for p^{eig}. As the polymer has a negligible vapour pressure, the vapour consists of purely gas. The composition of the liquid phase is determined by the summation condition, the void segment fraction of the gas phase ϕ_v^V and liquid phase ϕ_v^L, resembling the respective volumes are iterated independently. Since this is an one-dimensional root finding problem, a combined secant and bisection methods suits as a robust and fast method. The two-dimensional phase equilibrium condition is solved by a Newton method. The eigen pressure depends on the crystallinity and the void segment fraction of the liquid phase (eq. (3.3)). Hence, the predicted crystallinity of the CPP/FCA serves as variable, as does the amount of solved gas in polymer, which influences the void segment fraction of the liquid phase.

After a successful iteration, the new initial system pressure for a new weight fraction p_{w+1} is approximated linearly via the current pressure p_w and the previous pressure p_{w-1}, in order to enhance robustness of the numeric procedure:

$$p_{w+1} = 2 \cdot p_w - p_{w-1} \tag{4.82}$$

A special treatment is applied when using experimental data with insufficient characterization in terms of the branching degree. To access information about the architecture, the combined CPP and FCA is applied quasi reversed: The measured crystallinity at known temperature, molar mass and branching type are used to calculate the branching degree iteratively, which is shown in figure 4.5.
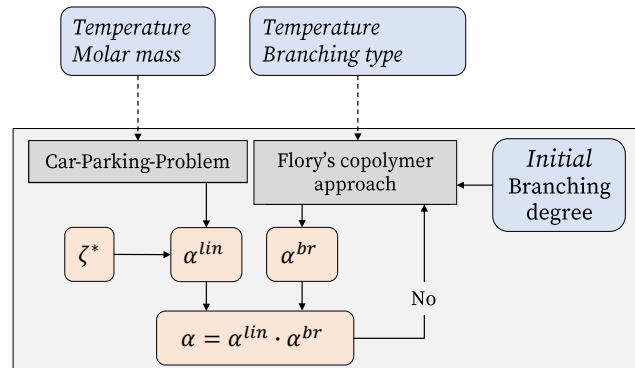

Figure 4.5: Numeric procedure for the determination of the branching degree with help of the temperature and the inverse CPP/FCA. Blue are input variables, orange calculations.

In case of ternary system, the calculation of the phase equilibrium is extended by the chemical potential of the second gas in the liquid and gas phase, whereby the latter is not pure any more (figure 4.6). The determination of the crystallinity, which is required for the calculation of the eigen pressure is analogous to the binary system (figure 4.4). In addition to the temperature and system pressure, the composition of the gas phase is given, while suitable initial values for the gas content in the liquid have to be guessed. Here, the individual gas solubilities at the corresponding partial pressure can serve as suitable initial values. Every successful iteration gives the partial solubility of both gases in the polymer. For the overall solubility, these partial solubilities must be added together.
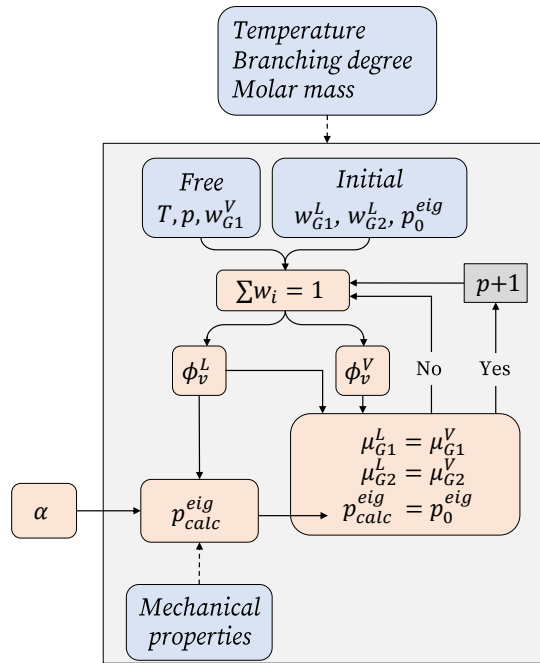
Figure 4.6: Numeric procedure for prediction of ternary system including two gases and a polymer. The left side including determination of the crystallinity α can be seen in figure 4.4. Blue are input variables, orange calculations.

For the sake of comparison, the sum of the independent binary gas solubilities can be formed at the corresponding partial pressure of the single gas systems:

$$w_{Sum}(p_i + p_j) = w_{i,0}(p_i) + w_{j,0}(p_j) \tag{4.83}$$

were $w_{i,0}(p_i)$ denotes the solubility of the pure gas i in the polymer at the pressure p_i. Eq. (4.83) rests upon the assumptions, that the partial pressure can be added to form the system pressure, which is the case for a mixture of ideal gases.

5 Results and discussion

In this chapter, results of the work are shown and discussed, starting with the prediction of crystallinities with the combined CPP/FCA approach. Subsequently, results of the parametrisation of pure components and gas solubilities in the melt are shown, followed by predictions of single- and multi-gas sorption in semi-crystalline polyethylene by the full framework.

5.1 Calculation of crystallinities

5.1.1 Linear polyethylene

Figure 5.1 shows both experimental data of electron microscope studies and predictions of ζ^* as a function of the segment number M for different temperatures.
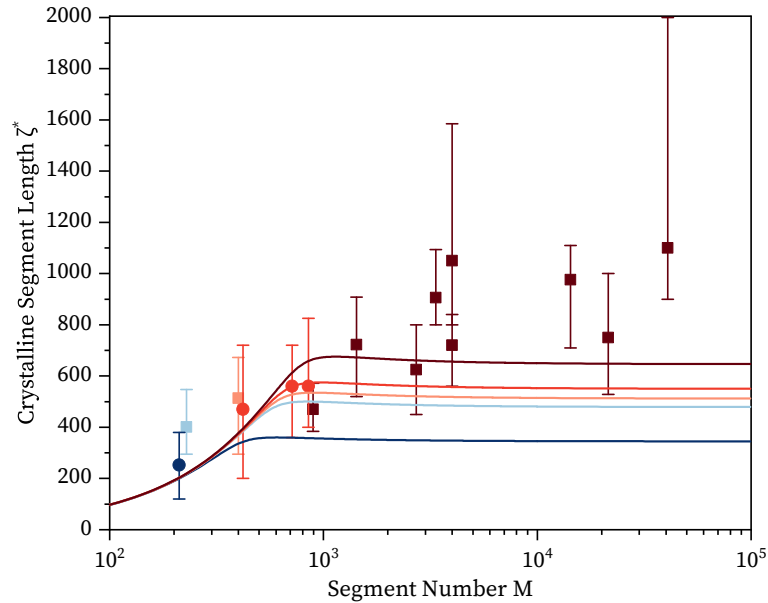
Figure 5.1: Plot of ζ^* as a function of M, calculated with eq. (4.55) for different temperatures. Parameters taken from table 4.1. Experimental data from Mandelkern (squares, [223]) and Anderson (circles, [224]) for T = 393.15 K (dark blue), T = 399.15 K (light blue), T = 400.15 K (light red), T = 401.15 K (red), T = 403.15 K (dark red), where bars represent the range of the electron microscope studies while the symbols depict the mean value.

To calculate ζ^*, eq. (4.55) is used which depends on the temperature and the segment number. The prediction of ζ^* runs exponential for low molecular weights independent of the temperature. In this area ζ^* corresponds roughly to the chain length. For higher molecular weights, ζ^* levels off and is independent of the molecular weight which is given by $\lim_{M\to\infty}\zeta^* = 8\sigma_e T_m^0/[\Delta h_u(T_m^0 - T)]$. The calculations reproduce the experimental data qualitatively considering the range of the measurements and experimental inaccuracies.

Applying the purely statistical eqs. (4.64)-(4.66) and (4.72), one can calculate the wasted space as a function of the crystallinity for different crystalline sequence lengths, which is shown in figure 5.2.
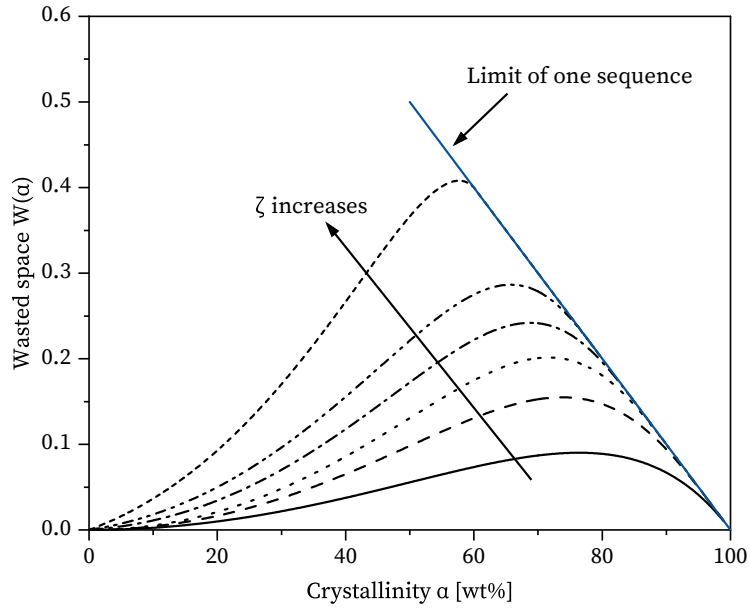

Figure 5.2: Wasted space as a function of the crystallinity α for different crystalline sequence lengths ζ at a chain length of M=10^5. Solid line: ζ=2, dashed line: $\zeta = 5$, dotted line: ζ=100, dash-dotted line: ζ=10000, dashed double dotted line: ζ=20000, short dashed line: ζ=40000. Calculated with eqs. (4.64)-(4.66). The blue line is the limit for one crystalline sequence (eq. (4.72)).

Coming from low crystallinities, $W(\alpha)$ increases slowly at first and drops after a maximum for $\lim_{\alpha\to 1} W$ to 0. The wasted space cannot decrease with increasing crystallinity, hence $\frac{\partial W(\alpha)}{\partial\alpha}$ must be positive in the physically useful range. This is why the maximum in $W(\alpha)$ simultaneously represents the maximal accessible amount of crystallinity.

For high amounts of crystallinity, the crystallinity is no longer prescribed by the CPP, but by the natural limit $W_{j=1}$ (eq. (4.72)), which denotes the wasted space having just one crystalline sequence and is represented by the blue line in figure 5.2. Since the interest lies in the estimation of the maximal crystallinity for a given crystalline sequence length, the maximum in figure 5.2 is of high relevance. Therefore in figure 5.3, the maximal crystallinity as a function of the ζ is given together with the limits $\alpha_{j=1}$ (eq. (4.71)) and $W_{j=1}$ (eq. (4.72)).
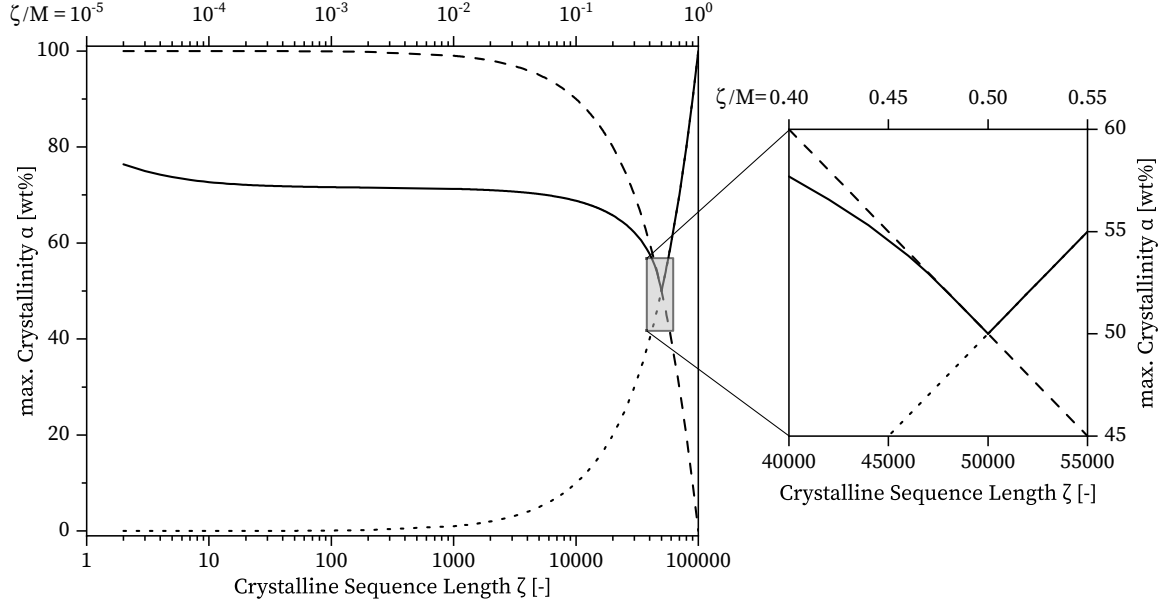
Figure 5.3: Maximal crystallinity as a function of ζ for a polymer chain consisting of $M = 1 \cdot 10^5$ segments by purely statistical treatment (straight line). The dotted line represents the crystallinity for a chain having one crystalline sequence $\alpha_{j=1}$ (eq. (4.71)) while the dashed line is the wasted space for one crystalline sequence $W_{j=1}$ (eq. (4.72)). A magnification is shown on the right-hand side.

For the straight line coming from left side, e.g. low crystallinities, the maximum crystallinity initially decreases and temporarily reaches a limit before decreasing again and finally running into the limit $W_{j=1}$ at about $\zeta/M = 0.48$. From $\zeta/M = 0.5$ on, the crystallinity is prescribed by the natural limit since only one crystalline sequence is present.

Figure 5.4 shows the maximal crystallinity when estimated by continuous treatment (eqs. (4.73)-(4.75)) considering the chronology in which the sequences crystallize. The result resembles qualitatively the route of the statistical treatment, which is depict as a blue curve. However, it gives higher crystallinities for $\zeta/M < 0.5$. Furthermore, the crystallinity tends to be asymptotic to Renyi's constant (≈ 0.748) at intermediate lengths of the crystalline sequences ($1 \cdot 10^{-3} \le \zeta/M \le 1 \cdot 10^{-2}$).

An interesting occurrence is the local maximum and minimum for $1/4 \le \zeta/M \le 1/2$. This originates from the continuous counting method. Coming from the right side and considering the interval $1/2 \le \zeta/M \le 1$, only one sequence can be accommodated in the polymer chain, resulting in a monotonic curve. Between $1/3 \le \zeta/M \le 1/2$, either one or two sequences can be accommodated according to the placement of the first sequence. While the incorporation of two sequences results in a higher crystallinity, at the same time the probability of placing two sequences decrease with increasing sequence length.
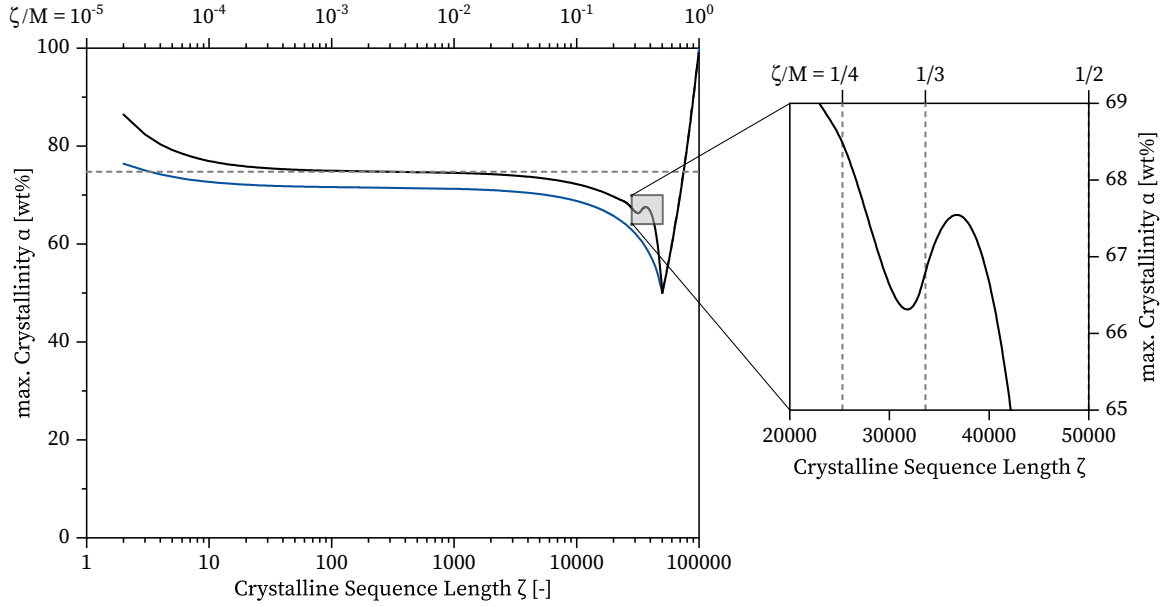
Figure 5.4: Maximal crystallinity as a function of ζ for a polymer chain consisting of $M = 1 \cdot 10^5$ segments by continuous treatment (black solid line). The blue solid line depicts the purely statistical treatment for the sake of comparability. Renyi's car parking constant (eq. (4.57)) in percent is shown by the dashed grey line. A magnification is shown on the right-hand side.

These two effects occasion the local maximum. $\zeta/M = 1/3$ represents the inflection point of the curve leading to the next interval $1/4 \leq \zeta/M \leq 1/3$, where analogous can be applied, resulting in the minimum. For $\zeta/M \geq 1/4$, although different numbers of sequences can be accommodated in one interval, the effect of different probabilities gets weaker and the curve of crystallinity is monotonic again.

Figure 5.5 shows the prediction of the crystallinity of linear polyethylene as a function of the segment number for five different temperatures for both statistical approach (dashed line) and the continuous treatment (straight line). Initially both curves run down from fully crystalline to 50 %, in this interval only one crystalline sequence exists and the crystallinity is predefined by the length of this sequence. After that, the crystallinity of the statistical treatment increases again due to the accommodation of more crystalline sequences in the polymer chain, levelling off at a crystallinity of about $\alpha = 0.72$. Meanwhile the continuous curve increases as well, but at a higher level and shows the local maximum already discussed. Subsequently, the continuous curve seems to run to an asymptotic limit close by the Renyi constant. However, the curve does not converge and exceeds the Renyi constant in case of low temperatures (hence short crystalline sequences) already in the range of reasonable change length. This exceeding of the Renyi constant for low crystalline sequence length became already apparent in figure 5.4.
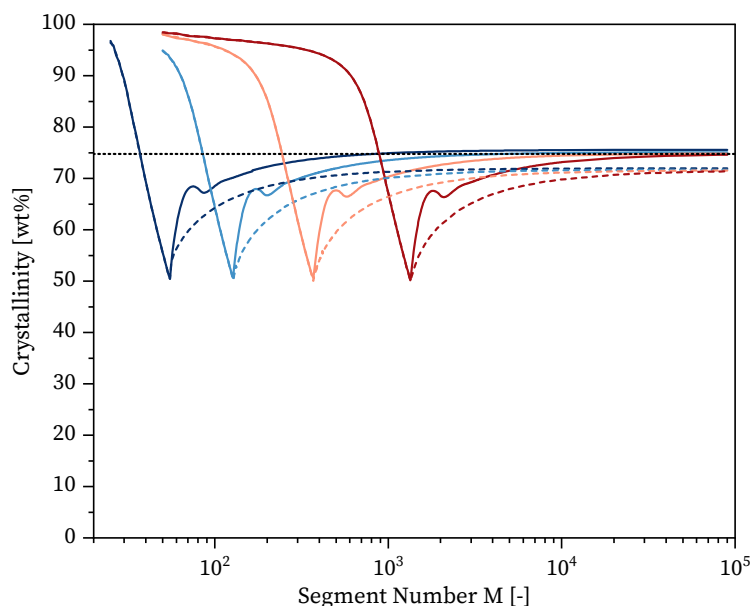
Figure 5.5: Prediction of the crystallinity of linear polyethylene as a function of the segment number M for different temperatures 144.15 K (blue lines), 296.15 K (light blue lines), 373.15 K (light red lines) and 403.15 K (red lines). The continuous treatment results in the straight line while the statistical approach leads to the dashed line. The dotted line indicates the Renyi-Limit.

5.1.2 Branched polyethylene

Model calculation for estimating the crystallinity of branched polyethylene were carried out in the following way: Via eq. (4.55) a crystalline sequence length ζ^* for the linear polyolefin was estimated. Subsequently, with help of ζ^* and the Car-Parking-Problem (eqs. (4.62)-(4.66) and (4.71) respectively eqs. (4.73)-(4.75)), a maximal crystallinity is calculated. Finally, by incorporating eq. 4.76, the crystallinity of branched polyethylene is predicted.

Figure 5.6 shows the predicted crystallinity as a function of chain branching with the combined CPP/FCA. The general trend the of experimental data is correctly reproduced by the model. In particular, the limiting crystallinity for unbranched polyethylene with help of the CPP between 70 % and 75 % is predicted accurately. Furthermore, figure 5.6 shows the dependence on the treatment of the CPP. Choosing the continuous treatment results in a higher limiting crystallinity for unbranched polyethylene compared to the statistical treatment. This effect was already observed in figure 5.5. The choice of treatment for the calculation of crystallinities and subsequently gas solubilities is far from trivial, as it is a choice of mathematical abstraction for a complex, multivariate physical behaviour. When considering a crystallization process, it seems obvious that sequences do not crystallize at exactly the same time. Even when considering quenched samples, there is probably a (very short) time lag between sequence crystallization due to inhibited motion or temperature gradients in the polymer. In view of

that, the continuous treatment seems to be the more accurate abstraction. Moreover, the continuous treatment results in the classic Renyi-limit for intermediate lengths of the crystalline sequences (figure 5.4 and 5.5). Henceforward, the continuous treatment is chosen for all further calculations.
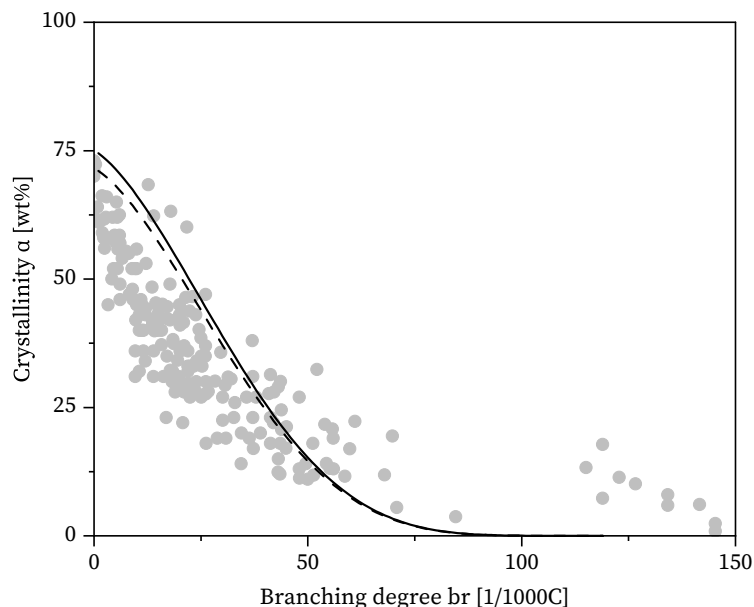

Figure 5.6: Model predictions for the crystallinity of branched polyethylene and its dependence on the counting method for the CPP with the parameters given in table 4.1 and $T = 273.15\,\mathrm{K}$, $M_N = 100\,\mathrm{kg\,mol^{-1}}$ and the length of the branch $n_{br} = 4$. Straight line: Continuous treatment, dashed line: Statistical treatment. Grey circles in the background represent the ensemble of experimental data from figure 3.3.

The target temperature, whose influence on the crystallinity is depict in figure 5.7, enters the predictive model as a variable in calculating ζ^* in eq. (4.55). However, its main influence is through incorporation of Flory's approach for branched polyolefins in eq. (4.76). This results in higher crystallinities for lower temperatures which reproduce the observation that was found in figure 3.3 from experimental data. According to Flory [4], at lower temperatures shorter crystallites can exist in equilibrium. Hence a rather short sequence that is enclosed between two branches must stay amorphous at higher temperatures but may crystallize at lower temperatures once this sequence is stable as a crystallite.

The influence of the molecular weight of polyethylene on the crystallinity which is shown in figure 5.8, affects just the crystallinity of the linear polyolefin. There is a slightly higher crystallinity for longer polyolefin chains. The exact limiting crystallinity can be discerned in figure 5.5. The type of branching n_{br} affects obviously only eq. 4.76 where branching is incorporated into the model. According to figure 5.9, longer branches result in a higher crystallinity which agrees with observations from figure 3.3.

Figure 5.7: Model predictions for the crystallinity of branched polyethylene and its dependence on the target temperature with the parameters given in table 4.1 and $M_N = 100\,\text{kg}\,\text{mol}^{-1}$, $n_{br} = 4$ and continuous treatment. Straight line: $T = 253.15\,\text{K}$, dashed line: $T = 273.15\,\text{K}$, dotted line: $T = 293.15\,\text{K}$. Grey circles in the background represent the ensemble of experimental data from figure 3.3.

Figure 5.8: Model predictions for the crystallinity of branched polyethylene and its dependence on the molecular weight with the parameters given in table 4.1 and $T = 273.15\,\text{K}$, $n_{br} = 4$ and continuous treatment. Straight line: $M_N = 10\,\text{kg}\,\text{mol}^{-1}$, dashed line: $M_N = 100\,\text{kg}\,\text{mol}^{-1}$, dotted line: $M_N = 1000\,\text{kg}\,\text{mol}^{-1}$. Grey circles in the background represent the ensemble of experimental data from figure 3.3.
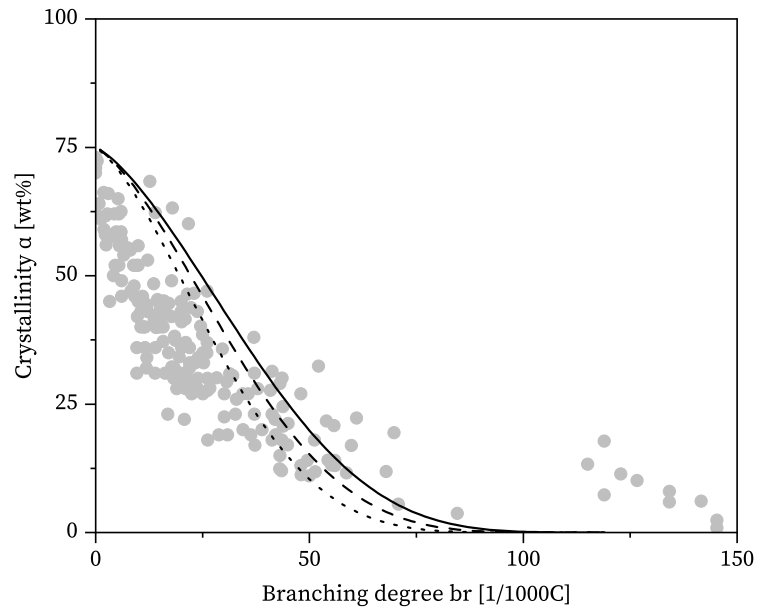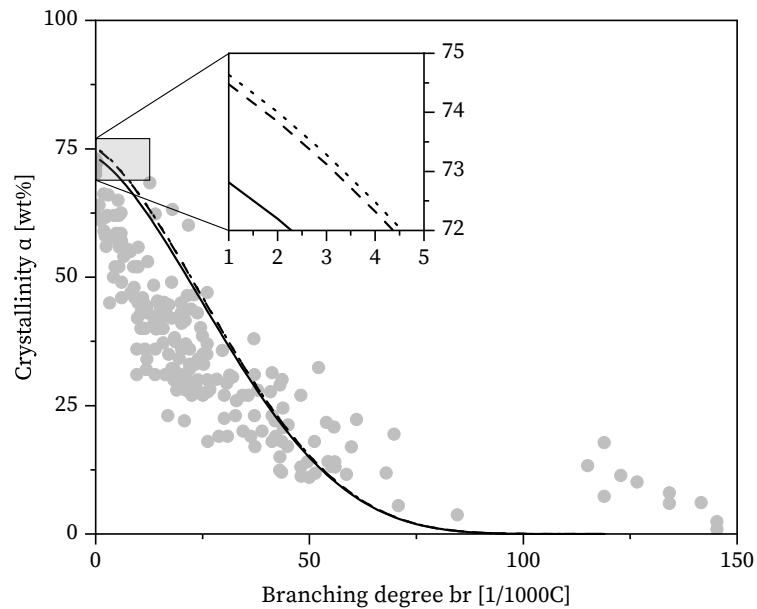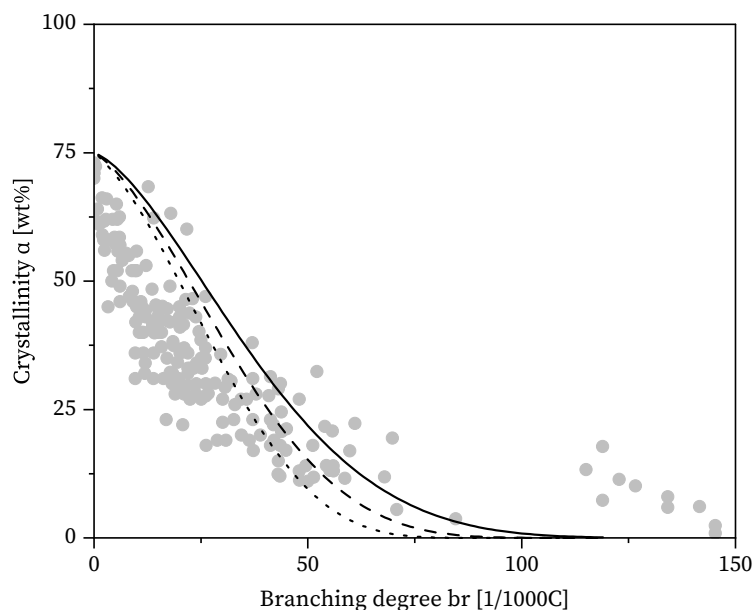
Figure 5.9: Model predictions for the crystallinity of branched polyethylene and its dependence on the type of branching with the parameters given in table 4.1 and T = 273.15 K, M_N = 100 kg mol^{-1} and continuous treatment. Straight line: n_{br} = 2, dashed line: n_{br} = 4, dotted line: n_{br} = 6. Grey circles in the background represent the ensemble of experimental data from figure 3.3.

In the next section, model predictions are compared with parts of the experimental data [75, 87, 148, 225] from figure 3.3. Since crystallinity depends on a variety of input variables, which have already been discussed, only measurements where sufficient input variables were available (at least target temperature, molar mass and branch type) will be considered.

Figure 5.10 shows the crystallinity of slowly cooled ethyl- and hexyl-branched polyethylene samples at T = 293.15 K and M_N = 78 kg mol^{-1} from [87]. The effect of lower crystallinity with increasing branching length is clearly visible. The model predicts the experimental data exceptional well, although there is a slight overestimation in the area of lower branching. The authors [87] performed measurements with samples polymerized with different catalysts. In figure 5.10 just experimental data with metallocene catalyst are included due to their narrow branching distribution. Samples with a Ziegler-Natta type of catalyst were excluded due to their broad branching distribution [87].

In figure 5.11, the influence of the side chain type on the crystallinity is depicted in form of ethyl-, propyl-, butyl- and hexyl-branched polyethylene samples. The samples were quenched at a temperature of T = 253.15 K having a molar mass of M_N = 100 kg mol^{-1} [75]. The trend of lower crystallinity with increasing branching length is observable again, but it is not as clearly as in figure 5.10.
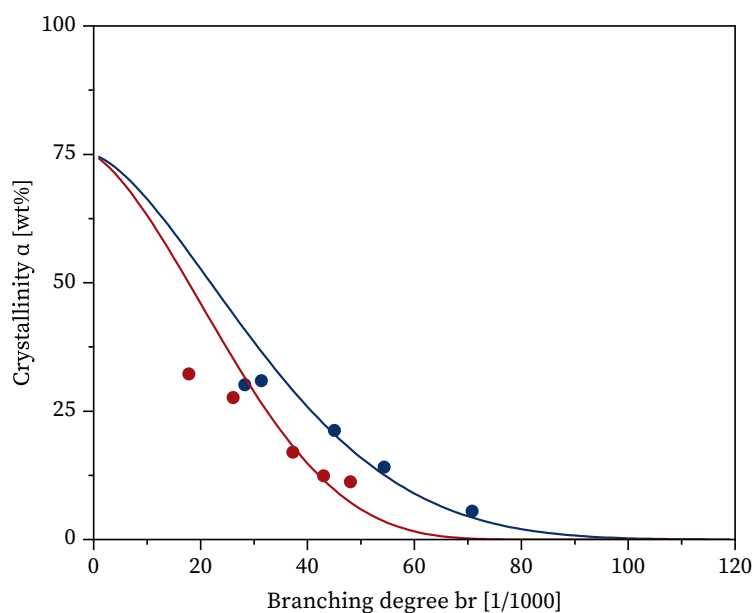
Figure 5.10: Predicted crystallinity of two slowly cooled sets of polyethylene samples each having ethyl (blue) and hexyl (red) branches with target temperature T = 293.15 K and M_N = 78 kg mol^{-1}, parameters are given in table 4.1. Experimental data taken from [87].

Figure 5.11: Predicted crystallinity of four quenched sets of polyethylene samples each having ethyl (blue), propyl (light blue), butyl (light red) and hexyl (red) branches with target temperature T = 253.15 K and M_N = 100 kg mol^{-1}, parameters given in table 4.1. Experimental data taken from [75].

71

This might be due to the fact, that the samples were quenched directly to 253.15 K instead of cooling them down slowly, thus being further away from a hypothetical equilibrium state. The combined CPP/FCA predicts the experimental data with very low deviations, especially in the area of higher branching and in the linear limit. However, the model overestimates the crystallinity in the area of lower branching. Reasons for this could be fact, that the samples were quenched rather than slowly cooled, as well as entanglements of polyethylene chains in the melt, inhibiting the crystallization process [3, 8–13, 138].

Figure 5.12 depicts the impact of the target temperature on a set of hexyl-branched polyethylene samples having a molecular weight of M_N = 78 kg mol^{-1} with a molecular weight distribution of approx. 2.35 [148, 225]. The target temperatures were 233.15 K and 293.15 K respectively. As the temperature increases, the crystallinity decreases, which is exceptional well reproduced by the model prediction.
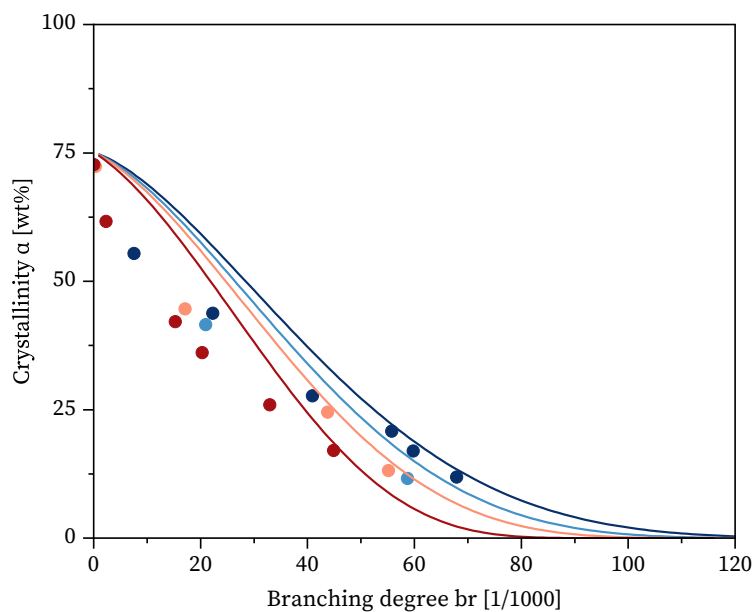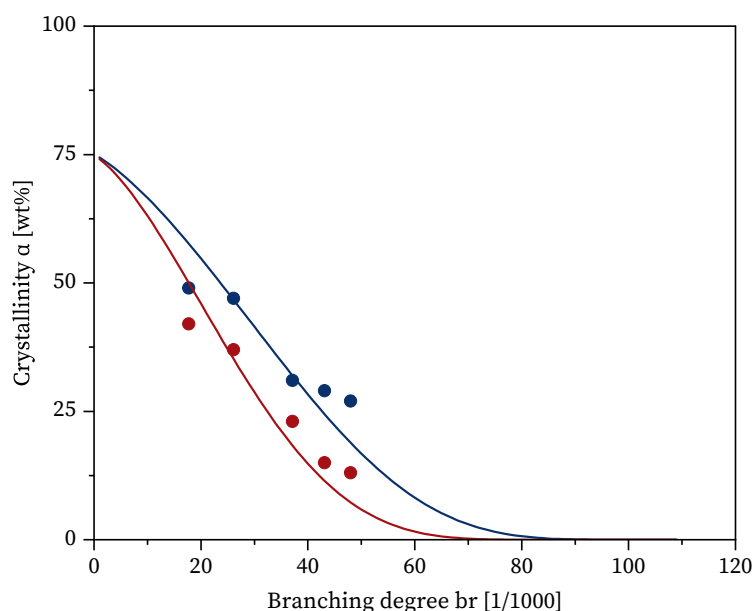

Figure 5.12: Predicted crystallinity of two slowly cooled sets of polyethylene samples having temperatures of T = 233.15 K (blue) and T = 293.15 K (red) with hexyl branches. No molecular weight is specified in the publication, so M$_N$=100 kg mol^{-1} is assumed, while parameters are given in table 4.1. Experimental data taken from [148, 225].

To investigate the temperature dependence of the crystallinity, figure 5.13 shows the crystallinity for fixed branching degrees as a function of the temperature. The model correctly predicts the sigmoidal course of the temperature dependence. The slightly branched samples from Kim et al. [226] are well reproduced by the combined CPP/FCA. However, the heavily branched sample, having 43.6 br 1000C^{-1} is significantly underestimated. On the contrary, another sample from Androsch & Wunderlich [227] having a similar branching degree (43.0 br 1000C^{-1}) shows

lower crystallinities which is in high agreement with the model. Both publications ([226] and [227]) use the heating run to measure the crystallinity having the same heating rates (10 K min^{-1}). Although the molecular weight differs from M_N=23 kg mol^{-1} [226] to M_N=78 kg mol^{-1} [227], the influence in this range should be negligible (figure 5.8). The discrepancy between both experimental data sets ([226] and [227]) is pronounced at lower temperature and almost vanishes in the range of the melting temperature. Possible reasons for the discrepancy could be differences in the production of the sample. Kim et al. [226] polymerized the samples in the laboratory with a metallocene catalysts, which results in a narrow branching distribution [65]. Androsch & Wunderlich [227] used a commercial polyethylene sample with unknown polymerization procedure. Moreover, additives may influence the crystallinity.
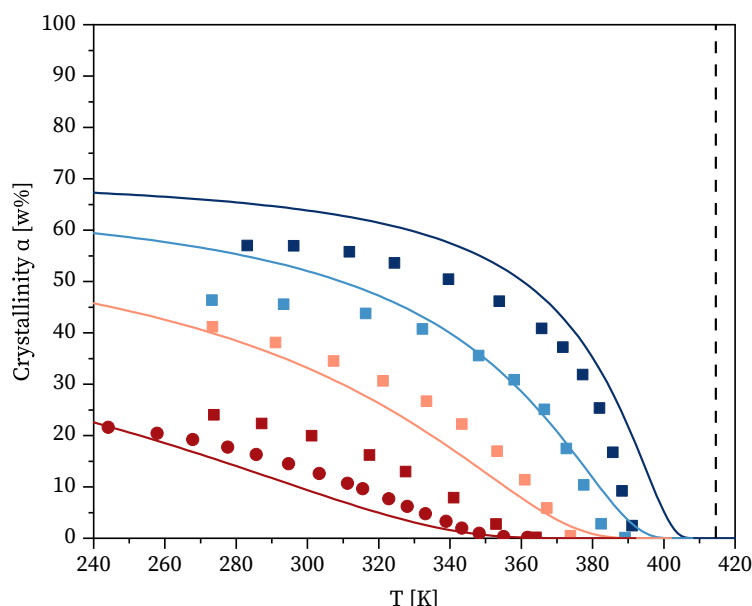
Figure 5.13: Temperature dependence of the crystallinity of hexyl-branched polyethylene having different branching degrees. Squares are from [226], having approx M_N=23 kg mol^{-1} and 9 br 1000C^{-1} (dark blue), 15.8 br 1000C^{-1} (light blue), 26.1 br 1000C^{-1} (light red) and 43.6 br 1000C^{-1} (dark red). Circles are from [227] having M_N=78 kg mol^{-1} and 43.0 br 1000C^{-1}. Straight lines are predictions with the combined CPP/FCA with parameters given in table 4.1. The dashed line denotes the melting temperature of linear polyethylene (414.6 K [70]).

The predicted melting point depression, i.e. the decrease of the melting point due to inclusion of branches, of the highly branched samples are in very good agreement with experimental data [226, 227]. However, the melting point depression of the slightly branched samples are smaller than the experiment [226].

5.2 Calculation of gas solubilities

In this chapter, the Lattice-Cluster-Theory is applied to gas solubility calculations. First, results of the parametrization of gases and polyethylene are discussed and the influence of architecture on the gas solubility in the polymer melt is investigated. Subsequently, the Car-Parking-Problem as well as the eigen-pressure approach are combined with the LCT and applied to binary calculations in semi-crystalline polyethylene. Finally, ternary systems are presented having dissolved two gases in polyethylene, whereby co- anti-solvent effects are investigated.

5.2.1 Parametrization of pure components

For the calculation of binary gas-polymer-systems, pure component parameters have to be determined. For the gases, namely the length of one cubic cell σ_i and the dispersion energy between two segments ϵ_{ii} are fitted to experimental data of the vapour pressure and the saturated liquid volumes [155–157, 161–165, 167, 170]. A range of 0.5 to 0.9 of the critical temperature T_c was used where possible. For polyethylene, σ_i and a temperature independent ϵ_{ii} are adjusted to experimental data of liquid volumes [71].

Table 5.1: Pure component parameters for the LCT with $z = 12$.

Component	M_i	σ_i[Å]	$\epsilon_{ii}^{(1)}$[K]	$\epsilon_{ii}^{(2)}$[K]	Used exp. data	data source
Polyethylene	a	2.9780	117.45	0	$v^L(1-1000\,\text{bar})$	[71]
Ethylene	2	3.4746	62.902	102.10	$p^{LV}, v^L(0.5T_c - 0.9T_c)$	[155]
1-propylene	3	3.3508	74.574	89.839	$p^{LV}, v^L(0.5T_c - 0.9T_c)$	[155]
1-butene	4	3.2718	82.187	71.493	$p^{LV}, v^L(0.5T_c - 0.9T_c)$	[161–164]
1-hexene	6	3.1937	88.963	59.998	$p^{LV}, v^L(0.5T_c - 0.9T_c)$	[165, 167, 170]
Carbon dioxide	3	2.7097	53.549	131.72	$p^{LV}, v^L(0.7T_c - 0.9T_c)$	[155]
Nitrogen	2	3.0709	29.243	36.924	$p^{LV}, v^L(0.5T_c - 0.9T_c)$	[155]
Methane	1	4.0623	50.664	111.41	$p^{LV}, v^L(0.5T_c - 0.9T_c)$	[155]
n-butane	4	3.3515	83.071	74.252	$p^{LV}, v^L(0.5T_c - 0.9T_c)$	[155]
n-pentane	5	3.3022	87.632	64.160	$p^{LV}, v^L(0.6T_c - 0.9T_c)$	[156]
n-hexane	6	3.2436	92.862	50.237	$p^{LV}, v^L(0.5T_c - 0.9T_c)$	[157]
n-heptane	7	3.2151	95.314	44.823	$p^{LV}, v^L(0.6T_c - 0.9T_c)$	[157]

a: $M_n/M_{Ethylene}$

ϵ_{ii} is assumed to have a temperature dependence according to eq. 4.33. The coordination number z is assumed to be 12 in all calculations. The two parameters for polyethylene as well as the three parameters for each gas are listed in table 5.1.

Figures 5.14 - 5.16 show calculations of the vapour pressure with the LCT for the alkanes n-butane, n-pentane, n-hexane and n-heptane; the small gases nitrogen, methane and carbon dioxide; and the alkenes ethylene, 1-propylene, 1-butene and 1-hexene respectively. Also shown is experimental data used for the parametrization and additional experimental data [155–157, 164, 165, 228]. The LCT is in strong agreement with experimental data over a wide temperature and pressure range, although longer molecules are represented with lower deviations.

Figure 5.14: Vapour pressure of parametrized n-alkanes. n-butane (straight line), n-pentane (dashed line), n-hexane (dotted line) and n-heptane (dash-dotted line). Filled symbols denote experimental data used for the parametrization [155–157], open symbols are other experimental data [155–157], stars are experimental critical points [155, 156, 228].

Figures 5.17 - 5.19 show calculations of the saturated liquid as well as vapour volume with the LCT for the same gases as in figure 5.14 - 5.16. There is a good agreement between the model and experimental saturated volumes for longer alkanes and alkenes, whereas deviations are higher for the smaller gases. The predictions for the saturated vapour volumes are in very good agreement for the ideal gas limit and worse for lower volumes. The critical point was in general overestimated by about 20 K.

Figure 5.15: Vapour pressure of parametrized small gases. Nitrogen (straight line), methane (dashed line) and carbon dioxide (dotted line). Filled symbols denote experimental data used for the parametrization [155], open symbols are other experimental data [155], stars are experimental critical points [155].

Figure 5.16: Vapour pressure of parametrized 1-alkenes. Ethylene (straight line), 1-propylene (dashed line), 1-butene (dotted line) and 1-hexene (dash-dotted line). Filled symbols denote experimental data used for the parametrization [155, 163–165, 167], open symbols are other experimental data [155, 164, 165], stars are experimental critical points [155, 164, 165].
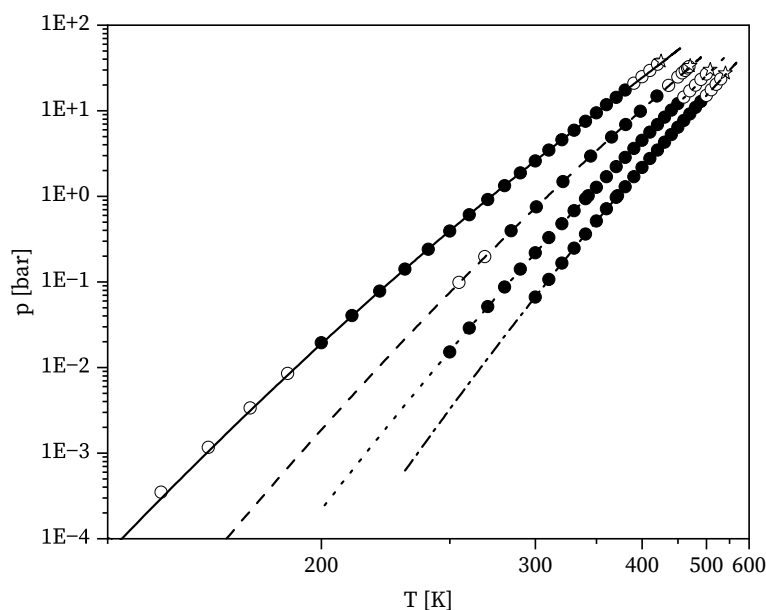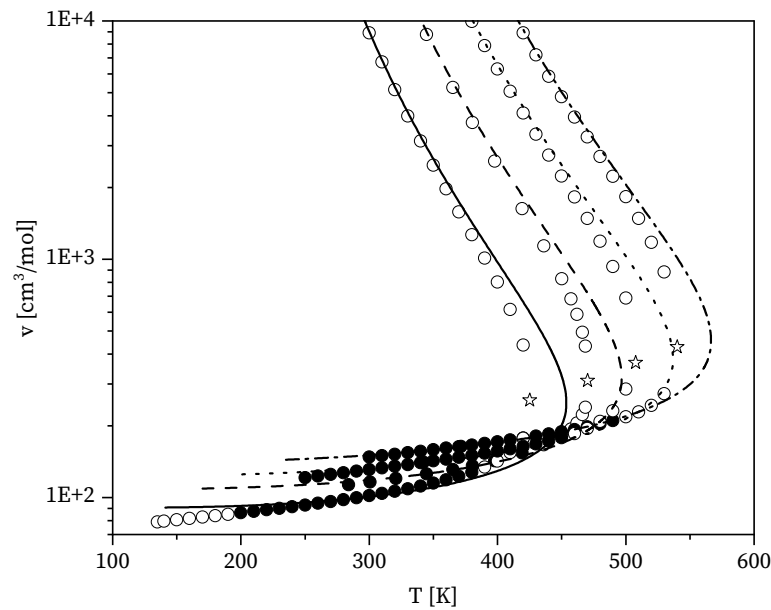
Figure 5.17: Saturated volumes of the parametrized n-alkanes. N-butane (straight line), n-pentane (dashed line), n-hexane (dotted line) and n-heptane (dash-dotted line). Filled symbols denote experimental data used for the parametrization [155–157], open symbols are other experimental data [155–157], stars are experimental critical points [155, 156, 228].
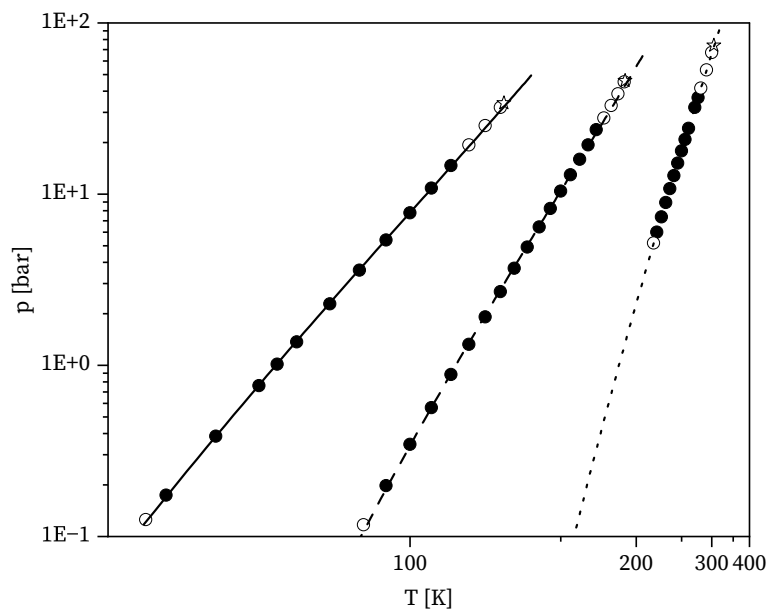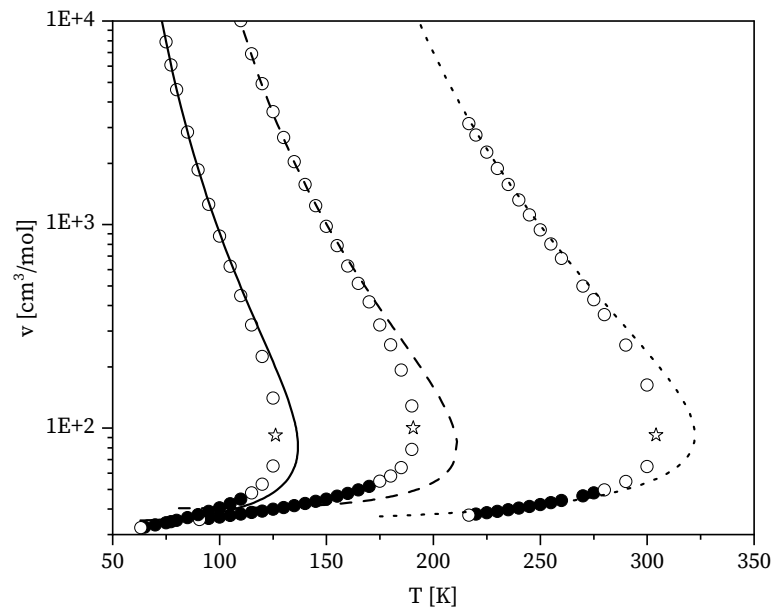

Figure 5.18: Saturated volumes of the parametrized small gases. Nitrogen (straight line), methane (dashed line) and carbon dioxide (dotted line). Filled symbols denote experimental data used for the parametrization [155], open symbols are other experimental data [155], stars are experimental critical points [155].
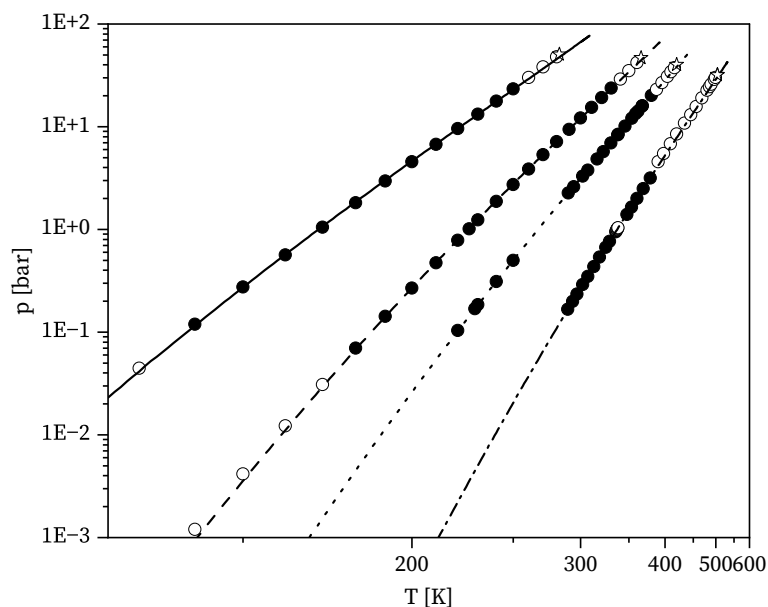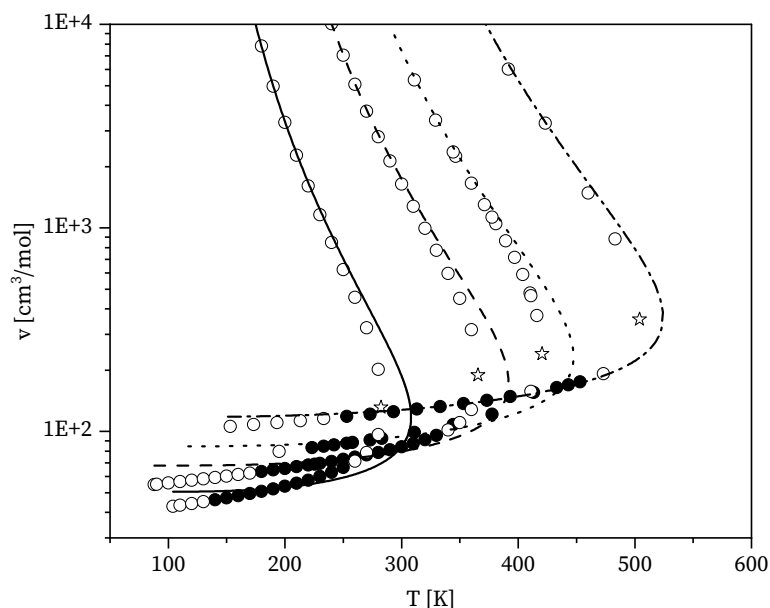
Figure 5.19: Saturated volumes of parametrized 1-alkenes. Ethylene (straight line), 1-propylene (dashed line), 1-butene (dashed line) and 1-hexene (dash-dotted line). Filled symbols denote experimental data used for the parametrization [155, 161, 162, 170], open symbols are other experimental data [155, 161, 162, 170, 171], stars are experimental critical points [155, 162, 228].

In order to investigate the physical relevance of the parameters and the scalability in terms of molar mass, the length of one cell over the segment number M is presented in figure 5.20. Included are alkanes and alkenes as well as a regression from Langenbach & Enders [211], who parametrized the LCT in contrast to this work with two parameters. σ_i decreases with increasing molar mass, which can be described by the fact, that shorter molecules have a higher amount of CH_3-groups occupying more space in comparison to CH_2-groups. Methane, composed of just one CH_4-group requires more than 4 Å cell length. Alkenes follow the same trend while having a slightly shorter cubic cell length compared to the corresponding alkane. This can be explained by the fact that alkenes contain two H-atoms less compared to alkanes, requiring less space. Moreover double bonds are shorter compared the single bonds [67]. Additionally the parameters are in high agreement with the results from Langenbach & Enders [211].

Figure 5.21 shows the dispersion forces per molecule $M \cdot \epsilon$ over the segment number M for alkanes, alkenes and a linear regression from the same set of parameters as mentioned above [211]. Since Langenbach & Enders [211] used a temperature independent dispersion energy parameter, an arbitrary temperature of 298.15 K was taken for eq. 4.33, in order to compare both sets of parameters. Clearly, the dispersive forces are proportional to the segment number and show similar results for alkanes and alkenes, as expected.
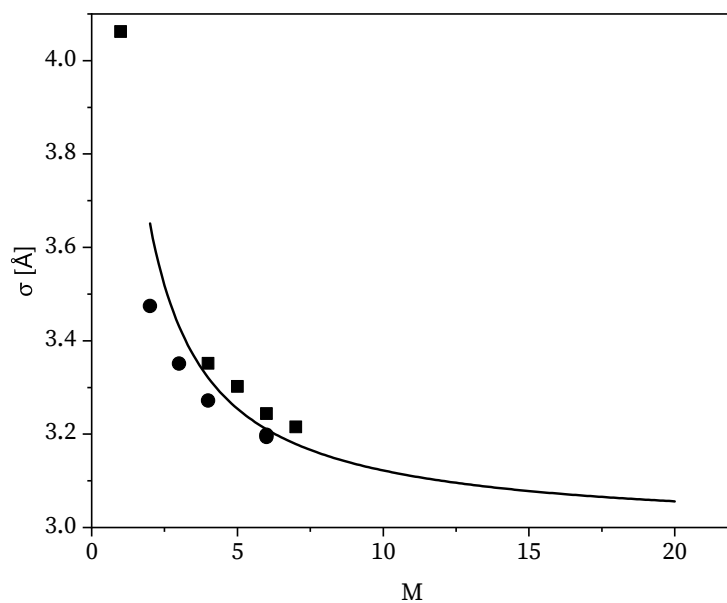
Figure 5.20: Length of one cell over the segment number. Squares are alkanes while circles are alkenes. The line denotes a regression from LCT alkane parameters from Langenbach [211].
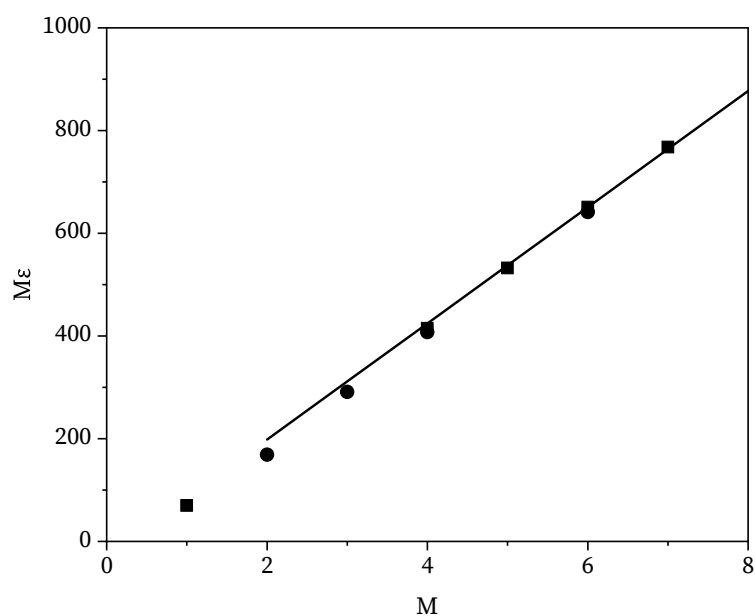
Figure 5.21: Dispersion energy of a molecule per segment number for 298.15 K. Squares are alkanes while circles are alkenes. The line denotes a linear regression from LCT alkane parameters from Langenbach & Enders [211].

There is a consistent trend towards slightly lower dispersion energies for alkenes compared to alkanes, which can be explained by the fact, that alkenes contain two H-atoms less, resulting in less dispersive forces between different molecules [67]. Furthermore the size of alkenes is lower due to the two missing H-atoms, since dispersive forces correlate with the surface, which leads to a slightly lower dispersion energy as well [67]. Lower dispersion energies are also the reason, why the boiling point of alkenes is always slightly lower than that of alkanes.

Figure 5.22 shows the adjusted liquid volumes of polyethylene between 1 bar and 1000 bar resulting in the parameters of table 5.1. A temperature independent dispersion energy and therefore only two parameters are used for polyethylene, since the representation of experimental data is in very good agreement and another temperature dependent dispersion energy parameter would be insignificant small and is therefore unnecessary.
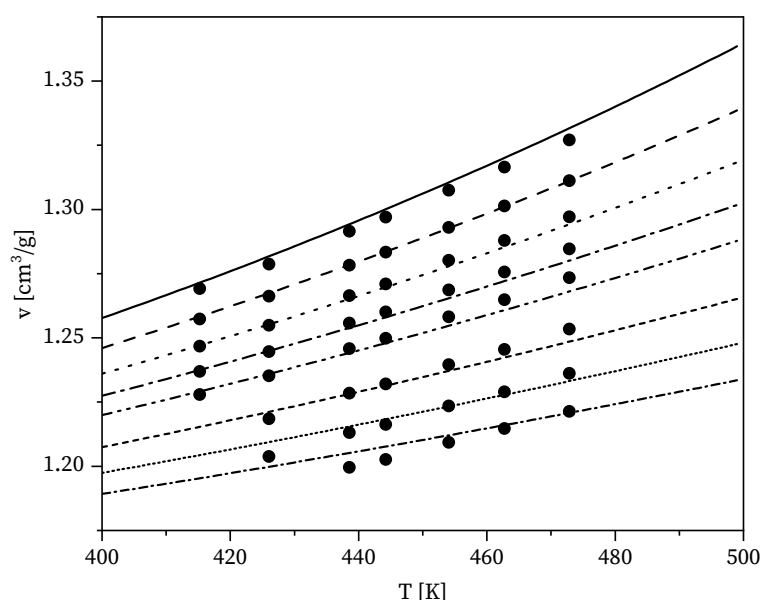
Figure 5.22: Liquid volumes of polyethylene used for parametrization at 1 bar (straight line), 100 bar (dashed line), 200 bar (dotted line), 300 bar (dash-dotted line), 400 bar (dash-dash-dotted line), 600 bar (short-dashed line), 800 bar (short-dotted line) and 1000 bar (short dash-dotted line). Circles denote experimental data used for the parametrization [71]. Polyethylene has a branching degree of 1.5 br 1000C^{-1} and a molar mass of 18 310 g mol^{-1}.

5.2.2 Binary systems

For the calculation of binary gas-polymer-systems, a temperature dependent binary interaction parameter k_{ij} is fitted to gas solubilities in the melt, which corrects the dispersion energy between unlike molecules $\Delta\epsilon_{ij}$ (eqn. 4.34 and 4.35). The coefficients for the calculation of the k_{ij} are listed in table 5.2. 1-hexene has no temperature dependence since only one isotherm in molten polyethylene was found in literature.

Table 5.2: Coefficients for the binary interaction parameter in eq. 4.35.

Gas + PE	$a_{ij} \cdot 10^3$	$b_{ij} \cdot 10^3$ K^{-1}	data source
Ethylene	-68.566	0.77660	[24]
1-propylene	82.997	0.072106	[24]
1-butene	-80.851	0.35244	[24]
1-hexene	34.655	0	[31]
Carbon dioxide	97.306	0.021823	[191]
Nitrogen	86.519	0.74649	[92]
Methane	-48.949	2.4810	[32]
n-butane	0.34275	0.19240	[201]
n-pentane	30.952	-0.0016420	[203]
n-hexane	0.17493	0.10327	[27]
n-heptane	-30.300	0.18337	[187]

5.2.2.1 Solubility in molten polyethylene

In this subsection, the solubility of gases in molten polyethylene, e.g. above the melting temperature, is investigated. First, the adjustment of the binary interaction parameter is discussed. Afterwards, the influence of the branching and the molecular weight is investigated and compared with experimental data from the literature [24, 31]. Ethylene is chosen as a model system, due to its high relevance as monomer in the polymerization process. Furthermore, plenty of experimental data considering this system can be found in literature [24, 31] and both the influence of branching and the molar mass can be evaluated quantitatively.

Figure 5.23 shows the calculated isotherms with the LCT at 413.15 K, 443.15 K and 473.15 K and k_{ij} according to table 5.2. There is a high agreement between the model and the experimental data.

Figure 5.23: Solubility of ethylene in molten polyethylene having M_N=1.94 kg mol^{-1} at 413.15 K (dark blue), 443.15 K (light red) and 473.15 K (dark red). Experimental data from [24] and lines are calculations with the LCT with k_{ij} according to table 5.2. Data points in brackets were not included in the adjustment.

However, the data points of the highest pressure were excluded from the adjustment due to questionable solubility values. This is probably due to the experimental difficulties of high-pressure measurements at that time. At high pressure, beyond ca. 500 bar, the LCT predicts a so-called inverse solubility behaviour. From this point on, the solubility increases with increasing temperature. The prediction is in agreement with results from Maloney & Prausnitz [89], who predicted a turnover point to inverse solubility behaviour at around 500 bar inside a temperature range of 423.15 K to 573.15 K with help of a free-volume theory.

The solubility of 1-propylene is shown in figure 5.24, accompanied by calculations with the LCT. The measurements are well described by the LCT, although the curvature at 413.15 K does not fit the experimental data exactly. This is due to the fact, that the critical point is calculated by the LCT to 391.5 K, which explains the beginning sigmoidal bending of the isotherm. The critical point, however, is overestimated by the LCT, which is why the experimental data do not show a significant bending at this temperature.

Figure 5.25 shows experimental data of 1-butene in molten polyethylene and calculations with the LCT. The data, which was used for the parametrization [24] is well described by the LCT. Moreover, additional experimental data at 493.15 K [104, 133] is predicted accurately. The solubility of 1-hexene is show in figure 5.26, whereby only a single isotherm is available in literature. The LCT is in well agreement with experimental data.
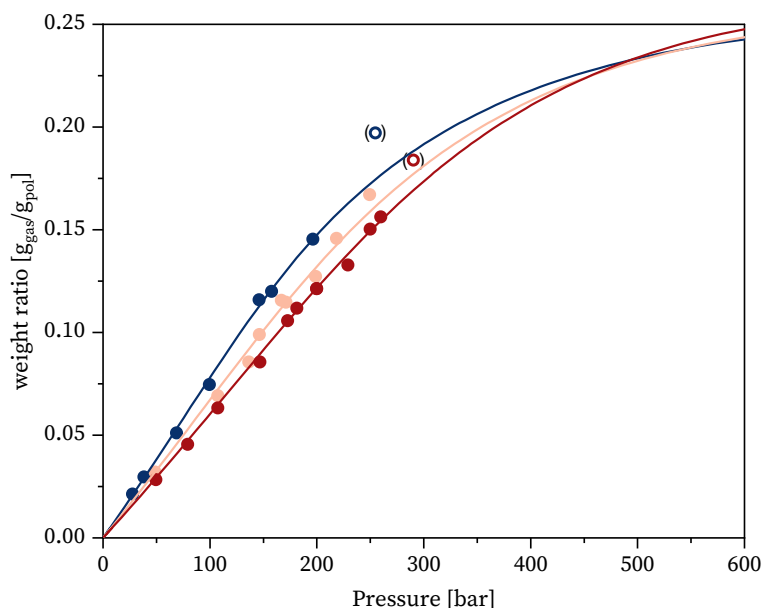
Figure 5.24: Solubility of 1-propylene in molten polyethylene having M_N=1.94 kg mol^{-1} at 413.15 K (dark blue), 443.15 K (light red) and 473.15 K (dark red). Experimental data from [24] and lines are calculations with the LCT with k_{ij} according to table 5.2.
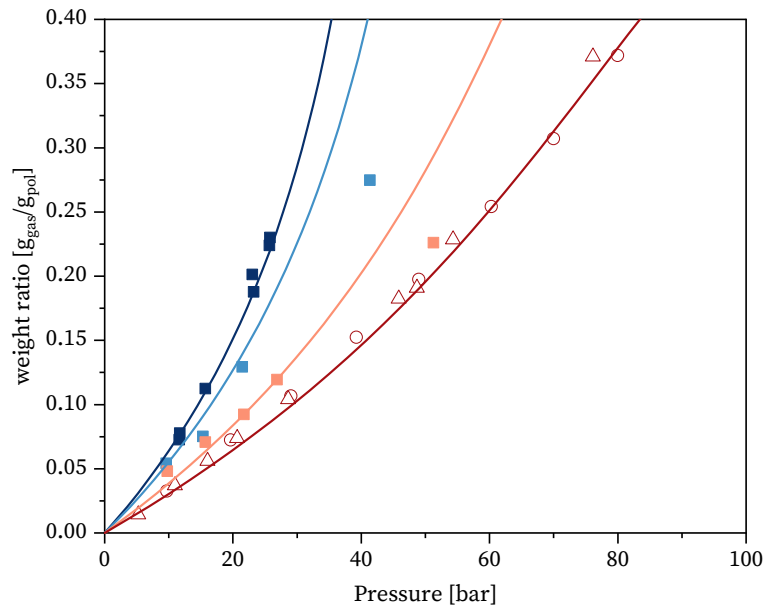
Figure 5.25: Solubility of 1-butene in molten polyethylene having M_N=1.94 kg mol^{-1} at 428.15 K (dark blue), 438.15 K (light blue), 468.15 K (light red) and 493.15 K (dark red). Filled symbols denote experimental data used for the parametrization (squares: [24]), open symbols are other experimental data (circles: [104], triangles up: [133]). Lines are calculations with the LCT with k_{ij} according to table 5.2.

Only at high amounts of dissolved gas there are some deviations, which can be explained by the fact, that in this area the overall pressure is close to the vapour pressure of 1-hexene, being 8.4 bar at 423.15 K according to the LCT. However, reliable experimental vapour pressure data is not available in this temperature range, and since the vapour pressure is strongly affecting the solubility in this pressure range, a small overestimation of the vapour pressure at 423.15 K leads to a significant underestimation of the solubility in this area.
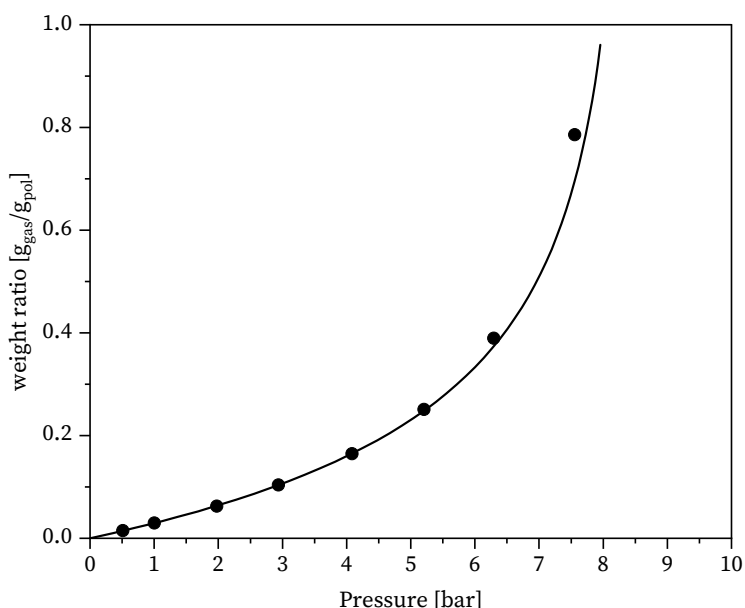
Figure 5.26: Solubility of 1-hexene in molten polyethylene at 423.15 K. No molecular weight was specified, hence M_N=20 kg mol^{-1} was assumed. Experimental data from [31] and lines are calculations with the LCT with k_{ij} according to table 5.2.

Figure 5.27 shows experimental data of carbon dioxide which was used for the adjustment of k_{ij} [191], accompanied by LCT calculations. The model is able describe the three isotherms precisely.

Figure 5.28 shows calculations of the solubility of nitrogen in polyethylene with the LCT and experimental data which was used for the reparametrization [33]. The LCT is able to describe the measurements at the low and medium pressure successfully. At higher pressure (>500 bar), the experimental data show more scattered behaviour which may be down to the novelty and experimental difficulties of the used pressure decay method at that time. Furthermore, swelling behaviour of the sample was ignored [32], which introduces inaccuracies especially at high pressure.

The solubility of methane in molten polyethylene is shown in figure 5.29. The molecular weight is not given in the publication [32]. However, the used polyethylene sample was characterized elsewhere [229], resulting in M_N=9 kg mol^{-1}.
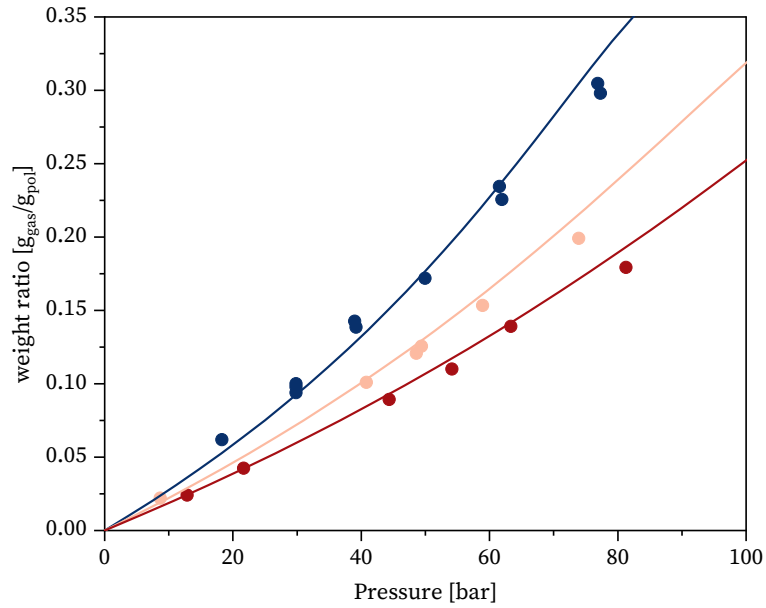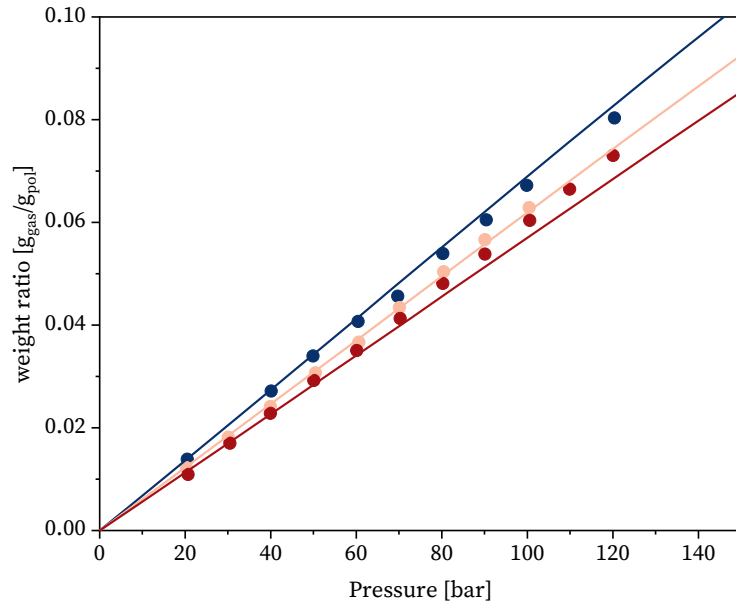
Figure 5.27: Solubility of carbon dioxide in molten polyethylene having M_N=15.2 kg mol^{-1} at 423.15 K (blue), 448.15 K (light red) and 473.15 K (dark red). Experimental data from [191] and lines are calculations with the LCT with k_{ij} according to table 5.2.


Figure 5.28: Solubility of nitrogen in molten polyethylene at 398.95 K (dark blue), 428.55 K (light blue), 431.4 K (light red) and 499.25 K (dark red). No molecular weight was specified, hence M_N=20 kg mol^{-1} was assumed. Experimental data from [33] and lines are calculations with the LCT with k_{ij} according to table 5.2.

Figure 5.29: Solubility of methane in molten polyethylene at different temperatures. Filled symbols denote experimental data used for the parametrization (squares: [32]), open symbols are other experimental data (circles: [95], triangles up: [33]). No molecular weight was specified, hence M_N=20 kg mol^{-1} was assumed. Lines are calculations with the LCT with k_{ij} according to table 5.2.

The results of the parametrization confirm the observation, that the isotherms lie close to each other, especially in the low-pressure region below 250 bar. Moreover, the LCT calculations may explain the different temperature dependencies, observed in figure 3.10. The data from Lundberg [32], used for parametrization show an inverse solubility behaviour mainly in the high-pressure region, correctly described by the LCT. However, the LCT shows a point of chance of the inverse solubility between 50 bar to 200 bar, depending on the temperature. The higher the temperature, the lower the point of change. Below this point, a higher temperature results in a lower solubility, which is in agreement with the lowest isotherm at 413.19 K of Lundbergs second publication [33]. This could also explain, why Lundbergs first measurements [32] at 140 bar show an inverse solubility behaviour considering the high temperatures pairs 461.55 K and 500.75 K, but a normal solubility behaviour for the lower temperature pairs 428.55 K and 461.55 K, correctly described by the LCT. A detailed investigation of the temperature influence is shown later.

The solubility of n-butane in molten polyethylene is shown in figure 5.30. Since the polyethylene was not characterized in terms of the molecular weight, a value of M_N=20 kg mol^{-1} was assumed, since at this magnitude, there is no significant influence of the molecular weight. Figure 5.31 shows the solubility of n-pentane in molten polyethylene having a molecular weight of M_N=76 kg mol^{-1}. The binary interaction of n-hexane was adjusted to solubility data at 1 bar with

a polyethylene sample having M_N=16.6 kg mol^{-1}, as shown in figure 5.32. The lowest isotherm was excluded from parametrization, since at 397.15 K, partial crystallization cannot be ruled out. Figure 5.33 shows the solubility of n-heptane in polyethylene having a molecular weight of M_N=13.7 kg mol^{-1}, precisely described by the LCT.
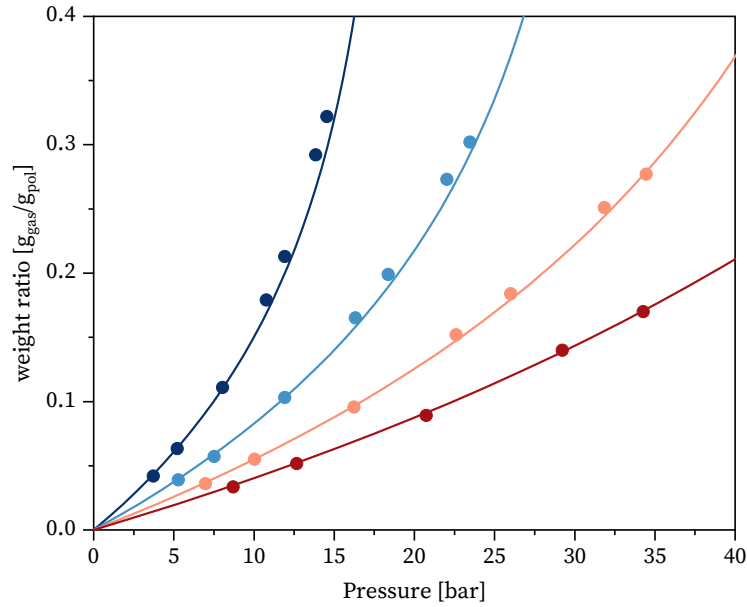
Figure 5.30: Solubility of n-butane in molten polyethylene at 383.15 K (dark blue), 413.15 K (light blue), 443.15 K (light red) and 473.15 K (dark red). No molecular weight was specified, hence M_N=20 kg mol^{-1} was assumed. Experimental data from [201] and lines are calculations with the LCT with k_{ij} according to table 5.2.
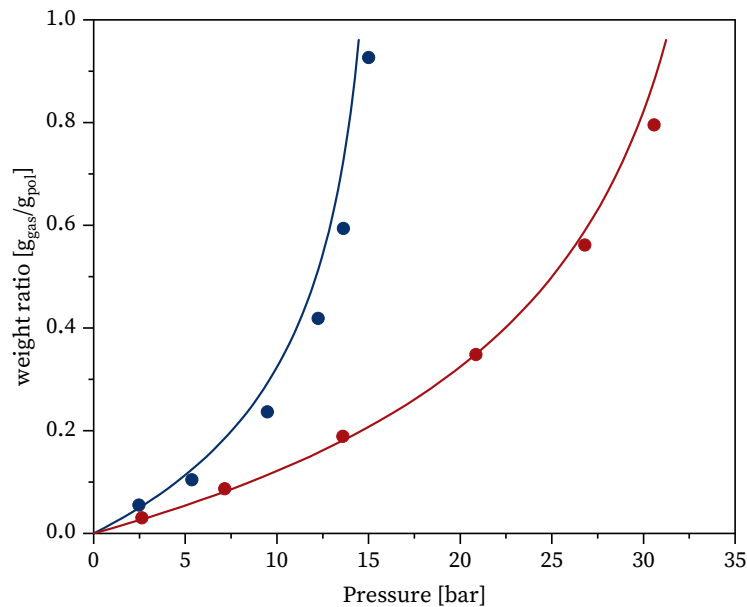
Figure 5.31: Solubility of n-pentane in molten polyethylene having M_N=76 kg mol^{-1} at 423.65 K (blue) and 474.15 K (red). Experimental data from [203] and lines are calculations with the LCT with k_{ij} according to table 5.2.
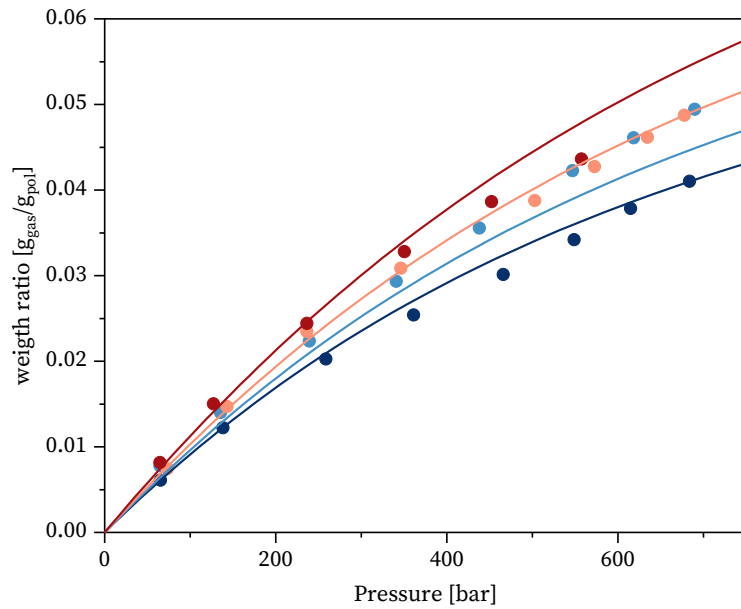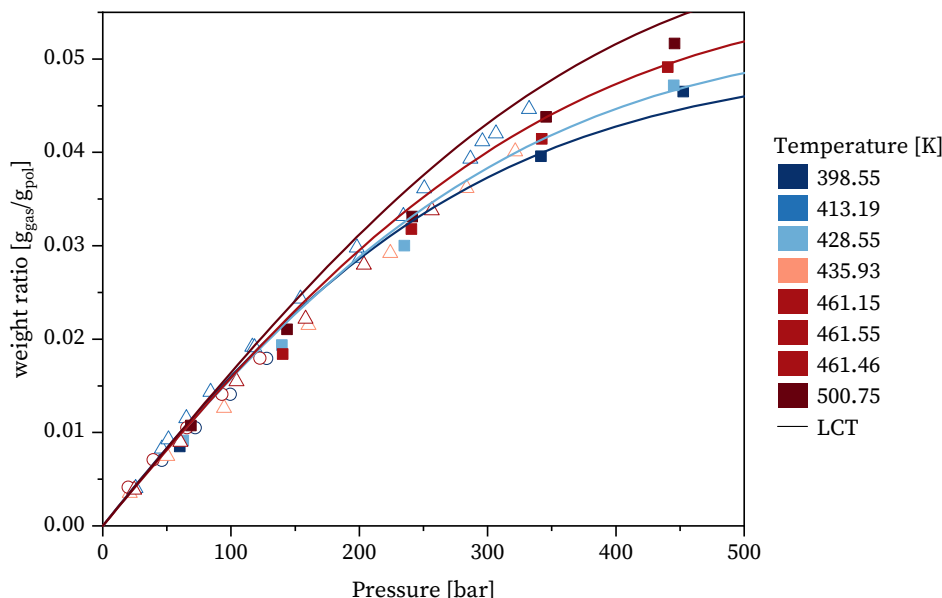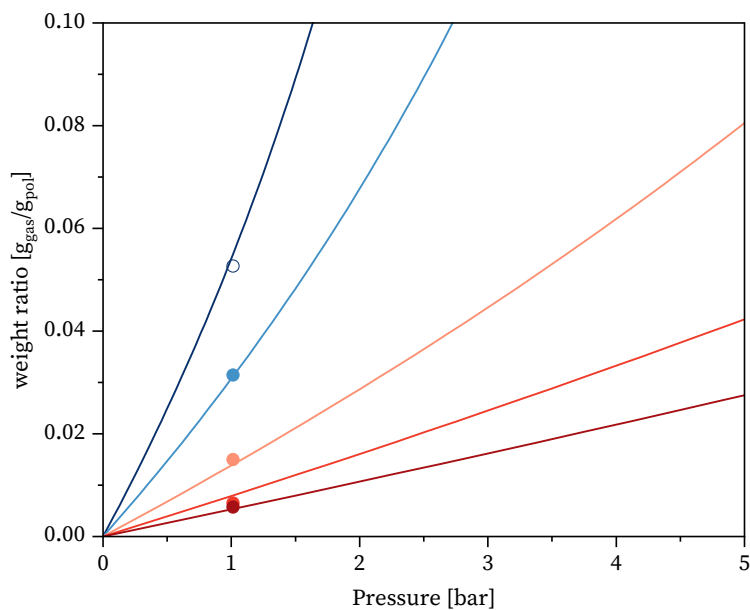
Figure 5.32: Solubility of n-hexane in molten polyethylene having M_N=16.6 kg mol^{-1} at 397.15 K (dark blue), 423.15 K (light blue), 473.15 K (light red), 523.15 K (red) and 573.15 K (dark red). Experimental data from [27]; filled symbols denote experimental data used for the parametrization, open symbols are other experimental data. Lines are calculations with the LCT with k_{ij} according to table 5.2.
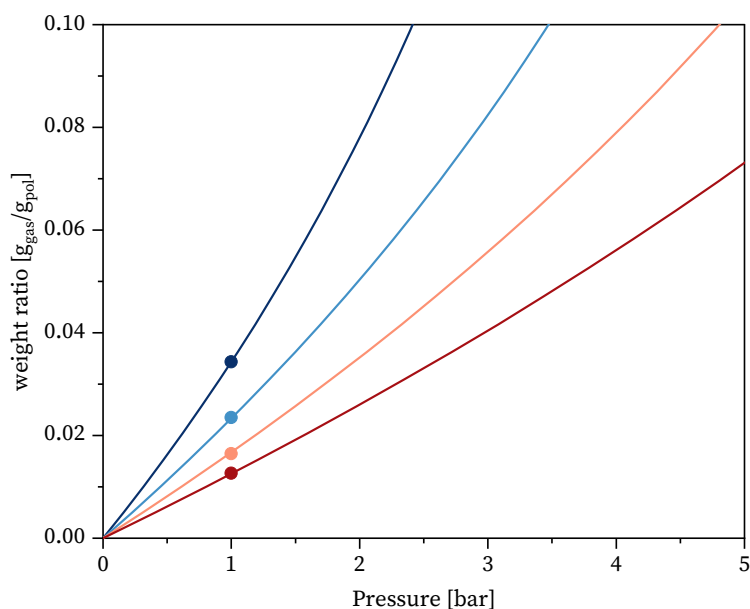
Figure 5.33: Solubility of n-heptane in molten polyethylene having molecular weights ranging from M_N=10 kg mol^{-1} to M_N=50 kg mol^{-1} at 443.15 K (dark blue), 463.15 K (light blue), 483.15 K (light red) and 503.15 K (dark red) having M_N=13.7 kg mol^{-1}. Experimental data from [187] and lines are calculations with the LCT with k_{ij} according to table 5.2.

Influence of temperature

Although, the gas solubility mainly decreases with increasing temperature, there are cases where the opposite is true, which is called inverse solubility. This behaviour depends on the type of gas and on the conditions, e.g. temperature and pressure. For gases having a low critical temperature [27, 45, 90], the inverse solubility behaviour can be found at temperatures and pressure, where gas solubility plays a role.

This applies for example to methane and nitrogen, whose solubility is shown over the temperature at a fixed pressure of 1 bar and 100 bar respectively in figure 5.34. A normal solubility behaviour, which can be found for bigger gases having a higher critical temperature, applies for low temperatures, while inverse solubility behaviour can be found for higher temperatures. The higher the pressure the more the minimum of solubility is shifted towards lower temperatures. It has to be mentioned that the solubility in figure 5.34 is calculated ignoring all effects of crystallinity. For a system below approx. 400 K, a significant lower solubility may be observed, depending on the branching degree. However, figure 5.34 is not just a hypothetical case, since for highly branched polyethylene, the sample would be completely amorphous, leading to the prescribed solubility.
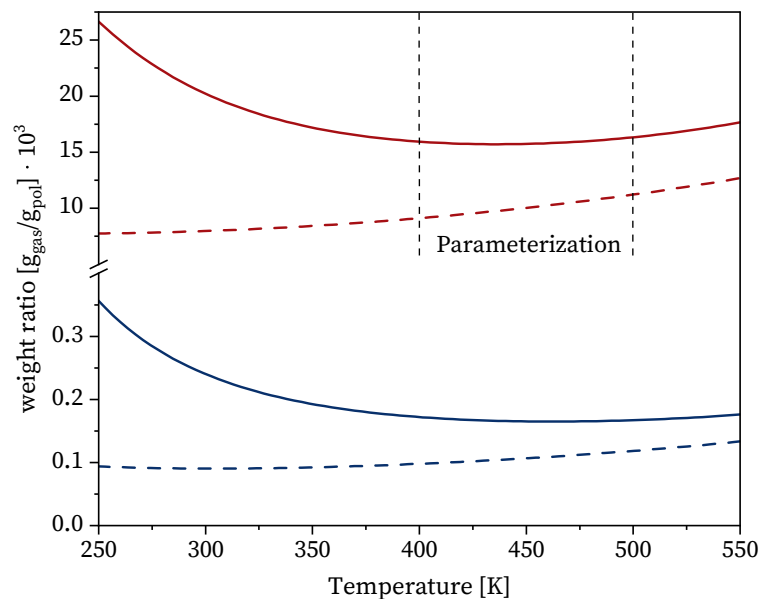
Figure 5.34: Gas solubility calculations with the LCT of methane (straight line) and nitrogen (dashed line) at 1 bar (blue lines) and 100 bar (red lines) over the temperature.

It now appears that the solubility of methane has a minimum of solubility between 400 K and 500 K for 100 bar, which is the range where the binary interaction parameter is adjusted (figure 5.29). This clarifies, why the experimental data concerning the solubility of methane in molten

polyethylene (figure 3.10) lie very close to each and show no clear temperature dependence, while the LCT shows intersecting isotherms below 200 bar (figure 5.29). Nitrogen, on the other hand, shows a weak inverse solubility behaviour between 400 K and 500 K for 100 bar, e.g. a slight increase of solubility with temperature, which is why experimental data concerning the solubility of nitrogen in molten polyethylene (figure 3.9) show isotherms lying close to each other, but still show a mainly consistent inverse solubility behaviour.

Influence of branching

After successfully describing the solubility in molten polyethylene, the influence of branching is investigated. Figure 5.35 shows three differently branched samples having a branching degree of $0\,\text{br}\,1000\text{C}^{-1}$, $19.4\,\text{br}\,1000\text{C}^{-1}$ and $23.8\,\text{br}\,1000\text{C}^{-1}$ from Novak et al. [31], not used for adjustment of k_{ij}, and the corresponding predictions with the LCT.
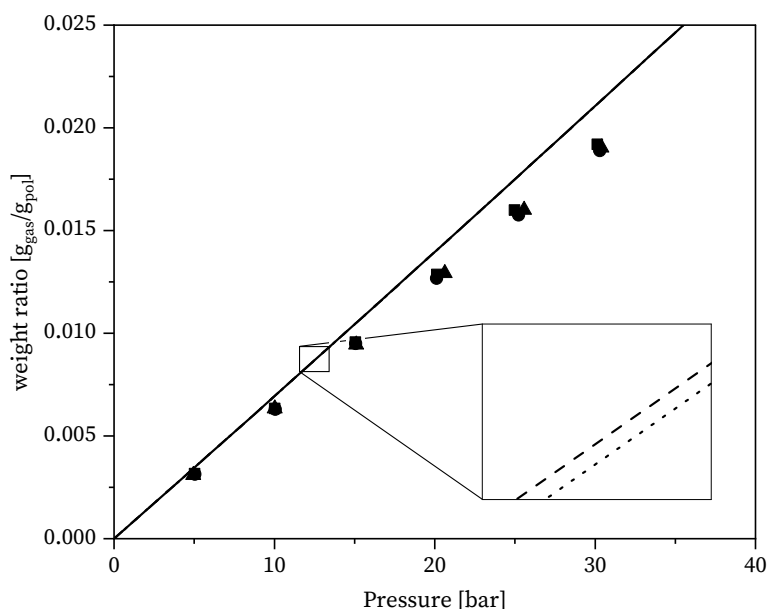
Figure 5.35: Influence of branching on solubility of ethylene in polyethylene melt at 423.15 K. Linear polyethylene with a branching degree of $0\,\text{br}\,1000\text{C}^{-1}$ (squares, straight line) as well as branched polyethylene with $19.4\,\text{br}\,1000\text{C}^{-1}$ (circles, dashed line) and $23.8\,\text{br}\,1000\text{C}^{-1}$ (triangles, dotted line). A molecular weight of $20\,\text{kg}\,\text{mol}^{-1}$ was assumed, experimental data from [31].

A slight overprediction of the solubility may be ascribed to the fact, that the polyethylene samples are not characterized in terms of molar mass and molar mass distribution, so a molar mass of $20\,\text{kg}\,\text{mol}^{-1}$ was assumed, since at this magnitude, there is no significant influence of the molecular weight (the influence of the molecular weight is investigated in the next section). Furthermore, additives can manipulate the solubility, especially because the polyethylene sample from the parametrization [24] was received from industry (VEB Leuna-Werke), while the

investigated sample in figure 5.35 was polymerized in the laboratory.

The model predicts, that there is no significant influence of chain branching on the gas solubility in the melt, which is in perfect agreement with the experimental data. This is an important and fundamental observation, as there is not much literature that has investigated the influence of chain branching individually while keeping other effects, such as molar mass distribution, different additives or experimental setups, unchanged. The model results are in agreement with findings from Newman & Prausnitz [100] and Schreiber et al. [30], who calculated interaction parameters from sorption experiments with different hydrocarbon-polyethylene-copolymers, which were mainly independent of the branching. Sorption experiments from Lundberg et al. [32, 33], high-pressure experiments from Cernia & Mancini [34] and Ehrlich [35] as well as molecular simulations from Banaszak et al. [101] reach the same result. Zimmermann et al. [36] measured the solubility of carbon dioxide in polyethylene having different branching degrees, finding no significant difference in the solubility. However, data from Hasan et al. [37], who measured the solubility of CO_2 in a branched and a linear polypropylene sample, show a significant difference between those two samples. Despite the fact, that this is of course another polymer, in the publication, two different fabricates of polymers of unknown molar mass, molecular weight distribution, tacticity and quantitive branching degree were compared, which is why the effect of varying gas solubility can be ascribed to any of these unknown input variables, whereby the tacticity is most likely the source of the varying solubility.

Figure 5.36 depicts the effect of the branching on the solubility of ethylene in molten polyethylene having a fixed molar mass of $20 \, \mathrm{kg \, mol^{-1}}$ at 423.15 K. Besides the fact that the influence is very small, it can be seen, that the solubility generally decreases with increasing branching degree. From about 150 bar on, however, there is an initial increase in the solubility at low branching degrees, which decreases after a maximum. This maximum is shifted towards higher branching degrees for higher pressures. Although, the quantitative effect is small, it is of interest, to outline the qualitative influence of the chain branching in molten polyethylene. An explanation for the general decrease of solubility with increasing branching could be chain entanglements, which can increase the tension when elongating a polymer [230, 231]. Thus, polymer swelling which occurs when solving a gas in the polymer matrix is constraint by entangled chains. The general decrease in solubility with increasing branching degree might therefore be down to the fact, that more branching leads to a higher probability of chain entanglements inhibiting the polymer swelling, which reduces the solubility of gas molecules.
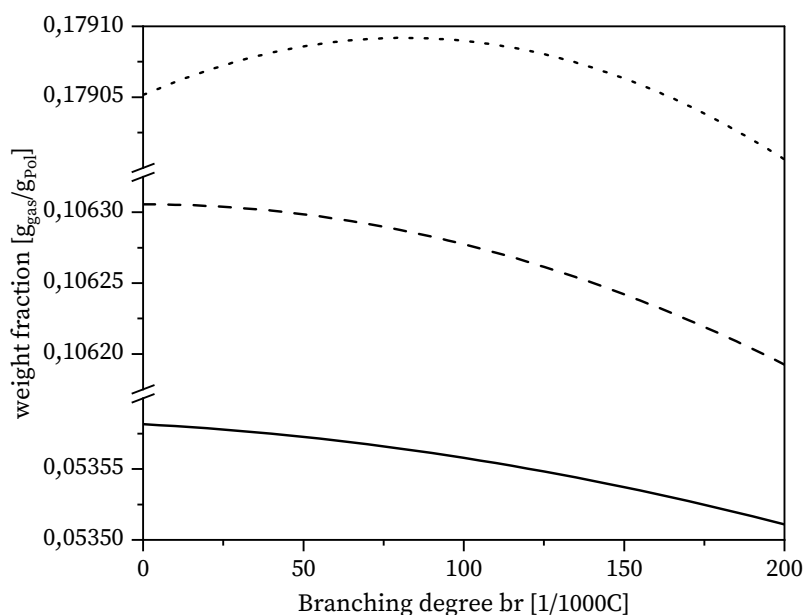
Figure 5.36: Gas solubility of ethylene in molten polyethylene at 423.15 K as a function of the branching degree at 75 bar (straight line), 150 bar (dashed line) and 300 bar (dotted line) and a molecular weight of 20 kg mol^{-1}.

However, this does not explain the initial increase in solubility and following maximum at high pressures. The reason for this might be a counter current effect caused by the volume of the pure polymer. As shown in figure 5.37, the polymers pure volume increases with increasing branching degree. A higher volume results in more space for gas molecules to penetrate the polymer matrix, provided that the pressure is high enough for a sufficient amount of gas molecules dissolving in order to make this effect significant. The increase of solubility due to this effect plays a role at low branching degrees because in this range there is a considerable increase of the pure polymer volume (figure 5.37), while at larger branching degrees the increase in volume levels off, and the effect of inhibited swelling dominates.

The system 1-hexene in polyethylene is another system whose influence on branching degree was investigated by Novak et al [31]. Figure 5.38 shows experimental data of a linear sample, which was used for adjusting the binary interaction parameter k_{ij} (table 5.2) and two branched polyethylene samples. The solubility differs by orders of magnitude compared to ethylene, also the curvature is as distinguished from ethylene. The calculations with the LCT are in good agreement with experimental data. Again, the LCT predicts correctly, that there is no significant influence of chain branching on the gas solubility.
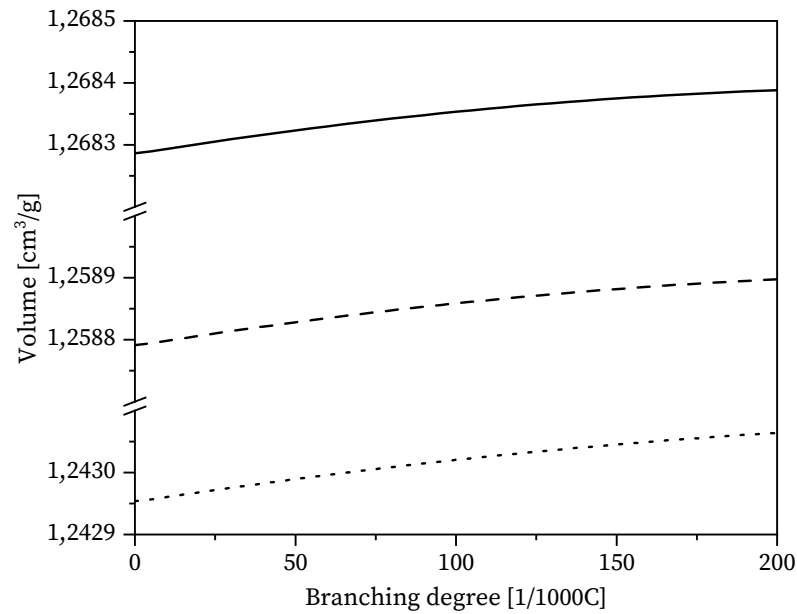
Figure 5.37: Volume of pure polyethylene at 423.15 K as a function of the branching degree at 75 bar (straight line), 150 bar (dashed line) and 300 bar (dotted line) and a molecular weight of 20 kg mol^{-1}.
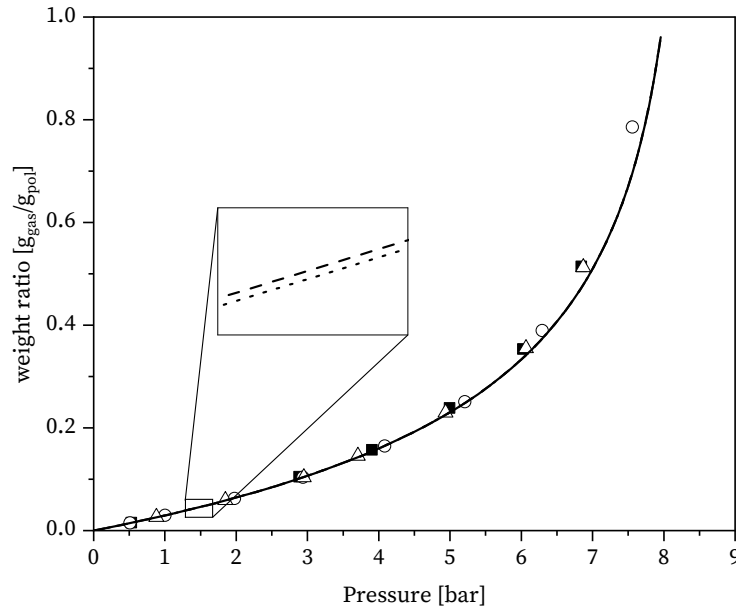
Figure 5.38: Gas Solubility of 1-hexene in polyethylene melt having different branching degrees at 423.15 K. Linear polyethylene (black squares, straight line) was used for adjusting k_{ij} (table 5.2), polyethylene with a branching degree of 19.4 br 1000C^{-1} (white circles, dashed line) and 23.8 br 1000C^{-1} (white triangles, dotted line) was predicted. A molecular weight of 20 kg mol^{-1} was assumed, experimental data from [31].

It is of course a challenging task to measure such small variations of solved gas in polyethylene melt as shown in figure 5.36, hence LCT predictions cannot yet be proven by experiments. Still, it is to my knowledge for the first time, that the actual influence of branching in the polyethylene melt, however small, is predicted. Nevertheless, it has to be clarified that the figures shown above and the associated considerations are for a constant molar mass of $20\,\text{kg}\,\text{mol}^{-1}$. A different polyethylene sample having a different branching degree probably has a different molecular weight distribution as well, potentially outweighing the influence of branching. For this reason, the next section investigates the influence of the molar mass on the gas solubility in molten polyethylene.

Influence of molecular weight

Figure 5.39 shows the influence of the molecular weight ranging from $1\,\text{kg}\,\text{mol}^{-1}$ to $20\,\text{kg}\,\text{mol}^{-1}$ on the solubility of 1-hexene in molten linear polyethylene. The gas solubility decreases with increasing molecular weight, whereby the effect becomes almost invisible at approx. $10\,\text{kg}\,\text{mol}^{-1}$. This upper limit where an effect of molecular weight in the solubility is discernible is in perfect agreement with experimental data, locating this limit at around $5\,\text{kg}\,\text{mol}^{-1}$ [25, 99] to $10\,\text{kg}\,\text{mol}^{-1}$ [27].
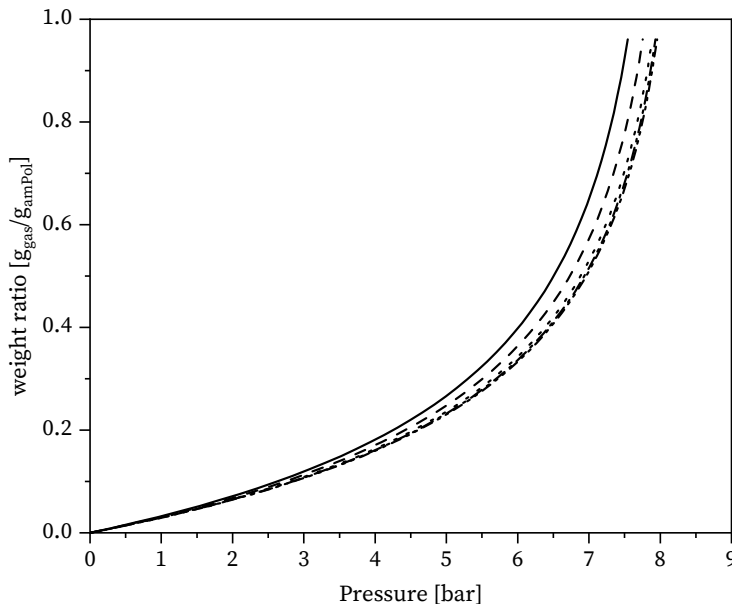
Figure 5.39: Gas Solubility of 1-hexene in polyethylene melt having different molar masses at 423.15 K and branching degree of $0\,\text{br}\,1000\text{C}^{-1}$. Molar masses are $1\,\text{kg}\,\text{mol}^{-1}$ (straight line), $2\,\text{kg}\,\text{mol}^{-1}$ (dashed line), $5\,\text{kg}\,\text{mol}^{-1}$ (dotted line), $10\,\text{kg}\,\text{mol}^{-1}$ (dash-dotted line) and $20\,\text{kg}\,\text{mol}^{-1}$ (dash-dash-dotted line).
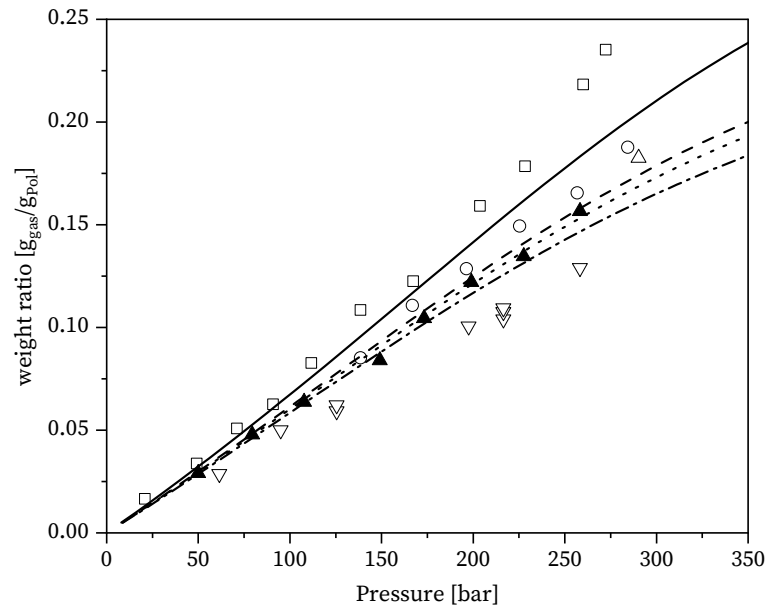
Figure 5.40: Gas Solubility of ethylene in polyethylene melt having different molar masses at 473.15 K and branching degree of 31.8 br 1000C^{-1}. Molar masses are 0.476 kg mol^{-1} (squares, straight line), 1.25 kg mol^{-1} (circles, dashed line), 1.94 kg mol^{-1} (triangles up, dotted line) and 19.5 kg mol^{-1} (triangles down, dash-dotted line). Filled symbols were used for the parametrization, open symbols are predictions. Experimental data from [24] and calculation with the LCT.

To quantitatively evaluate the predicted influence of the molecular weight on the gas solubility, figure 5.40 shows the solubility of ethylene in molten polyethylene having molecular weights ranging from 0.476 kg mol^{-1} to 19.5 kg mol^{-1}. The branching degree was determined to be 31.8 br 1000C^{-1} [24], which however has minor influence on the molten system, as explained above. The polyethylene sample having M_N=1.94 kg mol^{-1} was used for the adjustment of the binary interaction parameter, all other system are predictions. Although the solubility is orders of magnitude lower compared to the solubility of 1-hexene and curvature differs significantly, the effect of the molecular weight is the same: The lower the molecular weight the higher the gas solubility, which is in well agreement with data shown [24]. The effect of the molecular weight predicted by the LCT, however, is less pronounced compared to the experimental data. Nevertheless, the samples that were predicted are unspecified in the publication except for the molecular weight. A different molecular weight distribution, a strongly deviating branching degree or samples from different manufactures with different additives can result in experimental inaccuracies.

5.2.2.2 Solubility in semi-crystalline polyethylene

In this section, all the preliminary findings are combined to a framework, that is able to predict the gas solubility in semi-crystalline branched systems: After parametrizing the pure component parameters and the binary interaction parameters with the LCT, the crystallinity is predicted by the combined CPP/FCA depending on the polymers architecture and the temperature. Finally, the impact of the crystallinity upon the gas solubility is accounted by the eigen pressure (eq. (3.3)), were mechanical arguments were taken from the literature [232]. In all calculations, the compression modulus K is 66.6 MPa and the shear modulus G is 11.3 MPa [232].

Firstly, the influence of temperature, pressure and the polymers architecture on the gas solubility of four alkenes ethylene, 1-propene, 1-butene and 1-hexene are discussed, followed by a detailed study of branching on the solubility of methane, nitrogen and carbon dioxide at atmospheric pressure. Lastly, an approach for the prediction of gas solubilities without information of the polymers architecture is presented with n-butane, n-pentane, n-hexane and n-heptane.

Ethylene

Figure 5.41 shows the solubility of ethylene in semi-crystalline polyethylene at 353.15 K. The dashed line is a calculation with the LCT, standing for the amorphous limit disregarding the effects of the crystallinity on the gas solubility. Here, no intrinsic stress is considered and hence no eigen pressure acts on the amorphous domains of the semi-crystalline polymer. Three differently branched samples of polyethylene are shown as well having butyl as branches [108]. The straight lines of the LCT account for the semi-crystalline calculations according to the branching degree. A decreasing branching degree results in a higher crystallinity, which in turn lowers the solubility by applying the eigen pressure to the phase equilibrium.

The combined framework is able to predict the gas solubility with high accuracy, especially the lowest and highest branched sample. The intermediate sample having a branching degree of $23.3 \, \text{br} \, 1000\text{C}^{-1}$ is slightly overestimated. Besides the measurement uncertainty, this may be due to the molecular weight distribution, which is not specified for this sample. Although the molecular weight of this middle sample is lower compared to the two others ($32 \, \text{kg} \, \text{mol}^{-1}$ instead of $40 \, \text{kg} \, \text{mol}^{-1}$ and $43 \, \text{kg} \, \text{mol}^{-1}$), the effect of the molecular weight both directly on the gas solubility and on the crystallinity should be negligible in this area. Only entanglements of polymer chains, inhibiting crystallization, which are neglected in the model, could be a reason. Since the molecular weight is smaller, fewer entanglements would occur, increasing the crystallinity and hence lowering the solubility.
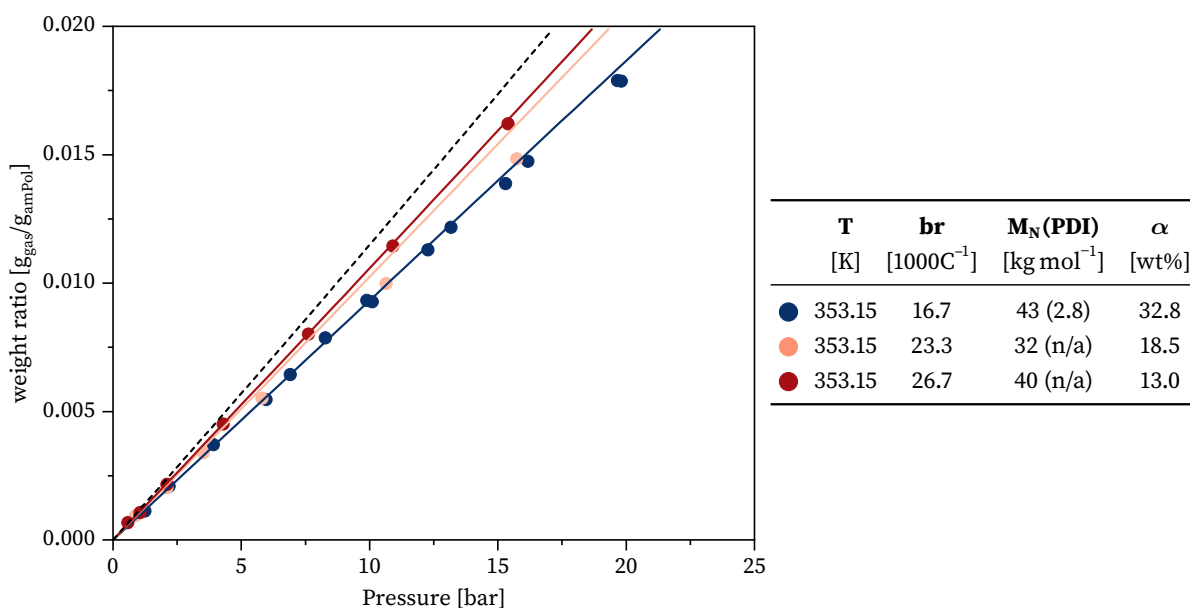
Figure 5.41: Predicted solubility of ethylene in semi-crystalline polyethylene at 353.15 K. Polyethylene has butyl branches with varying architecture, given in the legend: Branching degree and molecular weight are properties measured, the crystallinity is determined by CCP/FCA. Experimental data from [108]. Lines are the corresponding predictions with the LCT and the dashed line is the amorphous limit disregarding the crystallinity.

	T	br	M_N(PDI)	α
	[K]	[$1000C^{-1}$]	[$kg\,mol^{-1}$]	[wt%]
●	353.15	16.7	43 (2.8)	32.8
●	353.15	23.3	32 (n/a)	18.5
●	353.15	26.7	40 (n/a)	13.0

Figure 5.42: Predicted solubility of ethylene in semi-crystalline polyethylene at 358.15 K. Polyethylene has butyl branches with varying architecture, given in the legend: Branching degree and molecular weight are properties measured, the crystallinity is determined by CCP/FCA. Experimental data from [108]. Lines are the corresponding predictions with the LCT and the dashed line is the amorphous limit disregarding the crystallinity.

	T	br	M_N(PDI)	α
	[K]	[$1000C^{-1}$]	[$kg\,mol^{-1}$]	[wt%]
●	358.15	3.3	24 (n/a)	67.9
●	358.15	11.7	43 (2.6)	44.2
●	358.15	18.3	21 (2.9)	25.4

97

Figure 5.42 shows the same system at a temperature of at 358.15 K. Experimental data from the same author [108] is used, although the branching degree differs: Besides the amorphous limit, shown as dashed line, experimental data points with branching degrees ranging from 3.3 br 1000C^{-1} to 18.3 br 1000C^{-1} are shown. The branching degrees are lower compared to figure 5.41, which is why the crystallinity is higher, leading to a higher eigen pressure and hence lower gas solubilities. Moreover, the temperature is higher, resulting in a lower gas solubility as well.

	T	α
	[K]	[wt%]
	303.15	57.6
	313.15	55.7
	323.15	53.4
	333.15	50.4
	348.15	44.4
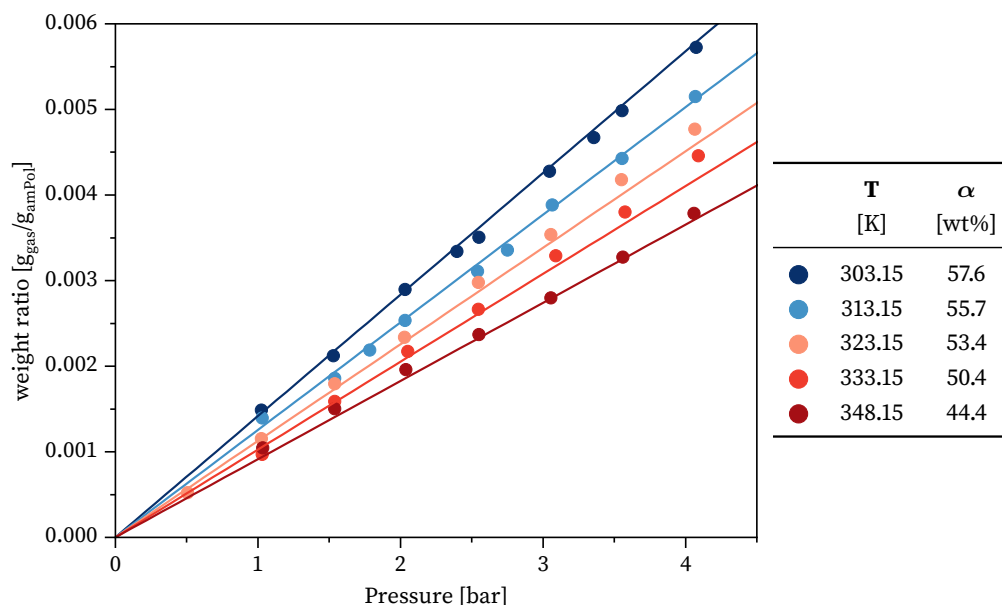
Figure 5.43: Predicted solubility of ethylene in semi-crystalline polyethylene, having a branching degree of 13 br 1000C^{-1} and a molecular weight of M_N=12.6 kg mol^{-1} (PDI=4.74). The crystallinity is calculated by the CCP/FCA. Experimental data from [176] and lines are the corresponding predictions with the LCT.

In order to study the influence of the temperature in more detail, figure 5.43 shows experimental data points of a single polyethylene sample having a branching degree of 13 br 1000C^{-1} and a molar mass of M_N=12.6 kg mol^{-1} (PDI=4.74) [176]. Here, two counteracting effects come into play: The gas solubility of ethylene in polyethylene generally decreases with increasing temperature, which can be seen for an amorphous state in figure 5.23. At the same time, a higher temperature results in a lower crystallinity, i.e. a lower eigen pressure and hence a higher gas solubility. However, the effect of decreasing solubility due to the shifted phase equilibrium prevails over the effect of lower crystallinity. This behaviour is predicted with high accuracy by the combined CCP/FCA and LCT framework.

1-butene

The solubility of 1-butene in semi-crystalline ethyl-branched polyethylene is shown in figure 5.44. Only one isotherm at 358.15 K was measured via pressure decay method [108] covering the pressure region until the vapour pressure of 1-butene. The prediction shows high agreement with experimental data except in the area near the vapour pressure of 1-butene, where the LCT predicts a lower solubility leading to a calculation beyond the vapour pressure. Here, a 1-butene rich phase with solved polyethylene emerges, building a liquid-liquid demixing. A reason for the discrepancy may be the calculation. Since lattice theories like the LCT underestimate the compressibility of gases, this could lead to inaccuracies in the high pressure region.

	T	**br**	**M_N(PDI)**	α
	[K]	[1000C^{-1}]	[kg mol^{-1}]	[wt%]
●	358.15	20.0	23 (n/a)	24.4
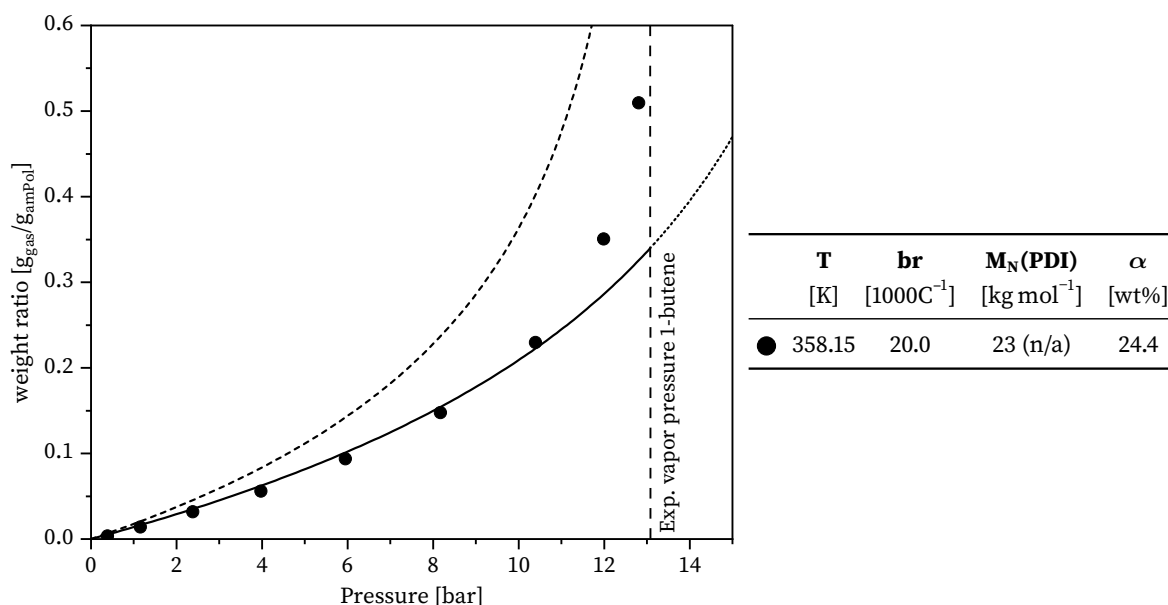
Figure 5.44: Predicted solubility of 1-butene in semi-crystalline ethyl-branched polyethylene at 358.15 K, having 20.0 br 1000C^{-1} and M_N=23 kg mol^{-1} (PDI=n/a) [108]. The straight line is the corresponding prediction with the LCT and the short dashed 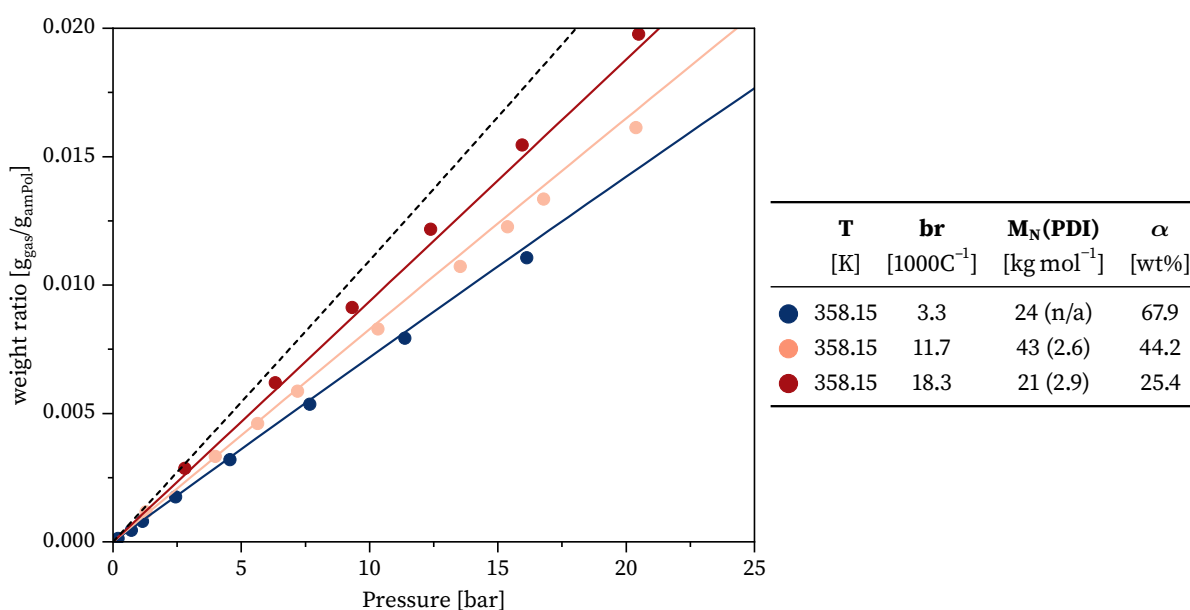line is the amorphous limit disregarding the crystallinity. The dashed line denotes the experimental vapour pressure of 1-butene at 358.15 K while the dotted line is the prediction beyond the vapour pressure.

On the other hand, experimental inaccuracies may be a reason for the discrepancy: The pressure decay method requires long experimental time, since a large amount of sample is needed (30 g in this case [108]). Moreover, especially at high amounts of solved gas, a precise swelling correction is necessary for the volume calculation. Since the swelling correction matters particularly at high solubilities, the low soluble system ethylene-PE from the same publication [108] in figure 5.41 and 5.42 is still in very good agreement, although the swelling correction may be insufficient. However, for the system 1-butene in polyethylene, a swelling correction is crucial. Yet, information about the swelling correction is not given in the paper [108].

1-hexene

Another system which was measured by the same author [108] is 1-hexene in polyethylene, shown in figure 5.45. Even though the qualitative course is correct, discrepancies between the experimental data and the prediction become apparent. Although, the swelling correction may introduce inaccuracies, already explained at the example of 1-butene, here, the disagreement is larger and manifests already in the low pressure area, where the effect of the swelling correction is small. There are two possible reasons for this: Due to scarce experimental data, only one single isotherm at 423.15 K was used for the adjustment of the binary interaction parameter in molten polyethylene (figure 5.26).

	T	br	M_N(PDI)	α
	[K]	[1000C^{-1}]	[kg mol^{-1}]	[wt%]
■	323.15	16.7	43 (2.8)	47.0
■	353.15	16.7	43 (2.8)	33.2
●	358.15	11.7	43 (2.6)	44.2
▲	358.15	18.3	21 (2.9)	25.4
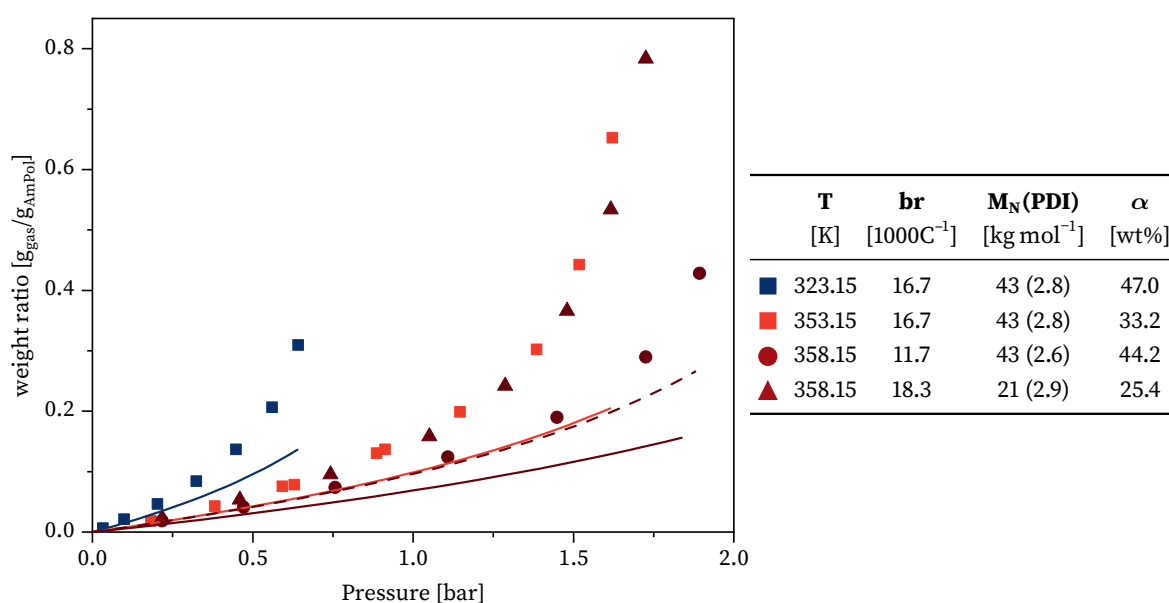
Figure 5.45: Predicted solubility of 1-hexene in semi-crystalline polyethylene at different temperatures from 323.15 K to 358.15 K. Experimental data points with hexyl branched polyethylene, with a branching degree varying from 11.7 br 1000C^{-1} to 18.3 br 1000C^{-1} are from [108]. The lines (the dashed one belongs to the triangles) are corresponding predictions with the combined LCT and CCP/FCA framework.

As a result of this, k_{ij} is not depending on the temperature, which may lead to inaccuracies when predicting a significantly lower temperature. On the other hand, in the publication [108] the methodology for determining the solubility of 1-hexene differs from that of 1-butene and ethylene. While the vapour and liquid density of ethylene and 1-butene, which are necessary for the determination of solubilities via pressure decay method, was determined by a highly accurate equation of state [233], they used in case of 1-hexene the ideal gas law for the vapour phase and estimations from saturated liquid density for the liquid density [108]. This can lead to deviations in the calculated solubility, especially when approaching the vapour pressure (which

all measurements do), where the ideal gas law is a precarious assumptions.

Despite the discrepancies between experimental data and calculations, the counteracting effects of the temperature, already investigated in figure 5.43, are in well agreement. The experimental data show almost the same solubility for 353.15 K and 16.7 br 1000C^{-1} and for 358.15 K and 18.3 br 1000C^{-1}. This is due the fact, that on the one hand, increasing temperature generally lowers the solubility of 1-hexene in polyethylene, but on the same time, an increase in temperature leads to a lower crystallinity and hence a higher solubility. In this case, both effects nearly cancel each other. This is exactly described by combined LCT and CPP/FCA framework. In order to investigate these discrepancies, observed in figure 5.45, another set of experimental data is shown in figure 5.46.

T	br	M$_N$(PDI)	α
[K]	[1000C^{-1}]	[kg mol^{-1}]	[wt%]
323.15	8.7	1126 (2.3)	63.4
323.15	16.4	915 (2.5)	48.0
323.15	29.2	947 (2.7)	24.0
323.15	37.1	875 (2.6)	13.4
323.15	49.4	83 (3.7)	4.0
323.15	73.4	80 (2.7)	0.1
323.15	16.7	43 (2.8)	47.0
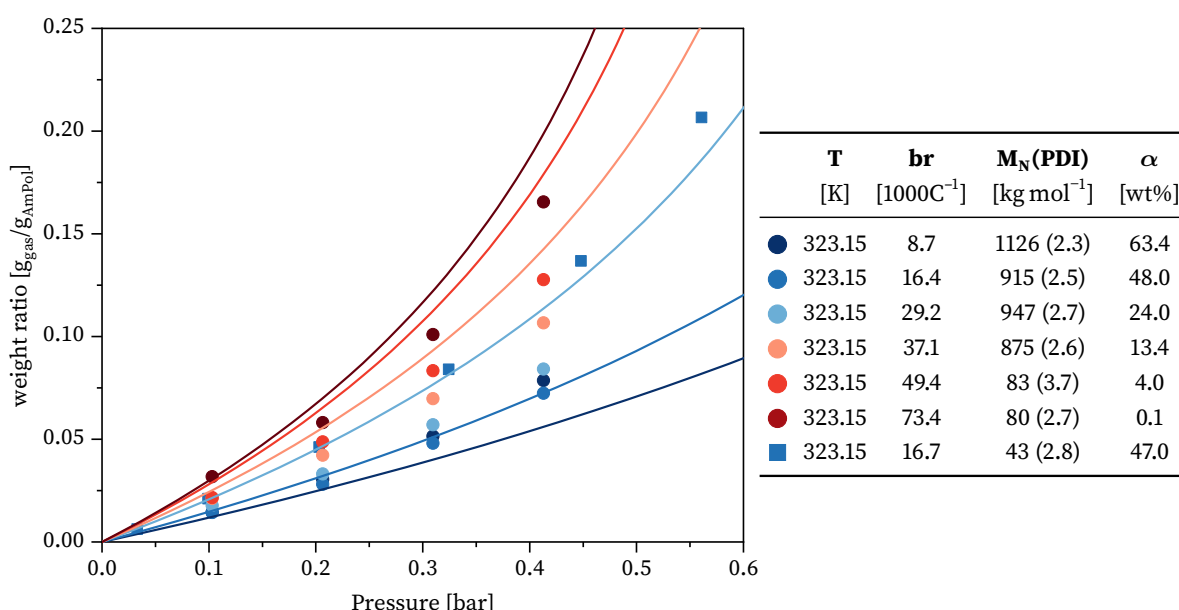
Figure 5.46: Predicted solubility of 1-hexene in semi-crystalline polyethylene at 423.15 K. Experimental data points with butyl branched polyethylene, with a branching degree varying from 8.7 br 1000C^{-1} to 73.4 br 1000C^{-1}, are from [188] (circles) and from [108] (squares). The lines are corresponding predictions with the combined LCT and CPP/FCA framework.

The solubility of 1-hexene in butyl-branched polyethylene was measured at 323.15 K via a quartz spring balance by Jin et al. [188]. Also included is the single measurement of figure 5.45 at 323.15 K [108], which is significantly higher compared to measurements of Jin et al. having a similar branching degree, confirming the above mentioned conjecture, that the experimental procedure in case of 1-hexene is questionable. Having said that, it has to be mentioned that the molecular weight between those two measurements differs by orders of magnitude. However, in this high molecular weight area, that does not explain the big discrepancies between those two measurements.

Carbon dioxide

Figure 5.47 shows the solubility of carbon dioxide in semi-crystalline polyethylene, alongside experimental data from Zimmermann et al. [36], measured at 353.15 K via magnetic suspension balance. Polyethylene has different branching degrees being 22 br $1000C^{-1}$ and 5 br $1000C^{-1}$.

	T	br	M_N(PDI)	α
	[K]	[$1000C^{-1}$]	[kg mol^{-1}]	[wt%]
●	353.15	22	11.4 (12.2)	20.3
●	353.15	5	4.5 (24.5)	59.7
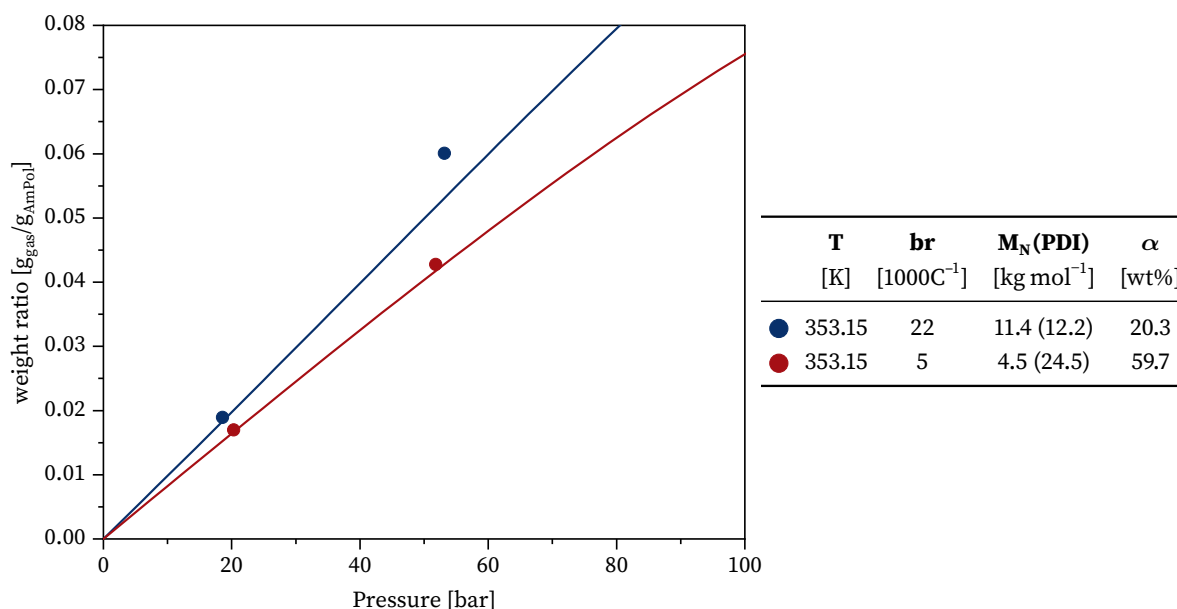
Figure 5.47: Predicted solubility of carbon dioxide in semi-crystalline PE at 353.15 K. Experimental data from [36] while the lines are the corresponding predictions with the CPP/FCA and LCT framework.

According to figure 5.47, the combined CPP/FCA and LCT framework is in high agreement with the experimental data [36]. Especially at low pressure and for the sparsely branched sample. The high pressure data point of the more branched sample is slightly underestimated by the model. One reason for the discrepancy could experimental difficulties at high pressure. However, the adjustment of the binary interaction parameter could be a source of error as well, as the solubility data in molten polyethylene scatter strongly in some cases (figure 3.8).

The next investigation on the solubility of carbon dioxide as well as the two following gas-polymer-systems including nitrogen and methane cover a detailed consideration of the influence of branching on the gas solubility in semi-crystalline polyethylene. Therefore, in the following figures (5.48-5.52), the solubility is plotted isobaric over the branching degree.

Figure 5.48 shows the solubility of carbon dioxide in polyethylene over the branching degree at 1 atm. Experimental data [111, 112, 153, 199] show an increasing solubility with rising branching degree, although the exact course of the data is not discernible due to scattering data. This could be down to the fact, that the solubility of carbon dioxide is very low, making reliable measurements difficult.
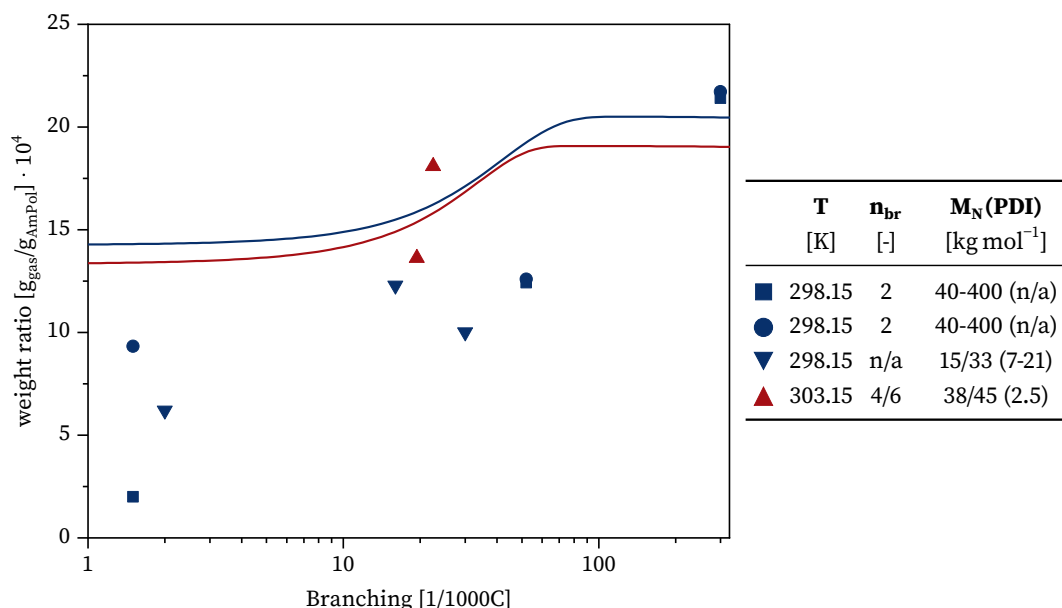
Figure 5.48: Predicted solubility of carbon dioxide in semi-crystalline polyethylene at 1 atm. Experimental data points from [111] (squares) [112] (circles), [199] (triangles down), [153] (triangles up). The lines are corresponding predictions with the combined LCT and CPP/FCA framework.

Furthermore, all the experiments were measurements of the diffusion and permeability via time-lag method, which were afterwards converted to the solubility. This may introduce inaccuracies due to kinetic effects during the experiment. The scattering of data from Pino et al. [199] (triangles down) is potentially due to the high polydispersity of the samples.

The branching degree has only minor influence on the solubility in amorphous PE, as was shown in the preceding section. Hence, solubility is only affected by the alteration of the crystallinity due to the branching degree. At 300 K, this mainly happens in the range up to $100\,\mathrm{br}\,1000\mathrm{C}^{-1}$, whereby at low branching degrees, a highly crystalline state is present which becomes completely amorphous at ca. $100\,\mathrm{br}\,1000\mathrm{C}^{-1}$, as can be seen in figure 5.7. For this reason, the solubility is just affected significantly up to ca. $100\,\mathrm{br}\,1000\mathrm{C}^{-1}$. For higher branching degrees, the influence of branching on the solubility, prescribed by the LCT is much lower, which can be seen in figure 5.36. The length of the branches n_{br} also influences the crystallinity (figure 5.9). Longer branches result in a lower crystallinity, leading to a higher gas solubility.

According to figure 5.48, the prediction of the combined LCT and CPP/FCA framework is in well agreement with experimental data, especially the data from Laguna et al. [153] at 303.15 K. Data from Michaels & Bixler [111, 112] is well reproduced in the high branching are, but overestimated in the area of lower branching. A strong temperature influence leads to a significant lower solubility at 303.15 K compared to 298.15 K, even if the crystallinity is considerable lowered by longer side chains between $20\,\mathrm{br}\,1000\mathrm{C}^{-1}$ and $50\,\mathrm{br}\,1000\mathrm{C}^{-1}$.

Nitrogen

Figure 5.49 shows the solubility of nitrogen at 1 atm over the branching degree. The experimental data sets [111, 112, 153, 199] are slightly scattered. The temperature has only minor influence on the solubility in the considered small range. This is due to the fact, that the LCT predicts a point of change to inverse solubility at 302.9 K (figure 5.34). Close to this minimum, the slope is very low, leading to a small temperature influence on the solubility. The increased solubility at 303.15 K is due to the fact, that the polyethylene sample has longer side chains, leading to a lower crystallinity and hence a higher solubility.

	T	n_{br}	M_N(PDI)
	[K]	[-]	[kg mol^{-1}]
■	298.15	2	40-400 (n/a)
●	298.15	2	40-400 (n/a)
▼	298.15	n/a	15/33 (7-21)
▲	303.15	4/6	38/45 (2.5)

Figure 5.49: Predicted solubility of nitrogen in semi-crystalline polyethylene at 1 atm. Experimental data points from [111] (squares) [112] (circles), [199] (triangles down), [153] (triangles up). The lines are corresponding predictions with the combined LCT and CPP/FCA framework.

Methane

The solubility of methane in polyethylene is shown in figure 5.50. The experimental data show similar behaviour compared to nitrogen in polyethylene. An increase in solubility until approx. 100 br 1000C^{-1} which is well reproduced by the theory. Here, the temperature influence is stronger at the considered conditions compared to nitrogen in polyethylene (figure 5.34). A higher temperature leads to a lower solubility, except between 20 br 1000C^{-1} and 50 br 1000C^{-1}, were the influence of the longer side chain on the crystallinity is pronounced and leads to a notable higher solubility.
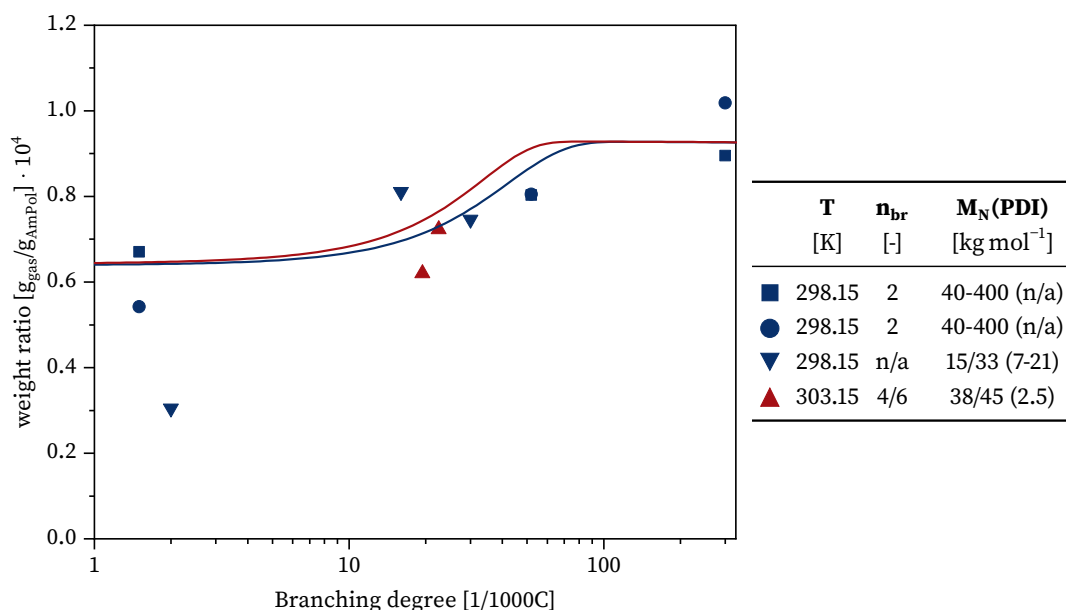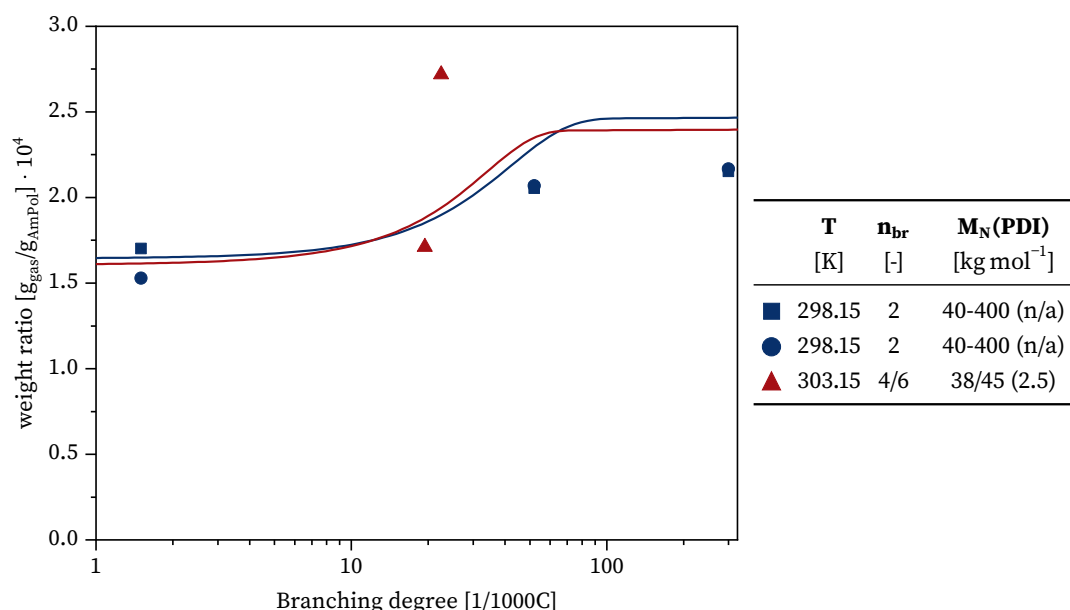
Figure 5.50: Predicted solubility of methane in semi-crystalline polyethylene at 1 atm. Experimental data points from [111] (squares) [112] (circles) and [153] (triangles up). The lines are corresponding predictions with the combined LCT and CPP/FCA framework.

n-hexane

In this last section of binary systems, solubility of the alkanes n-butane, n-pentane, n-hexane and n-heptane in semi-crystalline polyethylene is investigated and compared with experimental data from Castro et al. [202], measured gravimetrical by an electronic microbalance. Prediction of these systems require a special treatment, since no information about the architecture of the polymer on terms of branching degree were available in the publication [202]. Without information about the branching degree, the crystallinity cannot be determined as in the preceding gas-polymer-systems.

One first approach is to use the crystallinity, which was eventually measured and published alongside the solubility measurements. With this, the solubility without the CPP/FCA, only with the LCT and the eigen pressure approach can be predicted, which is shown in figure 5.51 as straight lines. The crystallinity was determined at 303.15 K via DSC [202]. This procedure yields already good results, which shows again the high predictive capability of the LCT and the eigen pressure approach. It becomes apparent that especially the isotherm at 303.15 K is in high agreement with experimental data. The lower isotherms are rather overpredicted while the higher isotherms are slightly underprecited. This is due to fact, that for the calculation of these isotherms, a crystallinity was used, which was not determined at this particular temperature. Since the temperature has a significant effect on the crystallinity (figure 5.7), especially for branched polyethylene samples, this introduces inaccuracies.
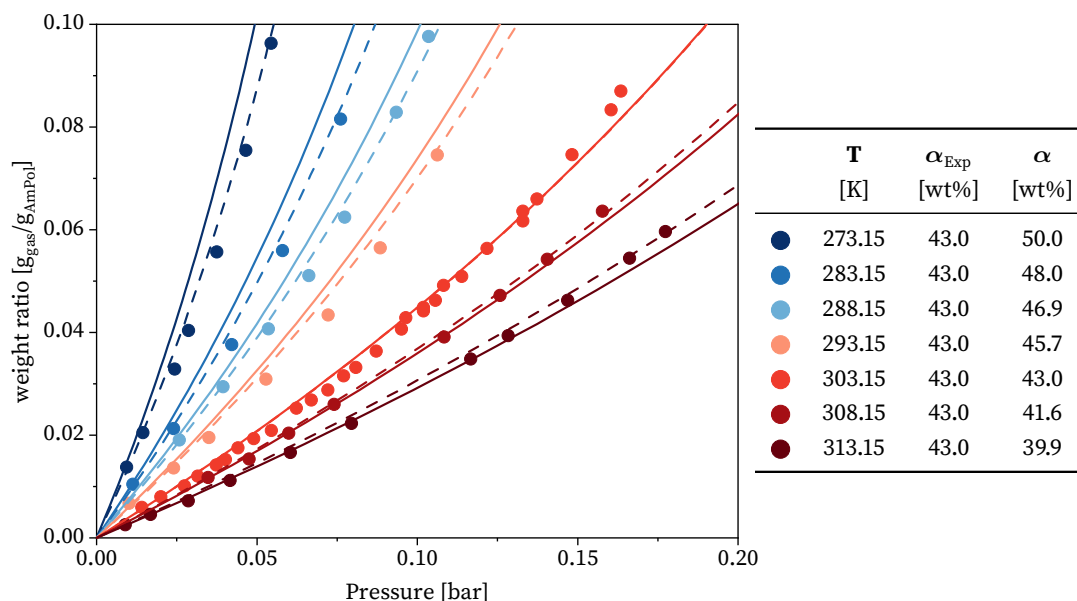
Figure 5.51: Predicted solubility of n-hexane in semi-crystalline polyethylene at different temperatures. The polyethylenes molecular weight is M_N=24.9 kg mol^{-1} (PDI=n/a). Straight lines denote the procedure with measured crystallinity. Dashed lines stand for predictions with the inverse CPP/FCA, resulting in 22.0 br 1000C^{-1}. Experimental data from [202].

To overcome this inability to successfully predict isotherms whose crystallinity has not been determined, the CPP/FCA can be used in an inverse manner according to the scheme in figure 4.5: With information of the crystallinity at one temperature and the molecular weight, the branching is determined iteratively via the inverse CPP/FCA. A branching length of 4 (butyl branches) is assumed, as butyl branching is the most abundant type of branching in LDPE [65] and at the same time represent a reasonable average value for the remaining branching of LDPE. Although, the influence of the branching length on the crystallinity is moderate (figure 5.9) and has a minor influence on the result. In this case, this leads to a branching degree of 22.0 br 1000C^{-1} which is within the expected range for LDPE, being between 20 br 1000C^{-1} and 25 br 1000C^{-1} [65]. The branching degree is a material property, only depending on the production condition and not on the temperature, in contrast to the crystallinity, which is a function of the temperature. The dependence of the temperature on the crystallinity can be seen in figure 5.12. Now, with help of the PCC/FCA and the iterated branching, the temperature dependent crystallinity can be predicted for different temperatures, as in the previous systems. This leads to an altered crystallinity according to the temperature, which can be seen in the legend of figure 5.51. A lower temperature results in a higher crystallinity and vice versa. Also shown are the predicted solubilities with the determined branching degree of 22.0 br 1000C^{-1} as dashed lines. The isotherm of 303.15 K does not change due to the different procedure, since

the crystallinity of this isotherm was used for the determination of the branching degree. For a lower isotherm and a correspondingly higher crystallinity, a lower solubility is predicted due to the higher eigen pressure, while the opposite is the case higher temperatures, which now is in excellent agreement with experimental data. This approach extends the predictive capability of the combined CPP/FCA and LCT to systems, where no information concerning the branching degree of the polyethylene sample is available.

n-butane

After successfully characterizing the polyethylene sample via the inverse CPP/FCA, other systems including the same sample can be investigated. This applies to the solubility of n-butane which is shown in figure 5.52.
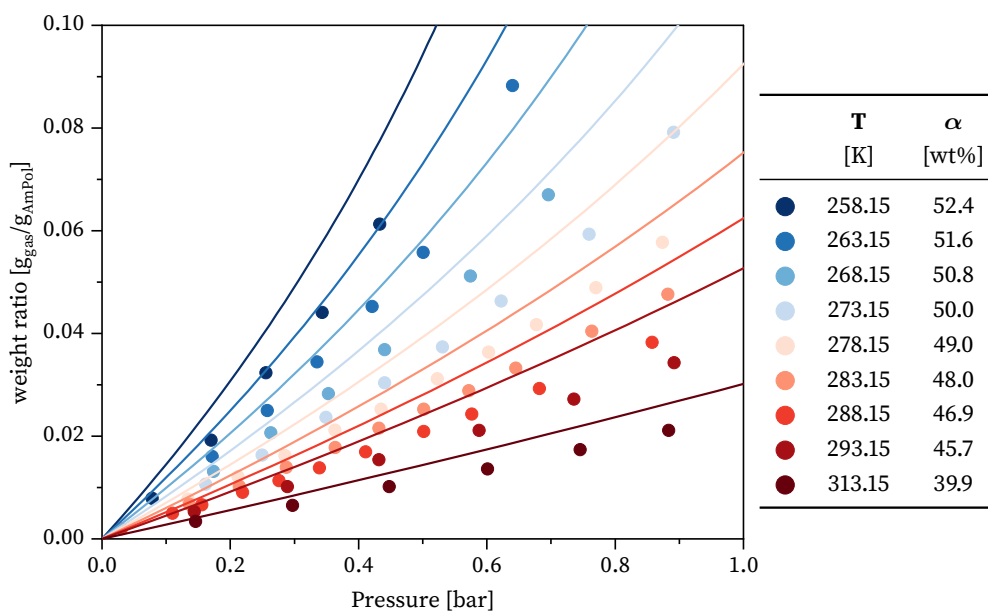
Figure 5.52: Predicted solubility of n-butane in semi-crystalline polyethylene at different temperatures. Polyethylene has a molecular weight of M_N=24.9 kg mol^{-1} (PDI=n/a) and a branching degree of 22.0 br 1000C^{-1}, determined by the inverse CPP/FCA. Lines are predictions with the LCT, experimental data is from [202].

Applying the determined branching degree of 22.0 br 1000C^{-1}, the solubility can be predicted by the combined CPP/FCA and the LCT. The influence of temperature is described qualitatively correctly by the model, which again shows that the CPP/FCA and LCT framework correctly accounts for two counteracting effects of higher crystallinity and hence lower solubility as well as higher solubility due to the phase equilibrium with an increase the temperature. However, the experimental data [202] are slightly overpredicted with an offset. Reasons for this could lie in the indirect characterization of the sample. Due to the determination of the branching

degree via inverse CPP/FCA, error sources could already lie in the measurement of the crystallinity. Moreover, the adjustment of the binary interaction parameter in the melt introduces inaccuracies. In case of n-butane, the polyethylene sample was not characterized in terms of the molecular weight, so a value of M_N=20 kg mol^{-1} was assumed. A different molecular weight may change the adjusted k_{ij}, leading to different results for the solubility in semi-crystalline systems.

n-pentane

The solubility of n-pentane in semi-crystalline polyethylene is shown in figure 5.53. Again, the branching degree of 22.0 br 1000C^{-1}, determined by the inverse CPP/FCA is used for the predictions.

|	**T**	α
	[K]	[wt%]
	263.15	51.6
	268.15	50.8
	273.15	50.0
	278.15	49.0
	283.15	48.0
	288.15	46.9
	293.15	45.7
	298.15	44.4
	303.15	43.0
	308.15	41.6

Figure 5.53: Predicted solubility of n-pentane in semi-crystalline polyethylene at different temperatures. Polyethylene has a molecular weight of M_N=24.9 kg mol^{-1} (PDI=n/a) and a branching degree of 22.0 br 1000C^{-1}, determined by the inverse CPP/FCA. Lines are predictions with the LCT, experimental data is from [202].

As was already for the system of n-butane, the solubility is overpredicted by an offset when comparing to experimental data [202]. Since n-hexane is predicted with higher accuracy compared to n-butane and n-pentane, the chain length of the gases may be introduced as a reason, because the LCT as a lattice theory generally has its strengths with long chains. However, other gases of comparable size or are even smaller are still described by very well by the LCT, as the preceding results show (figures 5.41-5.43 and 5.47).

n-heptane

Lastly, the system of n-heptane and semi-crystalline polyethylene is shown in figure 5.54. Here, a very good agreement between experimental data [202] and the combined CPP/FCA and LCT framework is achieved by using the determined branching degree of 22.0 br 1000C^{-1}. Especially the higher isotherms show excellent agreement. A slight overestimation can be seen for lower isotherm, which may be a result of the larger temperature difference between the parametrization in molten polyethylene and the prediction in semi-crystalline polyethylene.

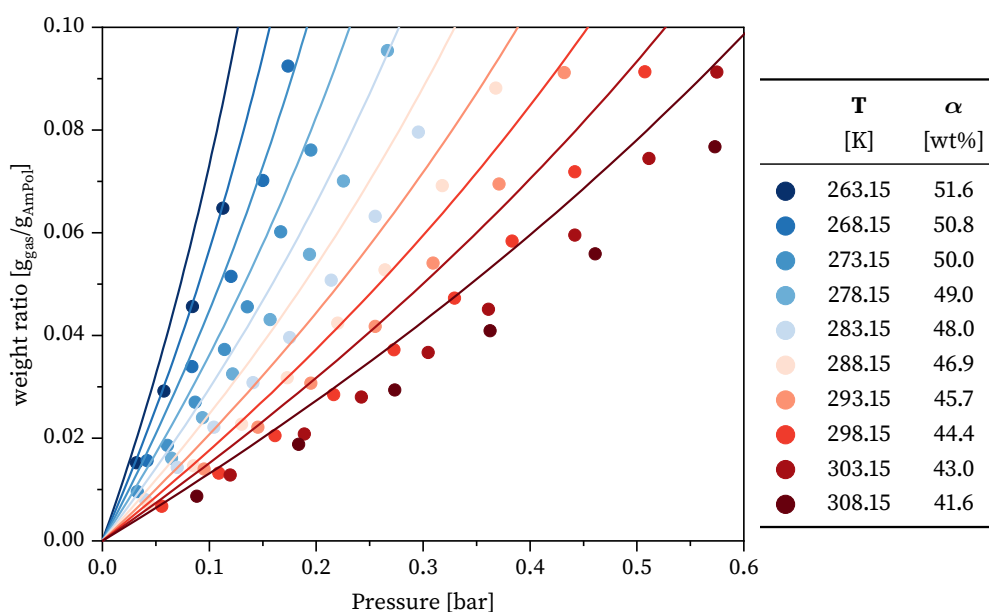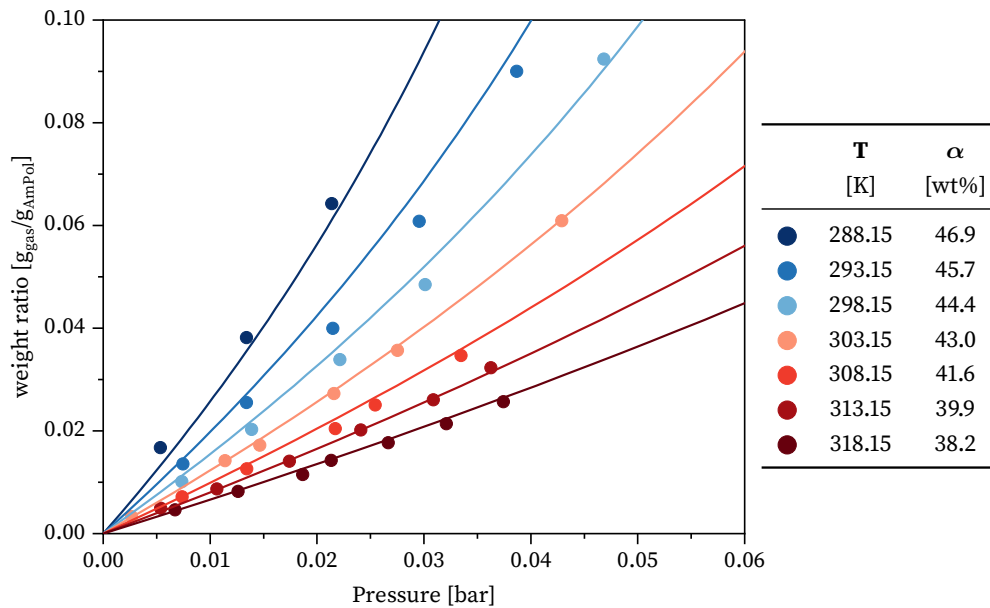| T	α
[K]	[wt%]
288.15	46.9
293.15	45.7
298.15	44.4
303.15	43.0
308.15	41.6
313.15	39.9
318.15	38.2

Figure 5.54: Predicted solubility of n-heptane in semi-crystalline polyethylene at different temperatures. Polyethylene has a molecular weight of M_N=24.9 kg mol^{-1} (PDI=n/a) and a branching degree of 22.0 br 1000C^{-1}, determined by the inverse CPP/FCA. Lines are predictions with the LCT, experimental data is from [202].

5.2.3 Ternary Systems

In this section, ternary systems are investigated which include two gases, solved in polyethylene. Generally, all phase equilibria are predicted with the binary interaction parameters in table 5.2, no additional parameters are introduced. Moreover, the interactions between the solved gases are assumed to obey the geometrical mixing rule (eq. (4.34)) with of $k_{ij}(T)=0$.

To first demonstrate whether the latter assumption holds true, figure 5.55 shows a vapour-liquid-equilibrium of the two gases ethylene and 1-propene between 233.15 K and 283.15 K. Together with LCT calculations and experimental data [234–237], PC-SAFT [38] results are shown for comparison, whereby for both equations, k_{ij} is zero. According to figure 5.55, the ideal mixing behaviour does represent the experimental data very well. At 283.15 K, ethylene is already in the supercritical state, and at 263.15 K and 273.15 K in the critical area. Since the LCT as a lattice theory generally overestimates the vapour pressure of pure ethylene, the phase equilibrium is slightly underestimated in the critical region of ethylene.
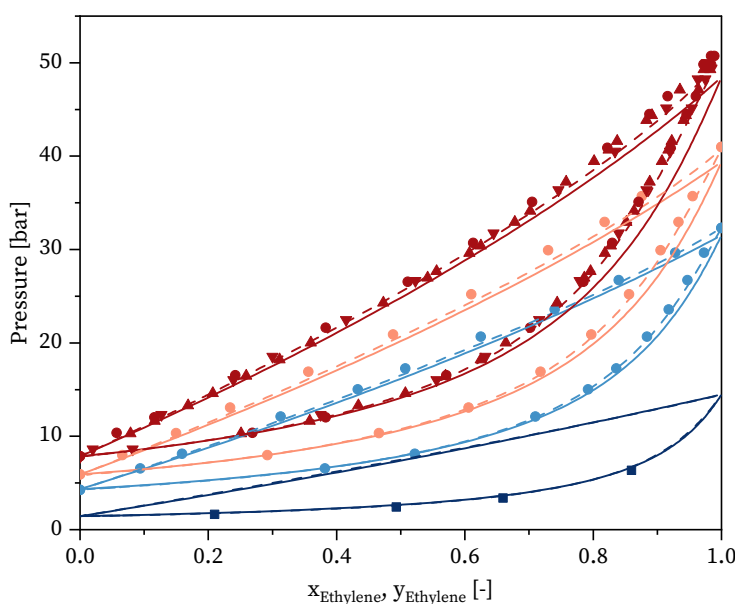
Figure 5.55: Vapour liquid equilibrium of ethylene and 1-propene at 233.15 K (dark blue), 263.15 K (light blue), 273.15 K (light red) and 283.15 K (dark red). Experimental data from Qian et al. [234] (squares), Bae et al. [235] (circles), Ohgaki et al. [236] (triangles up) and Kubota et al. [237] (triangles down). Straight lines denote LCT- while dashed lines are PC-SAFT [38] calculations for comparison. In both cases, k_{ij} is 0.

After successfully evaluating the geometrical mixing rule (eq. (4.34)) between the gases, a ternary system in investigated in figures 5.56 and 5.57. Here, ethylene and 1-hexene is solved in molten polyethylene at 423.15 K, whereby the sample has a molecular weight of 20 kg mol^{-1} and a branching degree of 0 br 1000C^{-1} (the influence of architecture on the binary cases is
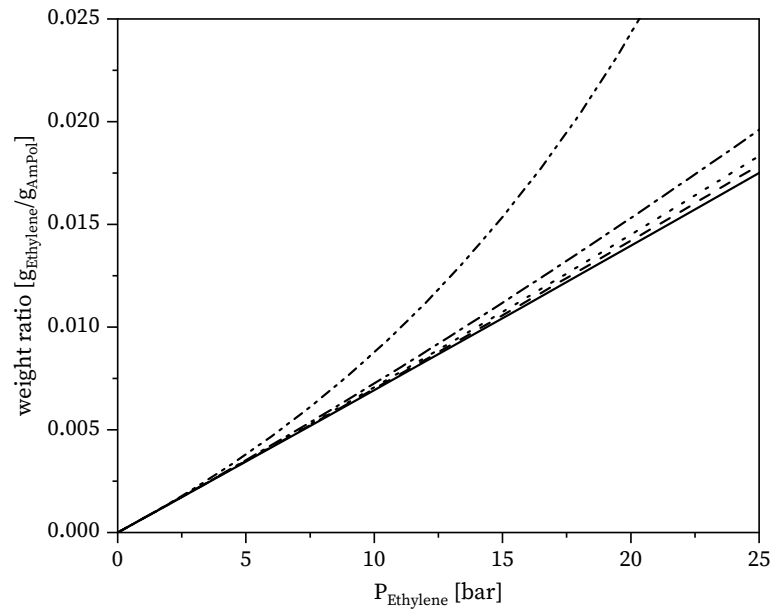
Figure 5.56: Partial Solubility of ethylene in a ternary system with 1-hexene and polyethylene at 423.15 K, having M_N=20 kg mol^{-1} and br = 0 br 1000C^{-1}. The straight line denotes the limiting binary case, while dashed line is 5 %, dotted line is 10 %, dash-dotted line is 20 % and dash-double-dotted line is 50 % of the 1-hexene in the gas phase.

Figure 5.57: Partial Solubility of 1-hexene in a ternary system with ethylene and polyethylene at 423.15 K, having M_N=20 kg mol^{-1} and br = 0 br 1000C^{-1}. The straight line denotes the limiting binary case, while dashed line is 5 %, dotted line is 10 %, dash-dotted line is 20 % and dash-double-dotted line is 50 % of the ethylene in the gas phase.

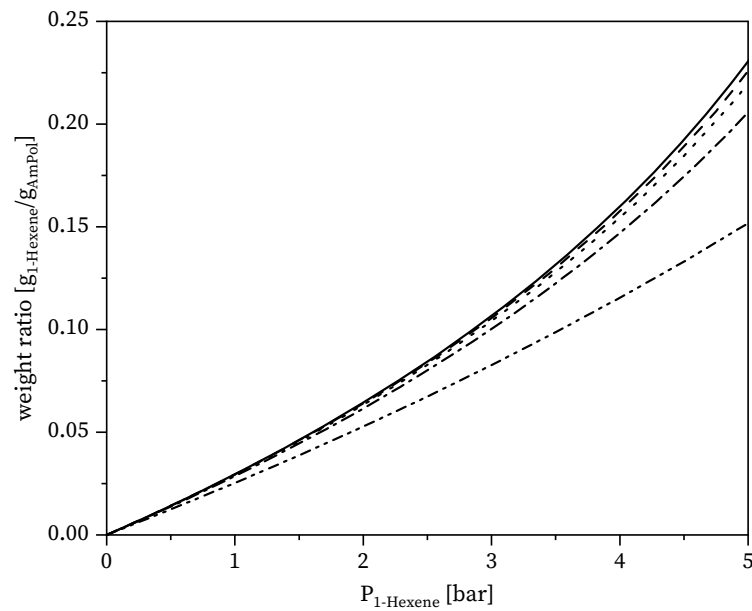discussed in section 5.2.2.1). To study co- and anti-solvent effects, the solubility of a single gas in ternary mixture is plotted over the partial pressure of that gas: Figure 5.56 shows the change of ethylene solubility by adding 1-hexene to the gas phase, figure 5.57 shows the opposite case. While the straight lines denote the limiting binary cases, the other lines stand for the partial solubility after adding a specific amount of the other gas to the system. Obviously, the presence of the other gas alters the solubility, which is not just decreases proportional to the decrease in partial pressure. In this case all lines would coincide with the limiting binary case (figures 5.56 and 5.57).

There are co-solvent and anti-solvent effects, coming from gas-gas interactions while solved in the polymer. According to figures 5.56 and 5.57 the solubility of ethylene in polyethylene is increased by the presence of 1-hexene, while the solubility of 1-hexene is decreased by the presence of ethylene. The more of the other gas is solved, the stronger the co- and anti-solvent effects become. This can be explained phenomenologically as follows: In case of ethylene, the bigger 1-hexene molecules are enlarging the polymer matrix, leading to polymer swelling. This enables the smaller ethylene molecules to find more space to dissolve. On the other hand, in case of 1-hexene, the smaller ethylene molecules occupy space in the polymer matrix, which is now not accessible for 1-hexene. To forge a bridge back to parking cars, that can be illustrated by a small car, occupying a much larger parking lot, on which a larger car that would fit can no longer be accommodated. The reason for the co- and anti-solvent effects are therefore mainly of entropic nature. Steric hindrance of interacting gas molecules in the polymer matrix lead to the altered solubility. Hence, the stronger the difference in size between the gas molecules, the stronger the co- and anti-solvent effects become.

Although, the partials solubilities may vary strongly depending on the presence of another, one question remains: How is the overall solubility affected by the simultaneous acting of co- and anti-solvent effects. This question is especially interesting, since in most cases, just the overall solubility is measured and not the partial solubility of the single gases. The latter would require further downstream measurements to characterize the single gases. Figure 5.58 shows the overall solubility of a ternary system containing ethylene, 1-hexene and molten polyethylene at 423.15 K, whereby the ethylene weight content in the gas phase is 10 %. Alongside the limiting binary cases of ethylene and 1-hexene, the sum of binary cases at its corresponding partial pressure is plotted as well. The latter denotes the totalized independent solubilities of both gases at their corresponding partial pressure according to eq. (4.83), which excludes all co- and anti-solvent effects.

The ternary prediction in figure 5.58 includes therefore both the co-solvent effect acting from 1-hexene to ethylene and the anti-solvent effect acting from ethylene to 1-hexene. However, the anti-solvent appears to be stronger, which reduces the ternary solubility in comparison to the sum of the limiting binary cases.
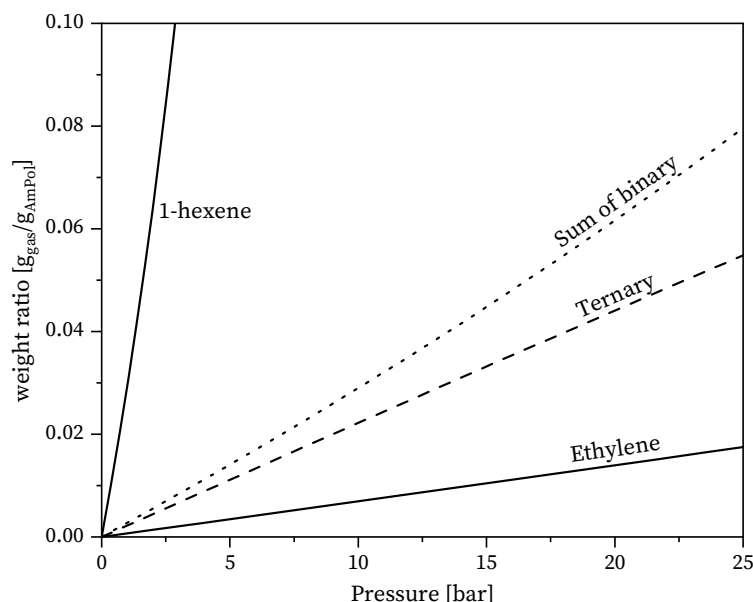
Figure 5.58: Simultaneous solubility of ethylene and 1-hexene in a ternary system with molten polyethylene at 423.15 K, having M_N=20 kg mol^{-1} and br = 0 br 1000C^{-1}. The fraction of 1-hexene in the gas phase is 10 wt%. The straight lines denote the limiting binary cases of ethylene and 1-hexene, the dashed line is the ternary system and the dotted line is the sum of the independent binary cases according to eq.(4.83).

In order to compare these model results with experimental data, a ternary system is required, where on the one hand the polymer sample is well characterized in terms of architecture, and on the other hand, measurements of the partial solubility of a single gas were carried out. While ternary solubility measurements not only include weighting of the gas loaded polymer sample, the determination of the partial solubility requires laborious downstream measurements of the gas composition. The group around Wohlfahrt [24] conducted experiments of the ternary system ethylene and 1-butene in molten polyethylene at 443.15 K and 50 bar. Polyethylene has a molecular weight of 1.94 kg mol^{-1} (PDI=n/a) and a branching degree of 31.8 br 1000C^{-1}. Figure 5.59 shows the experimental results accompanied by LCT predictions.

The bottom axis in figure 5.59 is the gas phase, while the binodal in the upper corner denotes the solubility of ethylene and 1-butene in polyethylene at different gas phase compositions. This system is above the melting temperature of polyethylene, e.g. completely amorphous. The LCT is able to predict the experimental data in very good agreement.
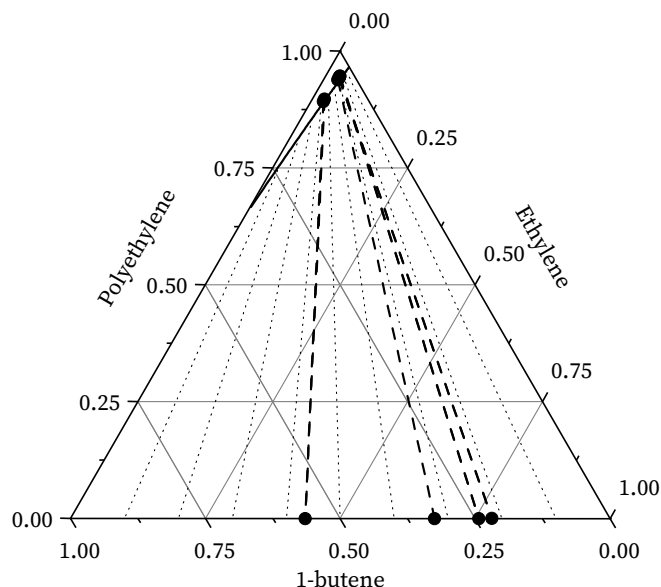
Figure 5.59: Solubility of ethylene and 1-butene in molten polyethylene at 443.15 K and 50 bar. Polyethylene has a molecular weight of 1.94 kg mol^{-1} (PDI=n/a) and a branching degree of 31.8 br 1000C^{-1}. Circles are experimental data [24] accompanied by dashed lines as tie lines. The straight line is the predicted binodal and the dotted lines are predicted tie lines with the LCT.

The ternary plot can be transformed into a partial solubility of one gas as a function of the partial pressure, which is shown in figure 5.60 for the case of ethylene. The illustrations in figure 5.60 include the calculation of the limiting binary case of pure ethylene. By introducing 1-butene into the gas atmosphere, the partial pressure drops up to approx. 30 bar. Due to the co-solvent effect, acting from 1-hexene onto ethylene, the solubility of ethylene is significantly higher compared the binary limiting case at the corresponding pressure. Both, the experimental data and the LCT show this behaviour in high agreement.

The experimental blue points in figure 5.60, corresponding to an ethylene weight fraction in the gas phase of 78.1 %, appear questionable since, according to the table in the publication [24], a higher ethylene content in the gas phase leads to a lower ethylene content solved in polyethylene.

After successfully evaluating co- and anti-solvent effects in ternary amorphous systems, in this last section, all the above observed and evaluated effects are combined, leading to ternary system of two gases, being solved in semi-crystalline polyethylene. Moore et al. [106] measured the simultaneous solubility of ethylene and 1-hexene in semi-crystalline polyethylene at 342.15 K. The weight fraction of ethylene in the gas phase is 85.9 %, while polyethylene has a molecular weight of 25.96 kg mol^{-1} and 1-butene as a co-monomer, leading to ethyl-branches.
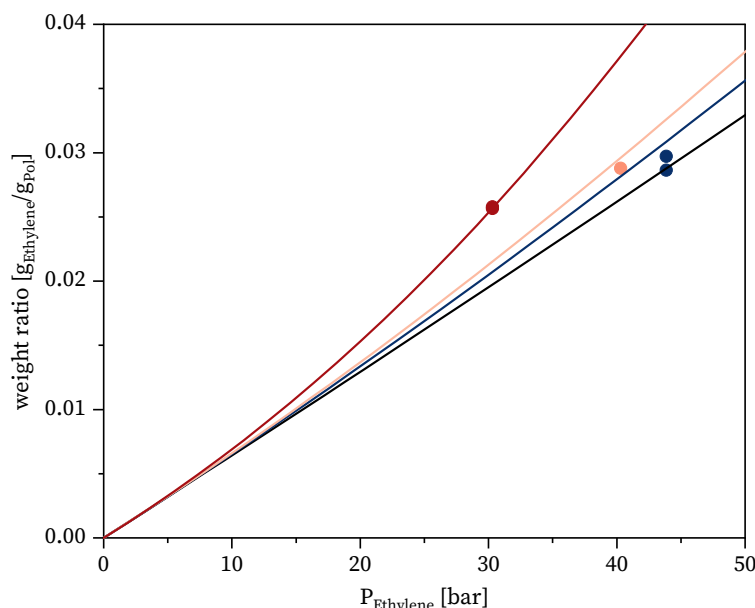
Figure 5.60: Partial Solubility of ethylene in a ternary system with 1-butene and polyethylene at 443.15 K and 50 bar. Polyethylene has a molecular weight of 1.94 kg mol^{-1} (PDI=n/a) and a branching degree of 31.8 br 1000C^{-1}. The black line denotes pure ethylene, blue is 78.1 % ethylene, light red is 67.5 % ethylene and red denotes 43.5 % ethylene in the gas phase. Circles represent experimental data [24] and lines are predictions with the LCT.

Unfortunately, the sample was not characterized in terms of the branching degree. For a start, a range of branching degree can be assumed, were LDPE with ethyl-branches is expected to lie. Therefore, figure 5.61 shows the simultaneous solubility of ethylene and 1-hexene for polyethylene between 15 br 1000C^{-1} and 30 br 1000C^{-1}, leading to a crystallinity of 43.1 % and 13.9 %, marked by the grey areas. Alongside the ternary system, the limiting binary cases of ethylene and 1-hexene are plotted as well as the sum of the limiting binary cases at the corresponding partial pressure according to eq. (4.83).

The solubility of the ternary case appears to be significant lower compared to the sum of binary systems, especially for higher pressure. Hence the anti-solvent effect, which lowers the solubility of 1-hexene outweighs the co-solvent effect. A typical value for the branching degree of low density polyethylene is 22.5 br 1000C^{-1} [65], being the mean value of the grey area. When comparing the predicted results for 22.5 br 1000C^{-1} via the combined CPP/FCA and LCT framework with experimental data [106], there seems to be a high agreement. Two experimental points are almost exactly reproduced by the isotherm having a branching degree of 22.5 br 1000C^{-1}, while the third point is slightly higher than the predicted results.

Further proof for the plausibility of a branching degree of 22.5 br 1000C^{-1} provides the measured crystallinity of the publication [106], which was determined via DSC to be 47.0 %.
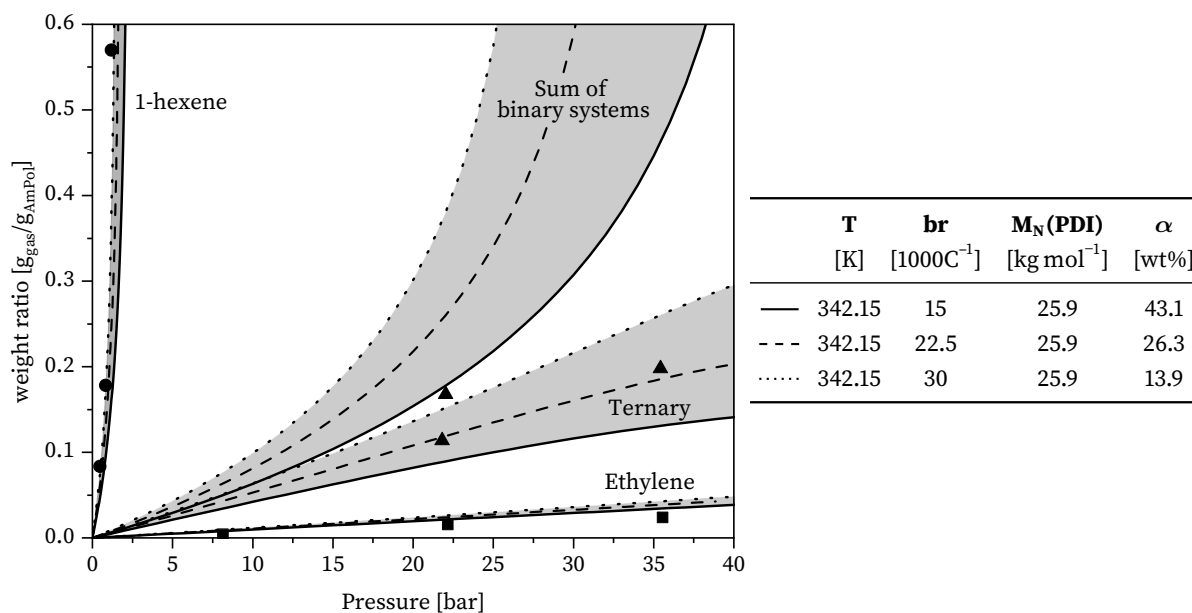
Figure 5.61: Simultaneous solubility of ethylene and 1-hexene in a ternary system with semi-crystalline polyethylene, having a molecular weight of 25.9 kg mol^{-1} at 342.15 K, while the ethylene weight fraction in the gas phase is 85.9 %. Triangles are the ternary experiments, the limiting binary case of ethylene are squares, while circles denote 1-hexene. Experimental data are from Moore et al. [106], while lines are calculations with the combined CPP/FCA and LCT framework at different branching degrees.

Unfortunately, the temperature, at which the crystallinity was determined, is not specified, so that the method of the inverse CPP/FCA according to figure 4.5 cannot be applied. However, at a temperature of 298.15 K, the assumed branching degree of 22.5 br 1000C^{-1} results via the CPP/FCA in a crystallinity of 47.4 %. Since the crystallinity is usually determined between 293.15 °C and 303.15 °C, often at room temperature, the assumed branching degree appears to be reasonable.

Yoon et al. [209] measured the simultaneous solubility of ethylene and 1-propene in highly branched polyethylene, having a branching degree of 206 br 1000C^{-1}, which leads to a fully amorphous sample according to the CPP/FCA. However, no molecular weight is specified in the publication [209]. Figure 5.62 shows measurements with temperatures ranging from 323.15 K to 363.15 K and partial pressures of 1-propene, ranging from 0.1 atm to 0.3 atm. A higher partial pressure of 1-propene at a constant mole fraction of ethylene increases the pressure, which increases the overall solubility. At the same time, an increase in temperature leads to decreasing solubility, which can be seen independently for ethylene and 1-propene in figures 5.23 and 5.24.

Both experimental behaviours are in well agreement with the model (figure 5.62), although there appears to be a slight overprediction, especially at low temperatures and high partial pressures of 1-propene. One reason for the discrepancy could lie in the insufficient character-

ization of the polyethylene sample in terms of the molecular weight, as M_N=20 kg mol^{-1} was assumed for the calculation. Moreover, lower temperatures show a higher deviation between experimental data and the model results, which could be a result from the adjustment of the binary interaction in the melt: The higher the temperature span between adjustment and prediction, the more noticeable inaccuracies of molten data or its adjustment become. One problem may be the fact, the polymer sample is a copolymer consisting of ethylene and 1-propene units, whereby the 1-propene units introduce the methyl-branches. These short branches can be accommodated to a certain amount in the crystal lattice, which is not included in the CPP/FCA. A small crystalline fraction due to the methyl-branches would then introduce an eigen pressure, which in turn slightly decreases the solubility. Since the crystallinity increases with decreasing temperature, the effect of lowered solubility would be larger for lower temperatures.
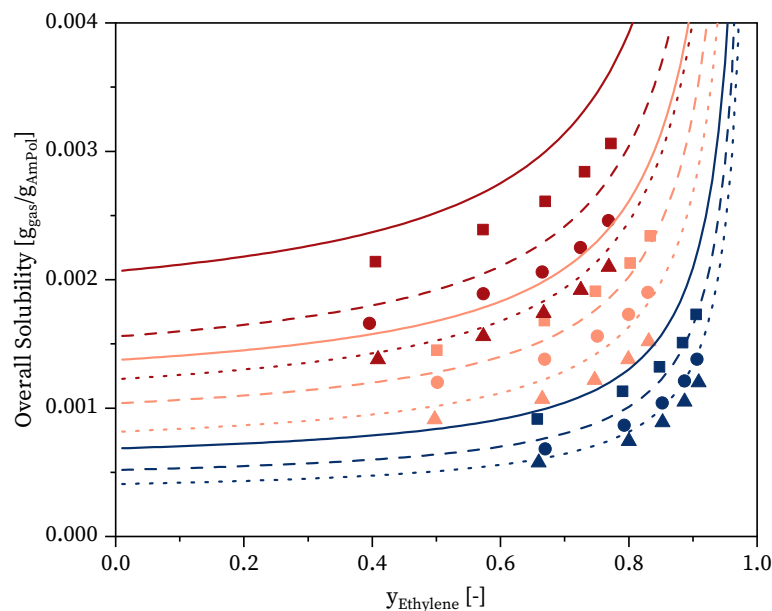
Figure 5.62: Simultaneous solubility of ethylene and 1-propylene in a ternary system with polyethylene at different temperatures. The branching degree is 206 br 1000C^{-1}, while no molecular weight is specified. Experimental data are from Yoon et al. [209]. The colour denotes constant partial pressure of 1-propene (blue: 0.1 atm, light red: 0.2 atm, red: 0.3 atm), while the shape of the line denotes the temperature (squares/straight lines: 323.15 K, circles/dashed lines: 343.15 K, triangles/dotted lines: 363.15 K).

Lastly, it appears that authors of the publication [209] did not account for the swelling of the polymer sample, which has already been contributed by Podivinska et al. [182]. Due to the negligence of the polymers swelling, the values of the experimental solubility appear lower than they actually are. Hence, accounting for the swelling of the polymer would increase the experimental solubility, especially for the higher partial pressures of 1-propene, where the swelling is more pronounced.

6 Conclusion and outlook

The aim of this work was the development of a framework, that is able to predict gas solubilities in semi-crystalline polyethylene taking into account the polymers architecture.

This was achieved by investigating the influence of the molecular structure (molecular weight and branching) on both the gas solubility and the crystallinity of polyolefins. The latter was modelled using a co-polymer approach from Flory (FCA) that accounts for the lowered crystallinity when increasing the amount of branches. The challenge of linear chains that do not show a fully crystalline behaviour, was successfully addressed by the incorporation of the Car-Parking-Problem (CPP), whereby isolated amorphous sequences, that are too short to build a stable crystallite are excluded from crystallization, analogous to the illustration of cars being parked randomly on a parking lot. The combination of both approaches revealed high agreement with experimental data, considering the influence of chain length, branching degree, branching type and temperature.

The Lattice-Cluster-Theory (LCT) was introduced due to its ability to directly account for the polymers architecture. First pure compound parameters of the ethylene, 1-propene, 1-butene, 1-hexene, nitrogen, methane carbon dioxide, n-butane, n-pentane, n-hexane and n-pentane as well as polyethylene were adjusted to experimental data. Subsequently, temperature dependent binary interaction parameters between the gases and polyethylene were adjusted to gas solubilities in molten polyethylene.

With this, the LCT revealed the influence of the architecture on the gas solubility. Of central importance was the knowledge, that the influence of chain branching is insignificant small, when keeping other impacts such as the chain length constant. This result confirms and explains experiments that have indicated this finding. With help of the LCT, the divers influence of chain branching on the solubility, however small, was investigated and discussed. Complex relations were revealed, where the influence of branching depends on the both pressure and the type of solved gas.

Subsequently, both approaches were combined to build a predictive framework for the calculation of gas solubilities in semi-crystalline systems. An eigen pressure was introduced, that accounts for the isotropic stress acting from the crystalline domains on the amorphous domains. The crystallinity, which is required for this, was directly predicted via the CPP and FCA as a function of the molecular structure and the temperature. Together with the LCT, the solubility of ethylene, 1-propene, 1-butene and 1-hexene in polyethylene was predicted in high agreement with experimental data over a wide pressure range. The influence of branching on the solubility of nitrogen, methane and carbon dioxide were investigated in detail at atmospheric pressure. Additionally, an approach was presented, to predict gas solubilities without information of branching degree of the polyethylene sample. This was achieved by using the CPP/FCA quasi inverse with help of the crystallinity at given temperature. This made it possible to calculate the branching degree, which is a material property and therefore does not depend on conditions such as the temperature. As a result, the crystallinity as a function of the temperature and hence gas solubilities can be predicted. Very good results were achieved with this method at the example of n-butane, n-pentane, n-hexane and n-heptane.

Finally, ternary systems were investigated, where two gases are simultaneously solved in poly-ethylene. Co-/ and anti-solvent effects were ascertained, whereby the smaller gas enhances the solubility of bigger gas and vice versa. The LCT, which had no additional parameters for the ternary systems, predicted gas solubilities in both amorphous and semi-crystalline systems, which were in high agreement with experimental findings.

In the course of this work, a few assumption were made, that could be a reason for deviations that were discerned between the model and experimental data. The crystallinity appears to depend on kinetic effects such as the cooling rate, e.g. quenched samples should have another crystallinity than slowly cooled samples, which is disregarded in the model. This may be the reason why the crystallinity of quenched samples is rather overpredicted by the model. The kinetic effects of the cooling rate could be related to entanglements which can decrease the crystallinity to a certain extend. In order to take kinetic effects such as the cooling rate into account, an additional kinetic approach would be necessary, as only the equilibrium state can be described with the current theory. Entanglements may be described by rheological models such as the reptation model which considers the polymer chain confined in virtual tubes being restrained in movement [238] or the application of the statistical knot theory to polymers [239]. A further assumption that was made, is that side chains are generally inhibited from being inside a crystal, which is true for most of the side chain. Methyl-chains, however, can be

incorporated into the crystal lattice to a certain amount which would lead to an increase of crystallinity for these systems. Furthermore, most polyolefins do not show a uniform architecture in terms of molecular weight and branching degree but a distribution, which is disregarded in this work by assuming a monodispers distribution. In order to account for the polydispers nature of polyolefins in terms of molar mass and chain branching, methods of continuos thermodynamics [240] may be introduced. Another assumption that has been made is that dissolved gas molecules do not affect the crystallinity of the polyethylene sample, which may not be the case [241]. When investigating gas crystallinity dependencies, the model has to be extended since the phase equilibrium calculation of the model considers the semi-crystalline state as a liquid with eigen pressure. However, care must be taken when investigating this effect, as sorption experiments often involve temperature changes that also affect the crystallinity.

References

[1]   A. W. deGroot, D. Gillespie, R. Cong, Z. Zhou and R. Paradkar, "Molecular Structural Characterization of Polyethylene", in: *Handbook of Industrial Polyethylene and Technology,* ed. by M. A. Spalding and A. M. Chatterjee, Wiley (2017).

[2]   L. Mandelkern, *Crystallization of polymers: Equilibrium concepts,* 2nd ed., vol. 1, Cambridge: Cambridge Univ. Press (2002).

[3]   L. Mandelkern, *Crystallization of polymers: Kinetics and Mechanisms,* 2nd ed., vol. 2, Cambridge: Cambridge Univ. Press (2009).

[4]   P. J. Flory, *Transactions of the Faraday Society* **51** (1955) 848–857.

[5]   P. J. Flory and D. Y. Yoon, *Nature* **272** (1978) 226–229.

[6]   L. Mandelkern, A. L. Allou and M. R. Gopalan, *The Journal of Physical Chemistry* **72** (1968) 309–318.

[7]   A. Moyassari, T. Gkourmpis, M. S. Hedenqvist and U. W. Gedde, *Polymer* **161** (2019) 139–150.

[8]   M. Psarski, E. Piorkowska and A. Galeski, *Macromolecules* **33** (2000) 916–932.

[9]   S. Yamazaki, M. Hikosaka, A. Toda, I. Wataoka and F. Gu, *Polymer* **43** (2002) 6585–6593.

[10] H. Bu, F. Gu, L. Bao and M. Chen, *Macromolecules* **31** (1998) 7108–7110.

[11] P. J. Flory, *Principles of polymer chemistry,* 10th ed., Ithaca: Cornell Univ. Press (1978).

[12] K. Iwata, *Polymer* **43** (2002) 6609–6626.

[13] F. Nilsson, X. Lan, T. Gkourmpis, M. S. Hedenqvist and U. W. Gedde, *Polymer* **53** (2012) 3594–3601.

[14] N. Stribeck, *Macromolecular Chemistry and Physics* **205** (2004) 1455–1462.

[15] F. Gornick and J. L. Jackson, *The Journal of Chemical Physics* **38** (1963) 1150–1154.

[16] A. Maltz and E. E. Mola, *Surface Science* **115** (1982) 599–605.

[17] M. Gordon and I. H. Hillier, *The Journal of Chemical Physics* **38** (1963) 1376–1380.

[18] A. Renyi, *Publications of the Mathematical Institute of the Hungarian Academy of Sciences* **3** (1958) 109–127.

[19] J. W. Evans, *Reviews of Modern Physics* **65** (1993) 1281–1329.

[20] B. Bonnier, D. Boyer and P. Viot, *Journal of Physics A: Mathematical and General* **27** (1994) 3671–3682.

[21] R. B. McQuistan and D. Lichtman, *Journal of Mathematical Physics* **9** (1968) 1680–1684.

[22] A. Maltz and E. E. Mola, *The Journal of Chemical Physics* **79** (1983) 5141–5144.

[23] F. Gornick and R. W. Freedman, *Journal of Mathematical Chemistry* **5** (1990) 265–274.

[24] T. Heuer, G.-P. Peuschel, M. T. Rätzsch and C. Wohlfarth, *Acta Polymerica* **40** (1989) 272–278.

[25]   P. Paricaud, A. Galindo and G. Jackson, *Industrial & Engineering Chemistry Research* **43** (2004) 6871–6889.

[26]   D. Patterson, *Polymer Engineering & Science* **22** (1982) 64–73.

[27]   D. P. Maloney and J. M. Prausnitz, *AIChE Journal* **22** (1976) 74–81.

[28]   C. W. Haschets, A. D. Shine and R. M. Secor, *Industrial & Engineering Chemistry Research* **33** (1994) 1040–1046.

[29]   A. Ghosh, W. G. Chapman and R. N. French, *Fluid Phase Equilibria* **209** (2003) 229–243.

[30]   H. P. Schreiber, Y. B. Tewari and D. Patterson, *Journal of Polymer Science: Polymer Physics Edition* **11** (1973) 15–24.

[31]   A. Novak, M. Bobak, J. Kosek, B. J. Banaszak, D. Lo, T. Widya, W. Harmon Ray and J. J. de Pablo, *Journal of Applied Polymer Science* **100** (2006) 1124–1136.

[32]   J. L. Lundberg, M. B. Wilk and M. J. Huyett, *Journal of Polymer Science* **57** (1962) 275–299.

[33]   J. L. Lundberg, *Journal of Polymer Science Part A: General Papers* **2** (1964) 3925–3931.

[34]   E. M. Cernia and C. Mancini, *Kobunshi Kagaku* **22** (1965) 797–803.

[35]   P. Ehrlich, *Journal of Polymer Science Part A: General Papers* **3** (1965) 131–136.

[36]   J. Zimmermann, S. Enders and M. Fischlschweiger, *to be published* (2025)

[37]   M. M. Hasan, Y. G. Li, G. Li, C. B. Park and P. Chen, *Journal of Chemical and Engineering Data* **55** (2010) 4885–4895.

[38]   J. Gross and G. Sadowski, *Industrial & Engineering Chemistry Research* **40** (2001) 1244–1260.

[39]   A. J. Haslam, N. von Solms, C. S. Adjiman, A. Galindo, G. Jackson, P. Paricaud, M. L. Michelsen and G. M. Kontogeorgis, *Fluid Phase Equilibria* **243** (2006) 74–91.

[40]   J. Chmelař, K. Smolná, K. Haškovcová, M. Podivinská, J. Maršálek and J. Kosek, *Polymer* **59** (2015) 270–277.

[41]   J. A. Moebus and B. R. Greenhalgh, *Macromolecular Reaction Engineering* **16** (2022) 2200017.

[42]   P. J. Flory, *The Journal of Chemical Physics* **10** (1942) 51–61.

[43]   M. L. Huggins, *Journal of the American Chemical Society* **86** (1964) 3535–3540.

[44]   I. C. Sanchez and R. K. Eby, *Macromolecules* **8** (1975) 638–641.

[45]   Y. Sato, K. Fujiwara, T. Takikawa, Sumarno, S. Takishima and H. Masuoka, *Fluid Phase Equilibria* **162** (1999) 261–276.

[46]   M. Fischlschweiger, A. Danzer and S. Enders, *Fluid Phase Equilibria* **506** (2020) 112379.

[47]   M. Minelli and M. G. De Angelis, *Fluid Phase Equilibria* **367** (2014) 173–181.

[48]   J. Dudowicz and K. F. Freed, *Macromolecules* **24** (1991) 5076–5095.

[49]   K. Langenbach, D. Browarzik, J. Sailer and S. Enders, *Fluid Phase Equilibria* **362** (2014) 196–212.

[50]   M. Fischlschweiger and S. Enders, *Journal of Molecular Liquids* **212** (2015) 436–443.

[51]   T. Zeiner, P. Schrader, S. Enders and D. Browarzik, *Fluid Phase Equilibria* **302** (2011) 321–330.

[52]   S. Enders, K. Langenbach, P. Schrader and T. Zeiner, *Polymers* **4** (2012) 72–115.

[53]   M. Fischlschweiger and S. Enders, *Macromolecules* **47** (2014) 7625–7636.

[54]   K. Langenbach, M. Fischlschweiger and S. Enders, *Molecular Physics* **114** (2016) 2717–2723.

[55] A. B. Michaels and R. W. Hausslein, *Journal of Polymer Science Part C: Polymer Symposia* **10** (1965) 61–86.

[56] F. Doghieri and G. C. Sarti, *Macromolecules* **29** (1996) 7885–7896.

[57] M. G. Bawendi and K. F. Freed, *The Journal of Chemical Physics* **88** (1988) 2741–2756.

[58] M. G. Bawendi, K. F. Freed and U. Mohanty, *The Journal of Chemical Physics* **84** (1986) 7036–7047.

[59] A. I. Pesci and K. F. Freed, *The Journal of Chemical Physics* **90** (1989) 2003–2016.

[60] A. M. Nemirovsky, M. G. Bawendi and K. F. Freed, *The Journal of Chemical Physics* **87** (1987) 7272–7284.

[61] K. F. Freed, *Journal of Physics A: Mathematical and General* **18** (1985) 871–877.

[62] J. Dudowicz, K. F. Freed and J. F. Douglas, *Macromolecules* **28** (1995) 2276–2287.

[63] Nemirovsky, J. Dudowicz and K. F. Freed, *Physical review. A, Atomic, molecular, and optical physics* **45** (1992) 7111–7127.

[64] H. R. Kricheldorf, O. Nuyken and G. Swift, *Handbook of polymer synthesis,* 2nd ed., New York: Marcel Dekker (2005).

[65] Y. V. Kissin, "Catalysts for the Manufacture of Polyethylene", in: *Handbook of Industrial Polyethylene and Technology,* ed. by M. A. Spalding and A. M. Chatterjee, Wiley (2017).

[66] S. L. Aggarwal and O. J. Sweeting, *Chemical Reviews* **57** (1957) 665–742.

[67] K. P. C. Vollhardt and N. E. Schore, *Organic chemistry, Structure and function,* 5th ed., New York: W.H. Freeman (2007).

[68] I. D. Burdett and R. S. Eisinger, "Ethylene Polymerization Processes and Manufacture of Polyethylene", in: *Handbook of Industrial Polyethylene and Technology,* ed. by M. A. Spalding and A. M. Chatterjee, Wiley (2017).

[69] R. G. Alamo, R. Domszy and L. Mandelkern, *The Journal of Physical Chemistry* **88** (1984) 6587–6595.

[70] B. Wunderlich and G. Czornyj, *Macromolecules* **10** (1977) 906–913.

[71] O. Olabisi and R. Simha, *Macromolecules* **8** (1975) 206–210.

[72] E. Hunter and W. G. Oakes, *Transactions of the Faraday Society* **41** (1945) 49–56.

[73] G. P. Johari, "Phenomenological aspects of glass transition and molecular motions in glasses", in: *Relaxations in complex systems,* ed. by K. L. Ngai and G. B. Wright, Naval Research Laboratory and Office of Naval Research (1985).

[74] M. J. Roedel, *Journal of the American Chemical Society* **75** (1953) 6110–6112.

[75] A. Alizadeh, L. Richardson, J. Xu, S. McCartney, H. Marand, Y. W. Cheung and S. P. Chum, *Macromolecules* **32** (1999) 6221–6235.

[76] K. Shirayama, S.-I. Kita and H. Watabe, *Die Makromolekulare Chemie* **151** (1972) 97–120.

[77] J. Hay and X.-Q. Zhou, *Polymer* **34** (1993) 1002–1005.

[78] H. Čačković, J. Loboda-Čačković, R. Hosemann and D. Weick, *Colloid & Polymer Science* **252** (1974) 812–818.

[79] A. Baker and A. Windle, *Polymer* **42** (2001) 651–665.

[80] J. A. Parker and R. H. Olley, *Journal of Polymer Science Part B: Polymer Physics* **43** (2005) 1986–1996.

[81] M. J. Richardson, P. J. Flory and J. B. Jackson, *Polymer* **4** (1963) 221–236.

[82] R. G. Alamo and L. Mandelkern, *Thermochimica Acta* **238** (1994) 155–201.

[83] D. J. Cutler, P. J. Hendra, M. Cudby and H. A. Willis, *Polymer* **18** (1977) 1005–1008.

[84] P. J. Holdsworth, A. Keller, I. M. Ward and T. Williams, *Die Makromolekulare Chemie* **125** (1969) 70–81.

[85] E. Martuscelli and M. Pracella, *Polymer* **15** (1974) 306–314.

[86] E. Pérez and D. L. VanderHart, *Journal of Polymer Science Part B: Polymer Physics* **25** (1987) 1637–1653.

[87] M. Y. Keating and I.-H. Lee, *Journal of Macromolecular Science, Part B* **38** (1999) 379–401.

[88] C. A. Sperati, W. A. Franta and H. W. Starkweather, *Journal of the American Chemical Society* **75** (1953) 6127–6133.

[89] D. Maloney and J. Prausnitz, *Industrial & Engineering Chemistry Process Design and Development* **15** (1976) 216–220.

[90] J. Sterr, B. S. Fleckenstein and H.-C. Langowski, *Food Engineering Reviews* **10** (2017) 14–33.

[91] J. G. Lee and R. W. Flumerfelt, *Journal of Applied Polymer Science* **58** (1995) 2213–2219.

[92] Y. L. Cheng and D. C. Bonner, *Journal of Polymer Science: Polymer Physics Edition* **16** (1978) 319–333.

[93] E. B. Atkinson, *Journal of Polymer Science: Polymer Physics Edition* **15** (1977) 795–804.

[94] P. L. Durrill and R. G. Griskey, *AIChE Journal* **12** (1966) 1147–1151.

[95] D. C. Bonner, *Polymer Engineering & Science* **17** (1977) 65–72.

[96] V. Ž. Bogdanović, A. Ž. Tasić and B. D. Djordjević, *Journal of Applied Polymer Science* **41** (1990) 3091–3095.

[97] V. Kobyakov, V. Kogan and V. Zernov, *Zhurnal Pikladnoi Khimii* **60** (1987) 81.

[98] J. A. Meyer and R. F. Blanks, *Journal of Applied Polymer Science* **28** (1983) 725–741.

[99] C. Peng, H. Liu and Y. Hu, *Chemical Engineering Science* **56** (2001) 6967–6975.

[100] R. D. Newman and J. M. Prausnitz, *AIChE Journal* **19** (1973) 704–710.

[101] B. J. Banaszak, D. Lo, T. Widya, W. H. Ray, J. J. de Pablo, A. Novak and J. Kosek, *Macromolecules* **37** (2004) 9139–9150.

[102] N. N. Li and R. B. Long, *AIChE Journal* **15** (1969) 73–80.

[103] W. Yao, X. Hu and Y. Yang, *Journal of Applied Polymer Science* **104** (2007) 3654–3662.

[104] C. Wohlfarth, U. Finck, R. Schultz and T. Heuer, *Die Angewandte Makromolekulare Chemie* **198** (1992) 91–110.

[105] L. M. Robeson and T. G. Smith, *Journal of Applied Polymer Science* **11** (1967) 2007–2019.

[106] S. J. Moore and S. E. Wanke, *Chemical Engineering Science* **56** (2001) 4121–4129.

[107] A. Alizadeh, J. Chmelař, F. Sharif, M. Ebrahimi, J. Kosek and T. F. L. McKenna, *Industrial & Engineering Chemistry Research* **56** (2017) 1168–1185.

[108] J. A. Moebus and B. R. Greenhalgh, *Macromolecular Reaction Engineering* **12** (2018) 1700072.

[109] J. Sun, H. Wang, M. Chen, J. Ye, B. Jiang, J. Wang, Y. Yang and C. Ren, *Journal of Applied Polymer Science* **134** (2016) 44507.

[110] A. S. Michaels and R. B. Parker, *Journal of Polymer Science* **41** (1959) 53–71.

[111] A. S. Michaels and H. J. Bixler, *Journal of Polymer Science* **50** (1961) 393–412.

[112] A. S. Michaels and H. J. Bixler, *Journal of Polymer Science* **50** (1961) 413–439.

[113] P. J. Flory and J. Rehner, *The Journal of Chemical Physics* **11** (1943) 521–526.

[114] D. R. Sturm, K. J. Caputo, S. Liu and R. P. Danner, *Fluid Phase Equilibria* **470** (2018) 68–74.

[115] B. J. Savatsky, J. A. Moebus and B. R. Greenhalgh, *Macromolecular Reaction Engineering* **13** (2019) 1900003.

[116] B. Bonavoglia, G. Storti, M. Morbidelli, A. Rajendran and M. Mazzotti, *Journal of Polymer Science Part B: Polymer Physics* **44** (2006) 1531–1546.

[117] P. Memari, V. Lachet and B. Rousseau, *Polymer* **51** (2010) 4978–4984.

[118] P. Memari, V. Lachet, M.-H. Klopffer, B. Flaconnèche and B. Rousseau, *Journal of Membrane Science* **390–391** (2012) 194–200.

[119] J. Zimmermann, S. Enders and M. Fischlschweiger, *Journal of Chemical & Engineering Data* **69** (2023) 526–537.

[120] R. M. Patel, "Processing-Structure-Property Relationships in Polyethylene", in: *Handbook of Industrial Polyethylene and Technology*, ed. by M. A. Spalding and A. M. Chatterjee, Wiley (2017).

[121] D. Campbell, *Polymer Characterization*, ed. by R. A. Pethrick and J. R. White, 2nd ed., Cheltenham: CRC Press (2000).

[122] J. C. Randall, *Polymer sequence determination, Carbon-13 NMR method*, New York: Academic Press (1977).

[123] J. P. Runt, *Encyclopedia of polymer science and engineering*, ed. by H. F. Mark, 2nd ed., New York: Wiley (1985).

[124] L. Mandelkern, J. G. Fatou, R. Denison and J. Justin, *Journal of Polymer Science Part B: Polymer Letters* **3** (1965) 803–807.

[125] R. G. Alamo, "Phase Structure and Morphology", in: *Molecular characterization and analysis of polymers*, ed. by J. M. Chalmers and R. J. Meier, Amsterdam: Elsevier (2008).

[126] S. Venkatram, J. McCollum, N. Stingelin and B. Brettmann, *Polymer International* **72** (2023) 855–860.

[127] Y. P. Khanna, *Journal of Applied Polymer Science* **37** (1989) 2719–2726.

[128] J. Mcbain and A. Bakr, *Journal of the American Chemical Society* **48** (1926) 690–695.

[129] Y. Yampolskii and R. Paterson, "Solubility of Gases in Polymers", in: *The Experimental Determination of Solubilities*, ed. by G. T. Hefter and R. P. T. Tomkins, Wiley (2003).

[130] Y. Kamiya, K. Mizoguchi, Y. Naito and T. Hirose, *Journal of Polymer Science Part B: Polymer Physics* **24** (1986) 535–547.

[131] J. K. Lee, S. X. Yao, G. Li, M. B. G. Jun and P. C. Lee, *Polymer Reviews* **57** (2017) 695–747.

[132] W. J. Koros and D. R. Paul, *Journal of Polymer Science: Polymer Physics Edition* **14** (1976) 1903–1907.

[133] C. Wohlfarth, *CRC handbook of thermodynamics data of polymer solutions at elevated pressures*, Boca Raton: CRC Press (2005).

[134] D. E. Axelson, L. Mandelkern, R. Popli and P. Mathieu, *Journal of Polymer Science: Polymer Physics Edition* **21** (1983) 2319–2335.

[135] G. Ver Strate and Z. W. Wilchinsky, *Journal of Polymer Science Part A-2: Polymer Physics* **9** (1971) 127–142.

[136] G. C. Han-Adebekun, M. Hamba and W. H. Ray, *Journal of Polymer Science Part A: Polymer Chemistry* **35** (1997) 2063–2074.

[137] M. Glotin and L. Mandelkern, *Colloid & Polymer Science* **260** (1982) 182–192.

[138] A. Moyassari, H. Mostafavi, T. Gkourmpis, M. S. Hedenqvist, U. W. Gedde and F. Nilsson, *Polymer* **72** (2015) 177–184.

[139] R. Seguela and F. Rietsch, *Polymer* **27** (1986) 703–708.

[140] I. G. Voigt-Martin, R. G. Alamo and L. Mandelkern, *Journal of Polymer Science Part B: Polymer Physics* **24** (1986) 1283–1302.

[141] P. Starck, K. Rajanen and B. Löfgren, *Thermochimica Acta* **395** (2003) 169–181.

[142] K. Jokela, A. Väänänen, M. Torkkeli, P. Starck, R. Serimaa, B. Löfgren and J. Seppälä, *Journal of Polymer Science Part B: Polymer Physics* **39** (2001) 1860–1875.

[143] M. Hedenqvist, A. Angelstok, L. Edsberg, P. Larsson and U. Gedde, *Polymer* **37** (1996) 2887–2902.

[144] Y.-L. Huang and N. Brown, *Journal of Polymer Science Part B: Polymer Physics* **29** (1991) 129–137.

[145] F. M. Mirabella and A. Bafna, *Journal of Polymer Science Part B: Polymer Physics* **40** (2002) 1637–1643.

[146] R. Quijada, R. Rojas, R. S. Mauler, G. B. Galland and R. B. Scipioni, *Journal of applied polymer science* **64** (1997) 2567–2574.

[147] J. C. W. Chien and T. Nozaki, *Journal of Polymer Science Part A: Polymer Chemistry* **31** (1993) 227–237.

[148] R. Androsch, *Polymer* **40** (1999) 2805–2812.

[149] D. E. Axelson, *Journal of Polymer Science: Polymer Physics Edition* **20** (1982) 1427–1435.

[150] R. G. Alamo and L. Mandelkern, *Macromolecules* **22** (1989) 1273–1277.

[151] C. France, P. J. Hendra, W. F. Maddams and H. A. Willis, *Polymer* **28** (1987) 710–712.

[152] S. Martín, M. T. Expósito, J. F. Vega and J. Martínez-Salazar, *Journal of Applied Polymer Science* **128** (2012) 1871–1878.

[153] M. F. Laguna, M. L. Cerrada, R. Benavente, E. Pérez and R. Quijada, *Journal of Polymer Science Part B: Polymer Physics* **41** (2003) 2174–2184.

[154] E. Pérez, D. L. VanderHart, B. Crist and P. R. Howard, *Macromolecules* **20** (1987) 78–87.

[155] R. H. Perry, D. W. Green and J. O. Maloney, *Perry's chemical engineers' handbook*, 7th ed., New York: McGraw-Hill (1997).

[156] S. Young, *J. Chem. Soc., Trans.* **71** (1897) 446–457.

[157] W. C. Reynolds, *Thermodynamic properties in SI, Graphs, tables and computational equations for 40 substances*, 2nd ed., Stanford: Department of Mechanical Engineering (1979).

[158] J. McMicking, *Vapor Pressures and Saturated Liquid and Vapor Densities of Isomeric Heptanes and Octanes*, PhD thesis, The Ohio State University (1961).

[159] J. Beattie and S. Marple, *Journal of the American Chemical Society* **72** (1950) 1449–1452.

[160] C. Coffin and O. Maass, *Journal of the American Chemical Society* **50** (1928) 1427–1437.

[161] R. C. Wackher, C. B. Linn and A. V. Grosse, *Industrial & Engineering Chemistry* **37** (1945) 464–468.

[162] R. H. Olds, B. H. Sage and W. N. Lacey, *Industrial & Engineering Chemistry* **38** (1946) 301–303.

[163] C. Luo and R. Miller, *Cryogenics* **21** (1981) 85–93.

[164] E. C. Ihmels, K. Fischer and J. Gmehling, *Fluid Phase Equilibria* **228–229** (2005) 155–171.

[165] P. Ma, Z. Fang, J. Zhang and Y. Ruan, *Gaoxiao Huaxue Gongcheng Xuebao* **6** (1992) 112–117.

[166] E. Sapei, A. Zaytseva, P. Uusi-Kyyny, K. I. Keskinen and J. Aittamaa, *Journal of Chemical & Engineering Data* **51** (2006) 2203–2208.

[167] D. L. Camin and F. D. Rossini, *The Journal of Physical Chemistry* **60** (1956) 1446–1451.

[168] P. Moodley, *Vapour-liquid equilibria studies for binary systems containing 1-hexene and n-hexane*, PhD thesis, University of KwaZulu-Natal (2009).

[169] L. Negadi, A. Belabbaci, A. Ait Kaci and J. Jose, *Journal of Chemical & Engineering Data* **52** (2006) 47–55.

[170] B. N. Kireev, *Nauchn. Tr. Kursk. Gos. Pedagog. Inst (Scientific Works of the Kursk State Pedagogical Institute)* **23** (1974) 40–45.

[171] T. Daubert and R. Danner, *Data Compilation of Pure Compound Properties*, Design Institute for Physical Properties Data, American Institute of Chemical Engineers (1987).

[172] B. Betken, R. Beckmüller, M. A. Javed, E. Baumhögger, R. Span, J. Vrabec and M. Thol, *The Journal of Chemical Thermodynamics* **176** (2023) 106881.

[173] G. S. Parks, *Selected values of properties of hydrocarbons and related compounds*, Thermodynamics Research Center, TexasA&M University, College Station, Texas (extant 1994).

[174] P. Rousseaux, D. Richon and H. Renon, *Journal of Polymer Science: Polymer Chemistry Edition* **23** (1985) 1771–1785.

[175] D. D. Liu and J. M. Prausnitz, *Industrial & Engineering Chemistry Fundamentals* **15** (1976) 330–335.

[176] B. Jiang, J. Dai, J. Sun, J. Ye, M. Chen, G. Han, J. Wang, J. Yang and Y. Yang, *Polymer Engineering & Science* **60** (2020) 1998–2007.

[177] R. Spahl and G. Luft, *Berichte der Bunsengesellschaft für physikalische Chemie* **85** (1981) 379–384.

[178] P. K. Davis, G. D. Lundy, J. E. Palamara, J. L. Duda and R. P. Danner, *Industrial & Engineering Chemistry Research* **43** (2004) 1537–1542.

[179] V. Compañ, L. F. Del Castillo, S. I. Hernández, M. M. López-González and E. Riande, *Journal of Polymer Science Part B: Polymer Physics* **45** (2007) 1798–1807.

[180] C. Kiparissides, V. Dimos, T. Boultouka, A. Anastasiadis and A. Chasiotis, *Journal of Applied Polymer Science* **87** (2002) 953–966.

[181] W. Yao, X. Hu and Y. Yang, *Journal of Applied Polymer Science* **103** (2006) 1737–1744.

[182] M. Podivinská, K. Jindrová, J. Chmelař and J. Kosek, *Journal of Applied Polymer Science* **134** (2017) 45035.

[183] Z. Yao, L.-J. Xu, F.-J. Zhu, Y.-F. Zhang, C. Zeng and K. Cao, *Journal of Chemical & Engineering Data* **60** (2015) 3033–3038.

[184] M. López-González, V. Compañ and E. Riande, *Journal of Applied Polymer Science* **105** (2007) 903–907.

[185] J.-S. Yoon, H.-S. Yoo and K.-S. Kang, *European Polymer Journal* **32** (1996) 1333–1336.

[186] M. L. D. Santos, N. F. Corrêa and D. M. Leitao, *Journal of Colloid & Interface Science* **47** (1974) 621–627.

[187] Z. H. Liu, M. Zhang, L. Zhao and P. Choi, *Macromolecules* **38** (2005) 4512–4520.

[188] H.-J. Jin, S. Kim and J.-S. Yoon, *Journal of Applied Polymer Science* **84** (2002) 1566–1571.

[189] J. Chmelař, K. Haškovcová, M. Podivinská and J. Kosek, *Industrial & Engineering Chemistry Research* **56** (2017) 6820–6826.

[190] M. Chen, J. Wang, B. Jiang and Y. Yang, *Journal of Applied Polymer Science* **127** (2012) 1098–1104.

[191] S. Areerat, Y. Hayata, R. Katsumoto, T. Kegasawa, H. Egami and M. Ohshima, *Journal of Applied Polymer Science* **86** (2002) 282–288.

[192] P. L. Durrill and R. G. Griskey, *AIChE Journal* **15** (1969) 106–110.

[193] B. I. Chaudhary and A. I. Johns, *Journal of Cellular Plastics* **34** (1998) 312–328.

[194] Y. Kamiya, T. Hirose, K. Mizoguchi and Y. Naito, *Journal of Polymer Science Part B: Polymer Physics* **24** (1986) 1525–1539.

[195] F. Sarrasin, P. Memari, M. Klopffer, V. Lachet, C. Taravel Condat, B. Rousseau and E. Espuche, *Journal of Membrane Science* **490** (2015) 380–388.

[196] R. Ash, R. Barrer and D. Palmer, *Polymer* **11** (1970) 421–435.

[197] N. Von Solms, J. K. Nielsen, O. Hassager, A. Rubin, A. Y. Dandekar, S. I. Andersen and E. H. Stenby, *Journal of Applied Polymer Science* **91** (2003) 1476–1488.

[198] T. Hirose, K. Mizoguchi and Y. Kamiya, *Journal of Polymer Science Part B: Polymer Physics* **24** (1986) 2107–2115.

[199] M. Pino, R. A. Duckett and I. M. Ward, *Polymer* **46** (2005) 4882–4890.

[200] H. Azimi, *Journal of Thermoplastic Composite Materials* **36** (2023) 4284–4295.

[201] M. Wang, Y. Sato, T. Iketani, S. Takishima, H. Masuoka, T. Watanabe and Y. Fukasawa, *Fluid Phase Equilibria* **232** (2005) 1–8.

[202] E. Castro, E. Gonzo and J. Gottifredi, *Journal of Membrane Science* **31** (1987) 235–248.

[203] R. K. Surana, R. P. Danner, A. de Haan and N. Beckers, *Fluid Phase Equilibria* **139** (1997) 361–370.

[204] N. F. Brockmeier, R. E. Carlson and R. W. McCoy, *AIChE Journal* **19** (1973) 1133–1139.

[205] L. V. Serna, J. L. Becker, J. R. Galdámez, R. P. Danner and J. L. Duda, *Journal of Applied Polymer Science* **107** (2007) 138–146.

[206] O. Vopička, K. Friess, H. V. Langenhove, J. Dewulf, M. Dingemans, V. Hynek and M. Šípek, *Separation Science & Technology* **45** (2010) 1260–1264.

[207] C. Liu and P. Neogi, *Journal of Membrane Science* **35** (1988) 207–215.

[208] N. Lützow, A. Tihminlioglu, R. P. Danner, J. Duda, A. De Haan, G. Warnier and J. M. Zielinski, *Polymer* **40** (1999) 2797–2803.

[209] J.-S. Yoon, C.-Y. Chung and I.-H. Lee, *European Polymer Journal* **30** (1994) 1209–1214.

[210] D. C. Bonner, *Journal of Macromolecular Science, Part C: Polymer Reviews* **13** (1975) 263–319.

[211] K. Langenbach and S. Enders, *Fluid Phase Equilibria* **331** (2012) 58–79.

[212] K. Langenbach, *Development of an equation of state incorporating molecular architecture*, PhD thesis, Technische Universität Berlin (2013).

[213] E. S. Clark, in: *Physical properties of polymers handbook*, ed. by J. E. Mark, 2nd ed., New York: Springer (2007).

[214] P. J. Flory, *The Journal of Chemical Physics* **17** (1949) 223–240.

[215] L. Mandelkern, J. G. Fatou and C. Howard, *The Journal of Physical Chemistry* **68** (1964) 3386–3391.

[216] L. Mandelkern, *Journal of Applied Physics* **26** (1955) 443–451.

[217] J. D. Hoffman, L. J. Frolen, G. S. Ross and J. I. Lauritzen, *Journal of research of the National Bureau of Standards. Section A, Physics and chemistry* **79A** (1975) 671–699.

[218] F. A. Quinn and L. Mandelkern, *Journal of the American Chemical Society* **80** (1958) 3178–3182.

[219] R. W. Freedman and F. Gornick, *Journal of Mathematical Chemistry* **13** (1993) 167–176.

[220] H. G. Kilian, *Colloid & Polymer Science* **202** (1965) 97–107.

[221] H. Baur, *Colloid & Polymer Science* **203** (1965) 97–107.

[222] B. Wunderlich, *Macromolecular physics*, vol. 2, New York: Academic Press (1976).

[223] L. Mandelkern, *Journal of Polymer Science Part C: Polymer Symposia* **15** (1967) 129–162.

[224] F. R. Anderson, *Journal of Applied Physics* **35** (1964) 64–70.

[225] R. Androsch and B. Wunderlich, *Macromolecules* **32** (1999) 7238–7247.

[226] M.-H. Kim, P. J. Phillips and J. S. Lin, *Journal of Polymer Science Part B: Polymer Physics* **38** (2000) 154–170.

[227] R. Androsch and B. Wunderlich, *Macromolecules* **33** (2000) 9076–9089.

[228] D. Ambrose and C. Tsonopoulos, *Journal of Chemical Engineering Data* **40** (1995) 531–546.

[229] A. P. De Boer and A. J. Pennings, *Journal of Polymer Science: Polymer Physics Edition* **14** (1976) 187–210.

[230] P. J. Flory, *Chemical Reviews* **35** (1944) 51–75.

[231] T. P. Lodge and P. C. Hiemenz, *Polymer Chemistry*, 3rd ed., Milton: Taylor & Francis Group (2020).

[232] A. S. Luyt and M. J. Hato, *Journal of Applied Polymer Science* **96** (2005) 1748–1755.

[233] R. Span and W. Wagner, *International Journal of Thermophysics* **24** (2003) 41–109.

[234] J.-W. Qian, J.-N. Jaubert and R. Privat, *Fluid Phase Equilibria* **354** (2013) 212–235.

[235] H. K. Bae, K. Nagahama and M. Hirata, *Journal of Chemical Engineering of Japan* **14** (1981) 1–6.

[236] K. Ohgaki, S. Nakai, S. Nitta and T. Katayama, *Fluid Phase Equilibria* **8** (1982) 113–122.

[237] H. Kubota, H. Inatome, Y. Tanaka and T. Makita, *Journal of Chemical Engineering of Japan* **16** (1983) 99–103.

[238] S. F. Edwards, *Proceedings of the Physical Society* **92** (1967) 9–16.

References

[239] D. W. Sumners, *Journal of Mathematical Chemistry* **1** (1987) 1–14.

[240] M. T. Rätzsch and H. Kehlen, *Progress in Polymer Science* **14** (1989) 1–46.

[241] P. Schneider, T. Chaloupka, L. Grunin and J. Kosek, *Polymer Testing* **127** (2023) 108174.